Dynamic Testing of Distance Protection

Dedi Mahendra

Master of Science Thesis

TU Delft

Dynamic Testing of Distance Protection

By

Dedi Mahendra

In partial fulfilment of the requirements for the degree of

Master of Science
in Electrical Sustainable Energy

at the Delft University of Technology,
To be defended publicly on Wednesday, 12 July 2017 at 9:30 AM

Supervisor:	Dr. Marjan Popov,	TU Delft
Thesis Committee:	Prof. M.A.A.M van der Meijden,	TU Delft
	Dr. A. Rodrigo Mor,	TU Delft
	Ir. Marc Achterkamp,	DNV GL – Kema Lab

Abstract

As the primary protection of high voltage (HV) and Extra high voltage (EHV) transmission networks, distance protection needs to operate properly under all possible fault conditions. It needs to operate as fast as possible for internal fault, while it also must be able to discriminate between the internal and the external faults to prevent unnecessary trip of the normal system. In real life application, the operational characteristic of commercial distance relays such as operating time and reach accuracy are usually defined using the steady state conditions. This leads to difficulty in understanding the operational characteristic of the relay under the dynamic conditions such as faults.

In this thesis, a dynamic test tool based on the latest IEC 60255-121 standard, suitable for performance analysis of distance protection during dynamic condition was developed and validated. The tools are built by using the ATP-EMTP Software and the Omicron secondary injection kit. The test results of two distance relays show that depending on the dynamic conditions, the operational performance of the relay might be affected. In some situations, the operating time of the relays was delayed, while, in other conditions, the accuracy of impedance measurement is affected causing the relay to overreach. Furthermore, this delayed tripping or overreach of distance protection could cause both security and dependability issue in power transmission protection. The dynamic test tool which has been developed can be expanded further to study other dynamic conditions that are not covered in this thesis.

Keywords: *ATP-EMTP, IEC 60255-121, distance protection, operating time, transient overreach*

Acknowledgments

I would like to give my sincere thanks to my supervisor, Dr. Marjan Popov for his guidance and encouragement during my thesis research. I have had a pleasure to learn a lot about this subject from him. I would like to also thank Mr. Marc Achterkamp and Mr. Herman Koerts from KEMA DNV-GL for their guidance and technical assistance with the protection testing.

I take this opportunity to express my gratitude to all my thesis committee members, Prof. Mart van der Meijden and Dr. Armando Rodrigo Mor for their recommendations.

Special thanks to LPDP scholarship for providing the opportunity for me to study in the Netherlands for the past two years.

I would like to express my greatest gratitude to my family for their constant support and caring, and to my friends whom I had the immense pleasure of knowing during my study at TU Delft.

.

“Knowledge is my companion, it is with me wherever I go. My heart is its container, not the bookshelf.”

- *Ali (RA)*

“In theory, theory and practice are the same. In practice, they are not.”

- *Albert Einstein*

Table of Contents

List of Figures

List of Tables

Glossary

A/D	Analog to Digital
ATP-EMTP	Alternative Transient Programs – ElectroMagnetics Transient Programs
CB	Circuit Breaker
COMTRADE	COMmon format for TRAnsient Data Exchange
CT	Current Transformer
CVT	Capacitive Voltage Transformer
DC	Direct Current
DFT	Discrete Fourier Transform
EHV	Extra High Voltage
FACTS	Flexible AC Transmission Systems
HVDC	High Voltage Direct Current
IEC	International Electrotechnical Commission
IEEE	Institute of Electrical and Electronics Engineers
LN	Line to Neutral (ground) fault
LL	Line to Line fault
LLN	Line to Line to Neutral (ground) fault
LLL	Line to Line to Line fault
OCC	Omicron Control Centre
SIR	Source Impedance Ratio
THD	Total Harmonic Distortion
VT	Voltage Transformer

1 Introduction

Distance protection is the primary protection of high voltage (HV) and extra high voltage (EHV) power transmission line. It detects disturbance (such as short circuit currents) by measuring the impedance between the faulted point and the relay location. The Impedance values are obtained by dividing the voltage and current at the relay location. When the measured impedance is *smaller* than the impedance setting, the protection will detect the internal fault and send a trip signal to the circuit breaker to isolate the faulted line. Distance protection needs to operate as quickly as possible for an internal fault condition, while it also must be able to discriminate between internal and external faults to prevent unnecessary disconnection of the healthy systems.

Distance protection has evolved over the years, from relatively simple mechanical relays with limited capability to the sophisticated numerical relays that involve extensive use of computers with superior capabilities. Numerical relays utilize advanced signal processing techniques and state-of-the-art algorithms to enhance their operational performance. As a result, they have a much faster operating time and better accuracy compared to the mechanical type.

The requirements for distance protection performance are defined in the IEEE standard (C37.90-2005 & C37.113-2015), and the IEC standard (IEC 60255-1, IEC 60255-16, & IEC 60255-121). The former standards only introduce requirements for distance protection steady-state performance. The requirements for dynamic performance of numerical distance protection has been incorporated into the latest IEC 60255-121:2014 standard. In the latest standard, the operational performance of distance protections is evaluated based on the operating time and the reach accuracy during dynamic conditions.

The operating time is defined as time interval between the instant when the fault occurs and the instant when distance protection operates (trip) [1]. Reach accuracy means that distance relay must not have overreach or underreach operation under all fault conditions. Overreach happens when the calculated impedance is less than the actual fault impedance causing the relay to trip for faults located outside of its protection zone. On the other hand, underreach arises when the calculated impedance is greater than the actual fault impedance causing the relay failed to trip for internal faults.

1.1 Literature Review

The first commercial numerical distance protection was developed in 1985 to replace the older static distance protection. Numerical distance relays were then developed into smart IEDs (Intelligent Electronic Devices) with different integrated functions and enhanced communication via fiber optics and data networks. The application of numerical distance protection results in faster tripping time in the order of one to two cycles (20 to 40 ms) for the instantaneous zone 1 [2].

There has been much research into analyzing the problem of distance protection under transient conditions. However, the research is usually conducted using computer simulations. Reference [3] describes the effect of fault variables to the performance of distance relay. Based on the simulation results, it was concluded that the fault resistance, type, and location have significant influences on the performance of distance protection due to an error in the measured impedance. The performance of distance relay during harmonics was reported in [6], it was concluded that due to the filtering effect, the harmonics have no significant effect on numerical distance type. In [5] and [7], the effect of capacitive voltage transformer (CVT)

transient was explained. It was found that CVT transient causes distance elements (mho and quadrilateral) to overreach. Reference [8] studied the effect of frequency deviation on numerical distance relay. In [10] the effect of arcing fault on distance protection performance are also studied.

Many test methodologies have also been presented on distance protections. Reference [13] shows the test methodology to evaluate the security and dependability of protection relay. The proposed methodology covers power network modeling, generating the test scenarios, and automating the simulation using a digital simulator. Two types of tests were performed: the conformance test and the compliance test. In [14], the dynamic testing is done by building a transient model in simulation software based on real network and machine data. Different short circuit conditions are simulated and tested into distance protection relays. Reference [15] proposes a testing concept and provides a general understanding of numerical protection testing. The proposed concept consists of two different tests. The first test is a type test for functional and technological verification, while the second test is an individual test for commissioning and periodic verification.

1.2 Objectives of The Thesis

While considerable research activity continues in the study of distance protection performance inside transient simulation software and developing test methodology for distance relays. Less work is being done in developing real testing tools for distance protection. Hence, this thesis focuses on developing testing tools that can be used to evaluate distance relay performance during transient conditions.

The research objectives of the thesis are:

- Study the performance of distance protection through transient simulation; getting used to the new standard for distance protection performance, i.e. the IEC 60255-121.
- Testing distance relays according to the IEC 60255-121 standard and additional transient conditions; evaluating the performance of commercial distance relay with a series of transient conditions and parameter variations.

1.3 Research Methodology

The dynamic testing of distance protection is performed in three steps. First, the IEC 60255-121:2014 standard has to be studied to obtain general information on how to evaluate the operational performance of distance protections and how to define which test cases should be included in the study. Second, a series of voltage and current signals are generated in compliance with the standard. The voltage and current signals are generated using the transient simulation software, i.e. ATP-EMTP. Finally, a dynamic test setup is developed. The test setup aims to inject transient signals into distance relays and to measure the operating time of the relay in the range of milliseconds. The test setup is developed using both software (Omicron control centre) and hardware (Omicron CMC 356) configurations.

After the tests are performed, an analysis will be performed by comparing the operating time and the accuracy of distance relays for different transient conditions. The summary of distance relay performance is then presented.

1.4 Thesis Layout

Chapter 1: Introduction
This chapter highlights past studies about the effect of transient to distance protection performance, and the test methodology developed. It continues with the objectives of the thesis and the research methodology, followed by the thesis structure.

Chapter 2: Distance protection theory and the IEC 60255-121 standard
This chapter contains the basic theory of distance protection and how transient condition affect its operation. In addition, the chapter also provides information about the latest IEC 60255-121 standard applied in this thesis.

Chapter 3: Test Methodology
This chapter deals with the test methodology performed in this thesis, including the test procedure and information about the hardware and software tools.

Chapter 4: Simulation of Dynamic Conditions
This chapter discusses the modeling and simulation of transient in power system. The simulations are performed in ATP-EMTP software. Simulation results describe the effect of various transients to distance protection operations.

Chapter 5: Dynamic Test of Distance Protection
This chapter presents the main work performed in this thesis. The results and analysis of all tests cases are presented.

Chapter 6: Conclusions and Recommendations
This final chapter summarizes the outcome of the thesis and recommendations for future research.

2 Distance Protection Theory and The IEC 60255-121 standard

2.1 Introduction

The distance protection detects fault conditions by continuously measuring the apparent fault impedance using voltage and current at the relay location. The measured impedance is then compared with the known line impedance setting. If the measured impedance is *lower* than the line impedance setting, an internal fault is detected, and the distance protection will send a trip signal to the circuit breaker according to the protection characteristics. The operating principle of distance protection is illustrated in Figure 2.1.

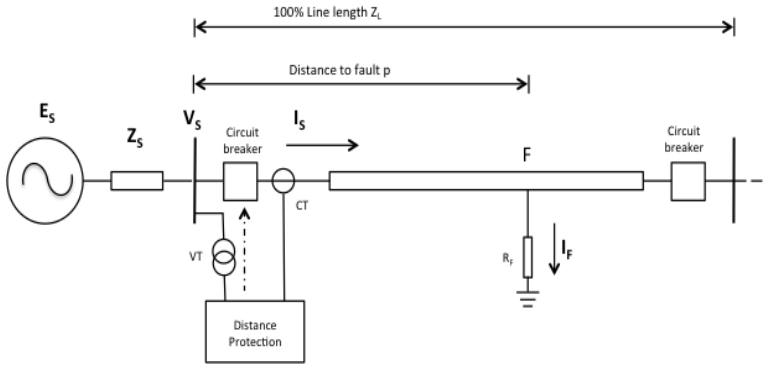

Figure 2.1 Operating principle of distance relay

The distance protection measures voltage (V_s) and current (I_s) signals and then calculate the apparent impedance (Z_m) between the relay location and the point of fault (F). The calculated impedance is then compared with the reach impedance setting of the transmission line (Z_L). If the apparent impedance is *smaller* than the impedance setting, the relay will send trip signals to the circuit breaker to disconnect the faulty network.

The apparent impedance (Z_m) is proportional to the distance (p) between the location of relay and fault. It can be explained using the following equations

$$V_s = \frac{E_s\, p\, Z_L}{Z_s + pZ_L} \tag{1}$$

$$I_s = \frac{E_s}{Z_s + pZ_L} \tag{2}$$

$$Z_m = \frac{V_s}{I_s} = pZ_L \tag{3}$$

The system impedance and the zone settings of distance protection are usually defined in an impedance (R-X) plane. The impedance diagram serves as the main tool to assess the relay operational characteristic as displayed in Figure 2.2.

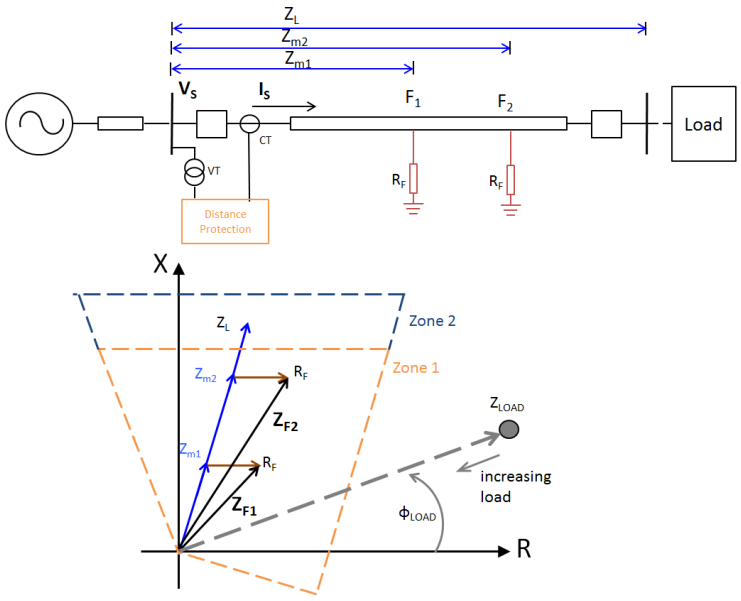

Figure 2.2 Load and short circuit impedance in R-X plane

During normal condition, the impedance is proportional to the load impedance ($Z_{load} = V_{line}^2 / P_{load}$). Meanwhile, during fault occurrence, the impedance value jumps to a much smaller short-circuit impedance (Z_m). The value depends on the distance between the location of the relay and the fault. Moreover, the fault resistance (R_F) that is present in the faulted point (F1) will shift the fault impedance because it adds a resistive component to the measured impedance as shown in the RX plane.

2.2 Impedance calculation methods

2.2.1 Multi-phases faults

The equations that relate fault voltages and currents with the fault impedance depend on the fault types. In a 3-phase system, there are ten possible fault types: one type of LLL, three types of LLN, three types of LL, and three types of LN. Normally, fault impedance is calculated based on the positive-sequence impedance regardless of the fault types [2]. The following section will explain how to calculate the positive-sequence impedance of multi-phases faults.

The first multi-phases fault type is the phase-to-phase fault. Consider a phase-to-phase fault (BC) occurs at location F as shown in Figure 2.3.

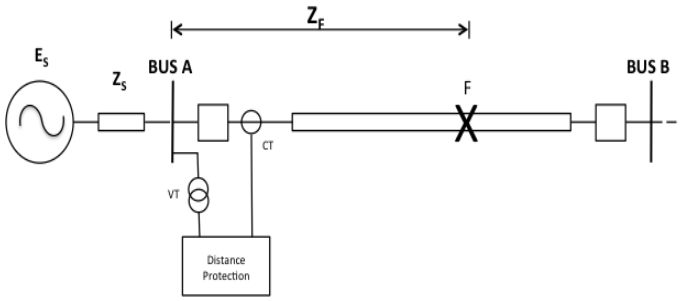

Figure 2.3 BC fault at location F

Its symmetrical component network can be arranged as shown in Figure 2.4.

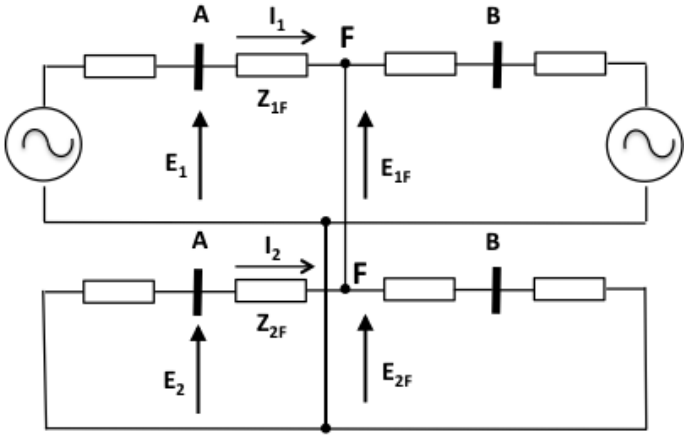

Figure 2.4 Symmetrical component network of BC fault

The positive- and negative- sequence voltages at the fault location are given by the following equations:

$$E_{1f} = E_{2f} = E_1 - Z_{1f}I_1 = E_2 - Z_{1f}I_2$$

Where:

E_1 and E_2 are positive- and negative- sequence voltage, respectively

I_1 and I_2 are positive- and negative- sequence current, respectively

From the above equation, it follows that:

$$\frac{E_1 - E_2}{I_1 - I_2} = Z_{1f}$$

The phase voltages at the relay location are given by:

$$E_b = a^2E_1 + aE_2 + E_0$$

$$E_c = aE_1 + a^2E_2 + E_0$$

Then,

$$(E_b - E_c) = (a^2 - a)(E_1 - E_2)$$

$$(I_b - I_c) = (a^2 - a)(I_1 - I_2)$$

Substitution and rearrangement of the equations lead to:

$$Z_{1f} = \frac{E_b - E_c}{I_b - I_c} = \frac{E_1 - E_2}{I_1 - I_2} \quad (4)$$

From Equation (4), it is shown that distance protections can calculate the positive-sequence impedance of BC fault by using the line-to-line voltage (BC) and the current difference between the faulted phases (IB - IC). Similar results can be obtained for the other phase-to-phase faults (i.e. AB and CA) if the appropriate voltages and currents are used.

The next multi-phases fault type is the double phase-to-ground (LLN) fault. The symmetrical component network of a BCG faults at the same fault location (F) can be seen in Figure 2.5.

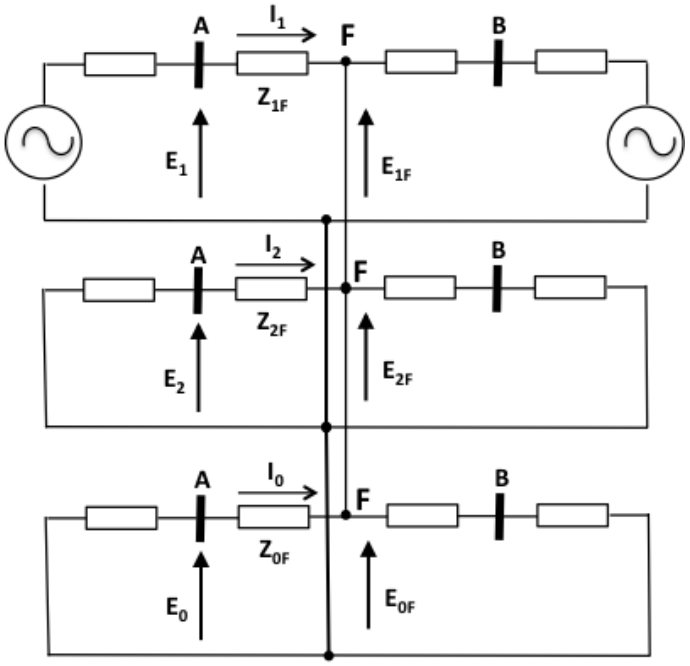

Figure 2.5 Symmetrical component network of BCG fault

The equations for positive- and negative-sequence components of double phase-to-ground faults are similar to the equations for phase-to-phase faults, except that they also have the zero-sequence component. Therefore, by using the line-to-line voltages and the current difference between the faulted phases as shown in Equation (4) before, the positive-sequence impedance of the double phase-to-ground fault can also be calculated.

The last multiple-phases fault type is the three-phase fault. The symmetrical component network for the three-phase faults is shown in Figure 2.6. It only consists of a positive-sequence network.

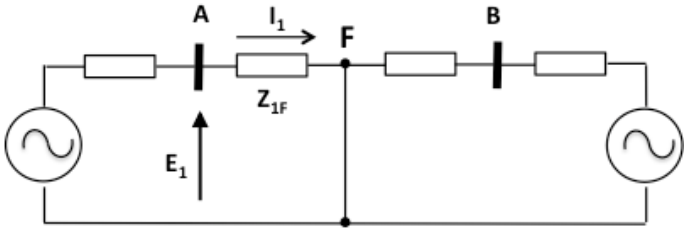

Figure 2.6 Symmetrical component network of ABC fault

The positive-sequence voltage for three-phase faults is given by the following equation:

$$E_1 = E_a = Z_{1f} I_1 = Z_{1f} I_a$$

Moreover, the negative- and the zero-sequence voltages and currents are zero:

$$E_2 = E_0 = 0$$

$$I_2 = I_0 = 0$$

Based on the network configurations, the positive-sequence impedance for three-phase faults can be calculated using the following equations:

$$Z_{1f} = \frac{E_a - E_b}{I_a - I_b} = \frac{E_b - E_c}{I_b - I_c} = \frac{E_c - E_a}{I_c - I_a} \quad (5)$$

The differences of the phase voltages and the phase currents, as shown in Equation (5), are called *the delta voltages and currents*. Similar with the phase-to-phase and double phase-to-ground faults, the positive-sequence impedance of three-phase faults can also be calculated using the line-to-line voltages and the current difference of the faulted phases.

It can be seen that by using three complements of the delta voltages (V_{AB}, V_{BC}, and V_{CA}) and the delta currents (I_A-I_B, I_B-I_C, and I_C-I_A), the distance protection is able to detect the positive-sequence impedance of all the multi-phases faults such as phase-to-phase, double phase-to-ground, and three-phase faults.

2.2.2 Single-phase faults

When a single-phase-to-ground fault (AG) occurs at location F (Figure 2.3), its symmetrical component network can be arranged as shown in Figure 2.7.

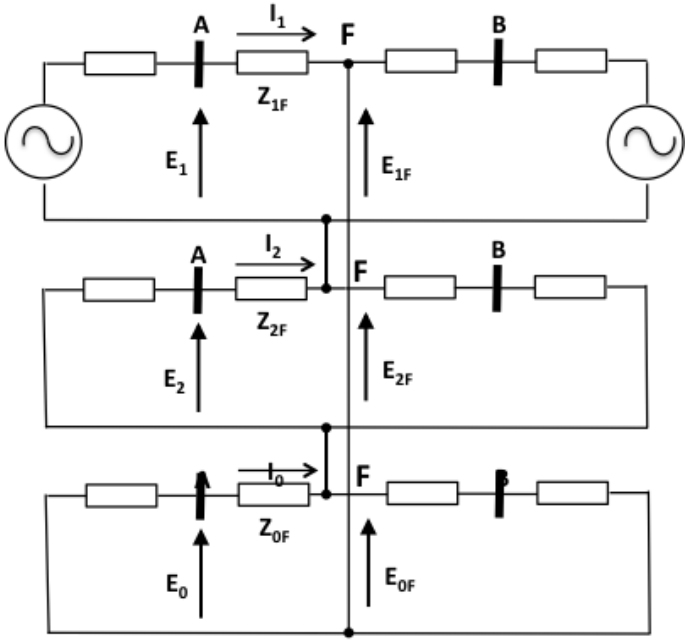

Figure 2.7 Symmetrical component network of AG fault

The positive-, negative-, and zero-sequence voltages for single phase-to-ground faults are given by the following equations:

$$E_{1f} = E_1 - Z_{1f} I_1$$

$$E_{2f} = E_2 - Z_{2f} I_2$$

$$E_{0f} = E_0 - Z_{0f} I_0$$

The phase A voltages and currents can be presented in terms of the symmetrical components:

$$E_{af} = E_{0f} + E_{1f} + E_{2f}$$

$$E_{af} = (E_0 + E_1 + E_2) - Z_{1f}(I_1 + I_2) - Z_{0f}I_0 = 0$$

$$E_a - Z_{1f}I_a - (Z_{0f} - Z_{1f})I_0 = 0$$

With,

$$I_a = I_0 + I_1 + I_2$$

Therefore, the positive-sequence impedance of the fault can be calculated using the equation:

$$Z_{1f} = \frac{E_a}{I_a + mI_0} \tag{6}$$

Where m is the compensating factor as given by the following equation:

$$m = \frac{Z_0 - Z_1}{Z_1} I_0 \tag{7}$$

From Equation 6, it is shown that the positive-sequence impedance of single-phase-to-ground faults can be calculated by dividing the faulted phase voltage with a compensated fault current. For AG faults, the phase A voltage is divided by Phase A current plus the compensation factor (mI_0). Using the same principle for the other faulted phases, distance protection is able to calculate the positive-sequence impedance of all single phase-to-ground faults using the voltages and the currents in all three phases (A, B, and C).

From the explanations of the multiple-phases faults and the single-phase faults, it is shown that, in order to provide complete protection against all short-circuit faults in the transmission network, the distance protection needs to have six impedance measurement elements.

2.3 Numerical distance protection

A numerical distance protection consists of several function blocks that are arranged to detect abnormal conditions in power system. The simplified function block of numerical distance protections is shown in Figure 2.8.

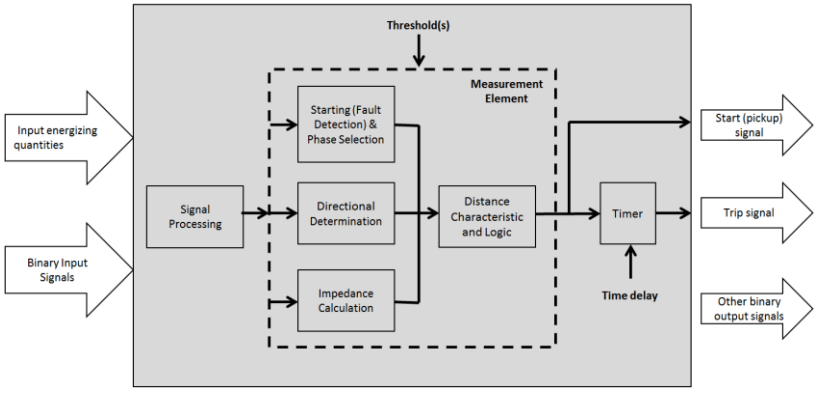

Figure 2.8 Simplified distance function blocks [1]

Numerical distance protections have two input signals. First, the *input energizing quantities* that consist of three voltages and three currents signal obtained from the voltage transformer (VT) and current transformer (CT), respectively. Second, *the binary input signal* that is usually

delivered from the other protection schemes such as circuit breaker status or permissive signals from the other relays.

The signal-processing block is used to filter noise from the analog input signals and then convert the signals into digital information containing the voltage and current phasor. The voltage and current phasor are then delivered to the measurement element blocks. Measurement element consists of four function blocks: (1) *the starting and phase selection block* is used to detect fault conditions in power system and to determine which phases are experiencing the short circuit. (2) *the directional determination block* provides the fault direction as seen by the distance protection. (3) *the impedance calculation block,* which calculates the apparent impedance of power system using voltage and current at the relay location. By measuring the fault impedance, distance protection can determine if the fault is located inside the protection zone or not. (4) *the distance characteristic and logic block* provides the decision if the relay must operate or not based on the information retrieved from the previous function blocks.

When the threshold values (such as protection characteristics and settings) are applied to the distance protection, it is expected that the distance protection will extract the fundamental frequency component of voltages and currents from the input energizing quantities, calculating the impedance of the fault, comparing the impedance value with the applied setting, and then operate if the fault occurs inside its protection characteristic. However, in the real power system, the voltages and currents during faults contain transient signals in the form of dc component, harmonics, and sub-harmonics. The transient signals could affect the operation of numerical protection type by delaying the operating time or introducing an error the measured impedance. To explain how the operation of numerical distance protection is affected by the transient signals, the basic processes and data flow inside the relay is shown in Figure 2.9.

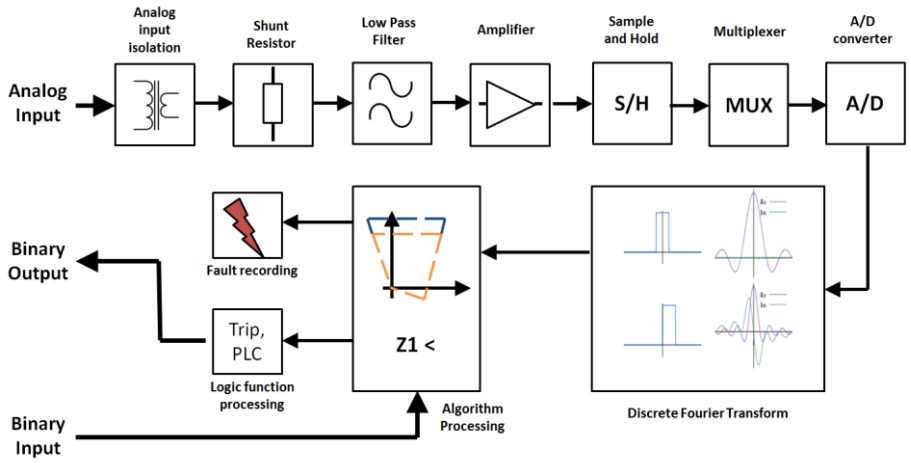

Figure 2.9 Signals and data flow inside numerical distance relay

The analog input signals containing voltages and currents at the relay location are processed inside several function blocks before they can be used in the algorithm processing. First, the voltages and currents are fed into an analog input isolation. The analog input isolation consists of step-down transformers that are used to lower the voltage and current to an acceptable level for the relays. This block also serves as an electrical isolation between the relay and the power system. Next, the current signals are passed through shunt resistors in order to convert them into voltage signals. This is because the analog-to-digital (A/D) converter can process only voltage signals.

A low-pass filter is used to provide anti-aliasing filtering of the signals. Aliasing is a phenomenon when the high-frequency components of a signal can appear to belong to the

fundamental frequency during the digital processing. It can affect the measurement accuracy of the relay. Low-pass filter passes the fundamental frequency component and blocks out all the remaining high-frequency components of the signal. The most common filter type used in numerical protection is the Butterworth type. Butterworth filter has the flattest amplitude response characteristic in the low-frequency ranges.

The amplitude response |H(ω)| of a Nth order of Butterworth is given by the following equation:

$$H(\omega) = \frac{1}{\sqrt{1 + (\omega/\omega_0)^{2N}}}$$

Where,
N is the order of the filter
ω_0 is the cut-off frequency of the filter

The order of low-pass filters determines the output signal quality. Higher order filters provide better filtering of the high-frequency components. However, higher order filter also means more computation and time are needed to process the signals. Hence, more operation time delays are introduced to the relays.

The sample-and-hold (S/H) and the analog-to-digital (A/D) converter operate together to sample the voltage signals at a specific time intervals and then convert them into digital information. The sampling process is crucial for the operation of distance protection as the digital information must represent the appropriate analog signals at the instant of sampling. Modern numerical distance protections have a fixed sampling rate that is a multiple of the fundamental-frequency, typically 12 - 20 samples per cycle.

After being digitalized, the sampled signals containing power system information are processed further using a digital filter. Digital filter aims to extract phasor information from the voltage and current signals to be processed further by the algorithm processing block. Many types of the digital filter have been developed for numerical protection application, including the Discrete Fourier Transform (DFT), the Least Squares Algorithm, and the Cosine Algorithm. In this section, the DFT algorithm will be explained as it is the most widely used digital filter in protection relays.

Discrete Fourier Transform (DFT) is a variation of Fourier analysis, which decomposes time-domain signals (f(t)) into frequency domain signals (f(jω)). Unlike the Fourier analysis that has continuous time duration from -∞ to +∞, the DFT analyse the signals for a small time window. The DFT can be explained using the following example:

A voltage signal in the time domain can be expressed as

$$v(t) = V_{max}\cos(\omega t + \theta)$$

The voltage is sampled N times per cycle and can be represented by Vk, where k = 0 - (N-1). The DFT processes each of the sampled value by multiplying it with the sine and the cosine coefficients.

The phasor of the voltage can be defined using the following equation:

$$V_h = \frac{2}{N}\sum_{k=0}^{N-1} v_k e^{-jn\frac{2\pi h}{N}} \quad (8)$$

Where:

V = Voltage phasor
N = number of samples in one data window
h = order of harmonics
v = Instantaneous value of voltage
k = nth sample in the data window

With the real and imaginary parts are given by the following equations:

$$V_{real} = \frac{2}{N}\sum_{k=0}^{N-1} v_k cos\left(\frac{2\pi kh}{N}\right) \quad (9)$$

$$V_{imag} = \frac{2}{N}\sum_{k=0}^{N-1} v_k sin\left(\frac{2\pi kh}{N}\right) \quad (10)$$

The magnitude and phase angle are then shown in Equations (11) and (12).

$$V_{mag} = \sqrt{{V_{real}}^2 + {V_{imag}}^2} \quad (11)$$

$$V_{angle} = \arctan\frac{V_{imag}}{V_{real}} \quad (12)$$

The DFT is capable of transforming a sinusoidal voltage signal to a phasor form. The phasor can be presented either in real and imaginary components or magnitude and phase angle components. The phasor of fundamental frequency components is obtained by setting the value of *h* to 1. The operation of distance protection heavily depends on the performance of the digital filter. During fault conditions, when the voltage and current signals are heavily polluted with noise, the digital filter needs to extract the correct fundamental frequency components from these signals so that the relay can calculate the correct fault impedance.

The transient response of numerical distance protection

When a fault occurs in a transmission line, the system voltages and currents abruptly change from normal state to the faulty state through a transient. The estimated impedances during transient are fluctuated and produce a trajectory that moves from the outside of protection zone into the protection zone. If the fundamental frequency components are extracted correctly from the transient signals, the impedance will stabilize after one sampling window. A typical fault impedance trajectory during the transient period, using a ten-sample DFT is shown in Figure 2.10. In each of the sampling step, the impedance values are calculated using the extracted fundamental frequency of voltages and currents.

It can be seen that fault impedance trajectory encroaches the protection zone at some point and excursion alternatively inside and outside the zone until it converges to a fixed value. During this period, it is essential for distance protections to measure the correct impedance values and to provide the appropriate operation criteria.

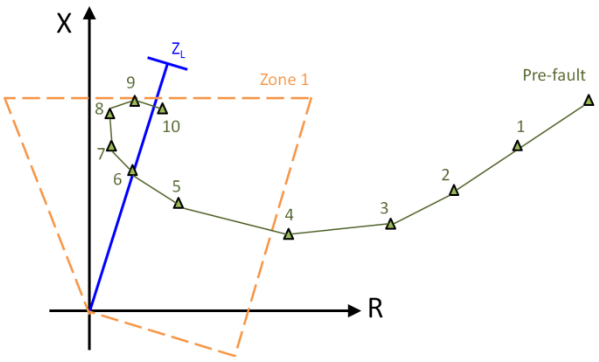

Figure 2.10 Fault impedance trajectory

The performance of distance relays during transients is a random nature. The operating time and the reach accuracy depend on the signal-processing techniques and the numerical algorithms utilized in the protection design. Moreover, the different shapes of transient waveform caused by dc-offsets, harmonics, and other components added more to the operation randomness. Hence, it is necessary to perform a large number of repetitive tests with different transient parameters to verify the operation of numerical distance protection under this condition.

2.4 The IEC 60255-121 standard

The IEC 60255-121 standard [1] specifies the minimum requirements for functional and performance evaluation of distance protections. The standard describes different tests to be performed and how to compare the test results of relays from different manufacturers. The IEC 60255-121 replaces the older standard IEC 60255-16: Impedance measuring relays.

Distance protection testing according to IEC 60255-121 can be divided into two parts: the accuracy test and the dynamic performance test. The accuracy test aims to measure the accuracy of the characteristic shape under steady state conditions, while the dynamic performance test seeks to evaluate the operational performance under simulated transient conditions. As the accuracy test can be easily performed using the steady state test available in relay injection kit, this thesis will only focus on the dynamic performance test of distance protection.

2.4.1 Dynamic performance tests

The dynamic performance of a distance protection represents the response of function blocks used in the relay to a disturbance condition such as short circuit fault. The IEC 60255-121 defines various benchmark networks that can be used to represent disturbance conditions in power system. The benchmark networks consist of three different configurations: (1) the single-feed transmission networks, (2) the double in-feed transmission networks, and (3) the parallel transmission networks. Figure 2.11 shows the parallel transmission network according to the standard.

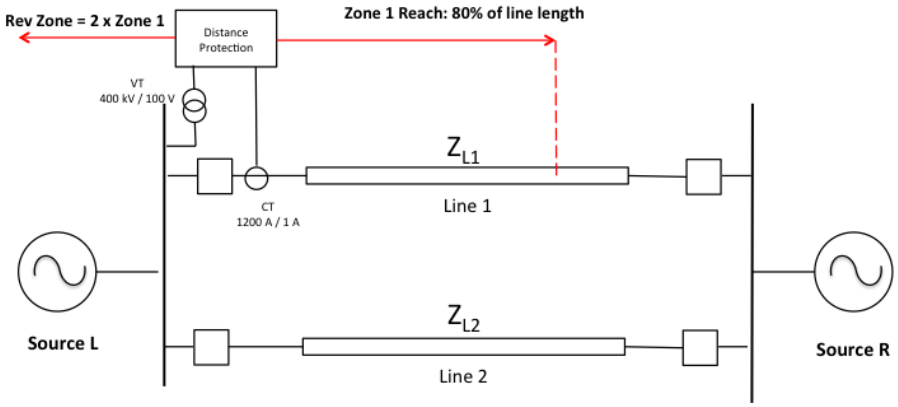

Figure 2.11 Parallel transmission network [1]

IEC 60255-121 standard defines various dynamic conditions that need to be simulated in a transient network simulator. The simulations are performed to check the operational perfomance of distance relay taking into account the following conditions:

- Effect of the decaying dc-offset
- Effect of the CVT transient
- Effect of the superimposed harmonics
- Effect of the frequency deviations
- Effect of the fault resistance with pre-fault load
- Effect of the evolving and the cross-country fault
- Effect of the current reversal condition

The dynamic performance of distance protection is defined in terms of the operating time and the reach accuracy. The operating time is defined as the time interval between the instant when the fault occurs and the instant when the distance protection operates (trips). The reach accuracy means that the relay must not have an overreach or an underreach operation under all dynamic conditions. Overreach operation happens when the calculated impedance of the distance relay is *less* than the actual impedance to the fault. While underreach operation arises when the calculated impedance of distance relay is *greater* than the actual impedance to the fault. The test results need to be presented using the source impedance ratio (SIR) diagrams, where the operating time of the relay is displayed as a function of fault positions, fault types, and source impedance ratios.

2.4.2 Ways to perform the test

The dynamic performance test according to IEC 60255-121 can be carried out using various testing methods. The first method is known as the offline test. The offline test uses pre-calculated fault voltage and current to check the relay operation. With this approach, the benchmark networks are modeled in transient simulation software. Then the test cases are simulated in the software, and the voltage and current signals are calculated. The signals are then injected into distance protection using a relay test set. The second approach is the closed-loop test. With the closed-loop test, the simulations are performed in a real-time digital simulator, and the response of distance protection during short circuit is fed directly into the simulation. In this way, the circuit breaker can be simulated as in real life conditions.

In this thesis, the dynamic performance test is realized using the offline method. The power system networks are modeled and simulated in ATP-EMTP software, while the transient signal injection is performed using the Omicron secondary injection kit. The detail explanation of the test methodology will be presented in the next chapter.

3 Test Methodology

3.1 Introduction

A dynamic test is defined as a test method that applies steady state pre-fault conditions, followed by fault conditions (transient and steady state conditions) to the protection relay input terminals [1]. It means testing the protection relays under *"real"* simulated power system conditions. In this thesis, the dynamic test according to the IEC 60255-121 standard is implemented using the test procedure in Figure 3.1.

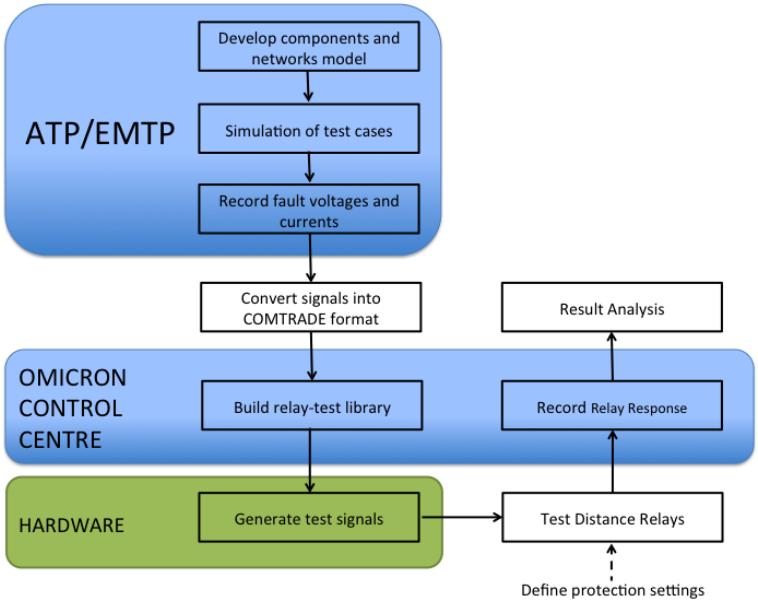

Figure 3.1 Dynamic test procedure

3.2 Transient simulation using ATP-EMTP

3.2.1 Developing the network and component models

The network and component models are developed based on the benchmark network of IEC 60255-121 standard. Three network configurations are defined, including single feed transmission lines (short and long), double in-feed lines, and parallel transmission lines. The transient effects of capacitive voltage transformer (CVT) are also simulated according to the standard. In addition, fault arc model developed by [10] is incorporated into the network to study the operation of numerical distance protection to arcing faults.

In this thesis, the modeling and simulation are carried out in ATP-EMTP [16]. Some considerations when performing transient simulations in ATP-EMTP are:

1. The size and type of the models
   The reduced-size models are typically used to minimize the computation process and time. It is crucial that the models can represent the power system sufficiently. The component models such as generator, transmission lines, CT, and CVT need to be modeled in such a way that they can represent similar transient response with the real

ones. Therefore, the selection of the model must be carefully made to get the accurate results.

2. Time step used in the simulation
   The simulation time steps can also affect the accuracy. Too large time steps will result in the insufficient transient information in the waveform, while too small time steps will increase the computation processes and the data sizes.

3.2.2 Simulating the test cases

The simulation of the test cases aims to explain how the dynamic conditions affect the operation of distance protection. Various dynamic conditions are simulated in this thesis, including:

- The effect of decaying dc-offset and source impedance ratio (SIR) to the tripping time and the reach accuracy of distance protection.
- The effect of CVT transient error to the tripping time and the reach accuracy of distance protection.
- The operation of distance protection when harmonics are superimposed on the voltage and current signals.
- The operation of distance protection during off-nominal frequency condition.
- The effect of fault resistance and remote in-feed current to the operating time and the reach accuracy of distance protection.
- The operation of distance protection against disturbance conditions that might occur in a parallel network configuration, such as:
  - Current reversal
  - Evolving faults
  - Cross-country faults
- The operation of distance protection during arcing faults.

3.2.3 Recording the voltages and currents

For each of the simulation case, the secondary value of voltages and currents at the relay location will be stored. The calculated values are stored using the XY-Plot of ATP-EMTP. Various file formats can be used to store the calculated values as shown in Figure 3.1. In this thesis, the PL4 format is used.

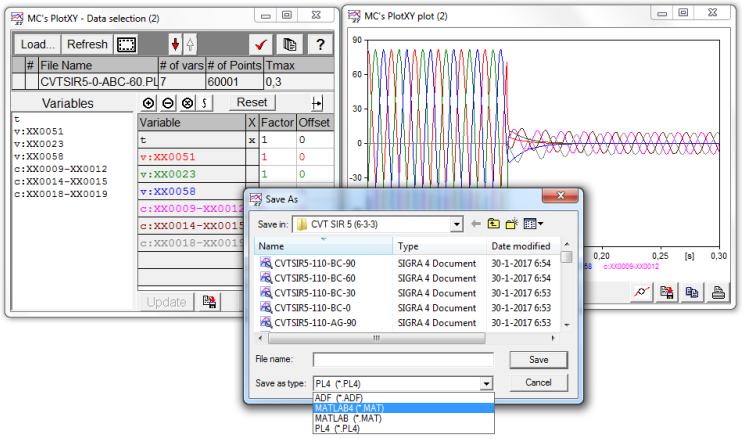

Figure 3.2 Record calculated voltage and current

3.3 Converting the signals to Comtrade format

COMTRADE (Common format for transient data exchange for power system) is a standardized file format from IEEE for recording analog and digital data related to transient conditions in the power system. The PL4 files containing voltage and current signals from ATP-EMTP are converted into COMTRADE format using the *advanced transplay* module of Omicron test universe. When converting the files, the ratio of the CT and VT needs to be defined correctly based on the simulated benchmark networks.

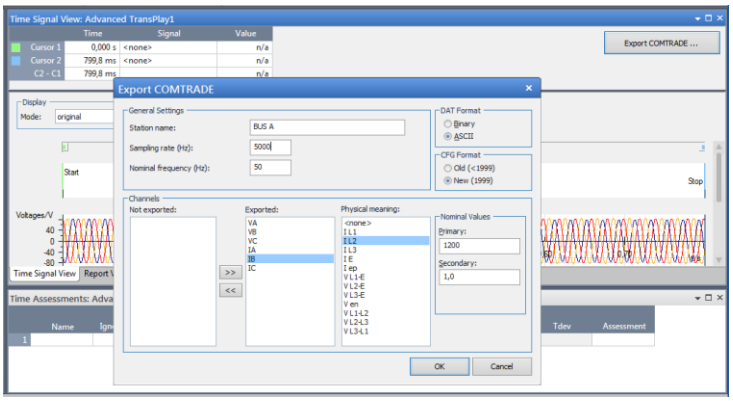

Figure 3.3 Convert signals into COMTRADE format

3.4 Developing the test library

The test library/database contains voltage and current signal at the relay location. In this thesis, Omicron Control Centre (OCC) is used to build the test library. Omicron Control Centre is a software package from OMICRON that allows the combination of individual testing functions into an overall test plan. For each defined test case, a separate test library will be built. When performing a test, each embedded function in OCC will be executed sequentially, and all test results will be created automatically. The library of analog signals and the operating time of the relay will be stored inside the OCC files after the test are carried out. For each test case, the voltage and current signals will be injected into the relay four times.

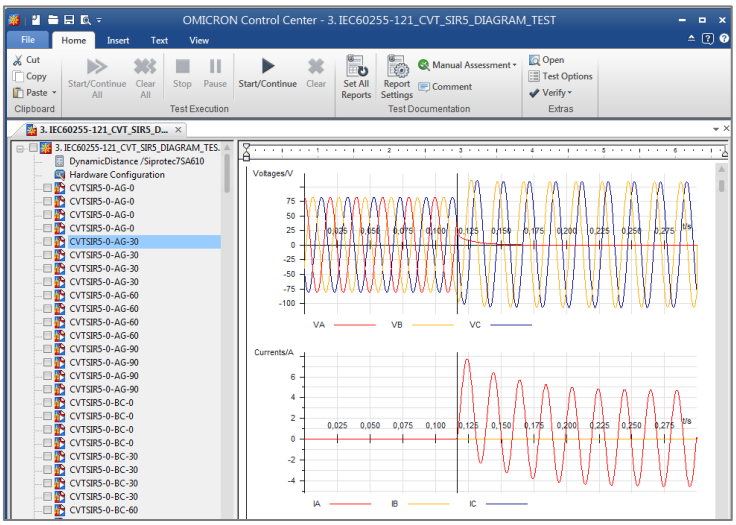

Figure 3.4 Relay test library in Omicron Control Centre

3.5 Developing the hardware setup

3.5.1 Generating the test signals

The Omicron CMC 356 is used to generate transient signals and inject them into the relay. The injected signals should have a sufficient accuracy and resolution to ensure that the relay will measure the voltages and currents similar to the one that occurs in the real power system. The Omicron CMC 356 provides possibilities for an accurate dynamic testing because of its wide ranging dynamic performance.

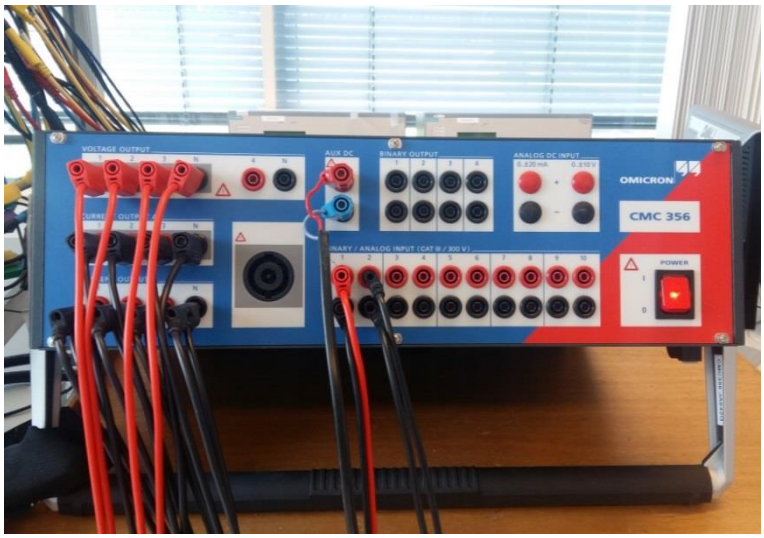

Figure 3.5 Omicron CMC 365 relay test set

The technical parameters of CMC 356 are displayed in Table 3.1.

Table 3.1 CMC 365 technical parameters

Parameters	Typical value
3 phase current output	3 x 0…64 A
3 phase voltage output	3 x 0…300 V
Current resolution	1 mA
Voltage resolution	5 mV
Phase Angle resolution	0.001º
Error	<0.05%
Range transient signals	DC…3.1 kHz

The schematic connection between Omicron CMC 356 and the tested relay is displayed in Figure 3.7. The hardware connection consists of two three-phase analog signals (voltage and current) and two binary signals (trip and pick-up).

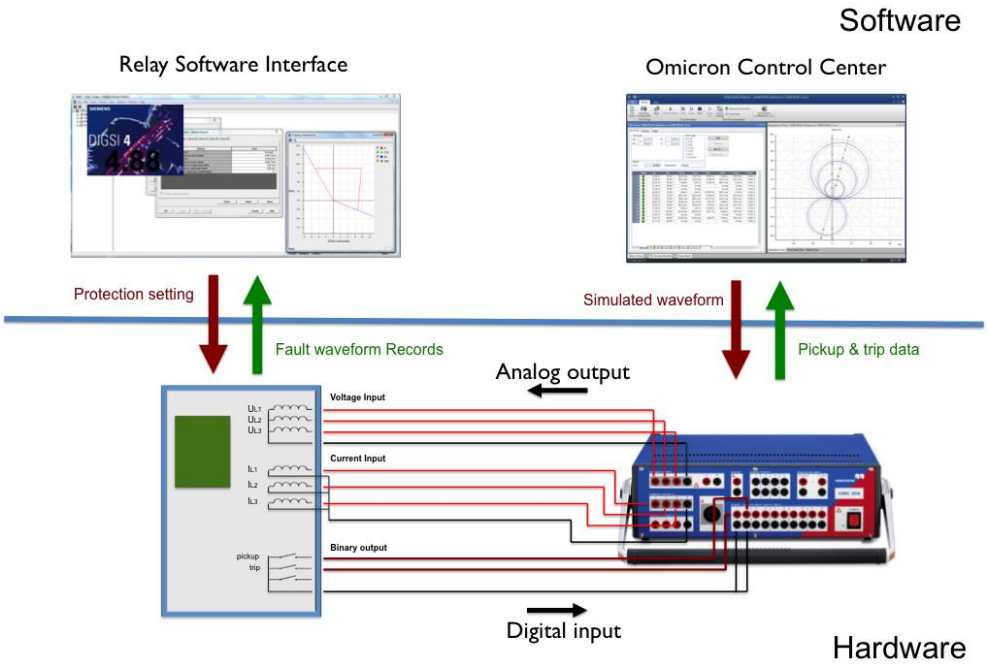

Figure 3.6 Schematic connection

3.5.2 Tested distance relay

Two distance relays from different manufacturers (relay M and relay N) are tested. These relays are multifunctional numerical distance relays utilized for high voltage (HV) and extra high voltage (EHV) transmission line protection. Detailed explanation about the tested distance relays and the protection settings applied in the testing will be given in Chapter 5.

3.5.3 Protection setting

The operation characteristics of the forward and reverse zones are tested. Zone 1 is set to protect the forward direction with no time delay (instantaneous), while Zone 3 is set to protect the reverse zone with a time delay. Moreover, the zone 2 setting is deactivated. The impedance reach setting of zone 1 is 80% of the transmission line length [1]. A summary of the impedance reach setting is given in Table 3.2, while the detail calculations are provided in Appendix I.

Table 3.2 Distance protection setting

	Short Network (20 km)	**Long Network (100 km)**	**Transient Oscillation (125 km)**	**Parallel Network (2 x 100 km)**
Zone 1	**Forward**	**Forward**	**Forward**	**Forward**
Characteristic	**Quadrilateral**	**Quadrilateral**	**Quadrilateral**	**Quadrilateral**
R ph-ph (ohm)	1.8	6.981	15.709	6.981
R ph-e (ohm)	2.699	6.981	15.709	6.981
X (ohm)	1.745	8.726	19.636	8.726
Characteristic Angle (o)	85	85	85	85
Time Delay (ms)	0	0	0	0
Zone 2	**Inactive**	**Inactive**	**Inactive**	**Inactive**
Zone 3	**Inactive**	**Inactive**	**Inactive**	**Reverse**
Characteristic	-	-	-	Quadrilateral
R ph-ph (ohm)	-	-	-	13.96224
R ph-e (ohm)	-	-	-	13.96224

X (ohm)	-	-	-	17.4528
Characteristic Angle (o)	-	-	-	85
Time Delay (ms)	-	-	-	500

3.6 Result analysis

The results of dynamic testing will be presented using the source impedance ratio (SIR) diagram [1]. SIR diagram shows the average operating time of distance relay as a function of the fault position and the source impedance ratio. Results analysis will also be performed using the impedance diagram where the trajectory of fault impedance will be displayed on an R-X plane with zone protection setting as shown in Figure 3.7.

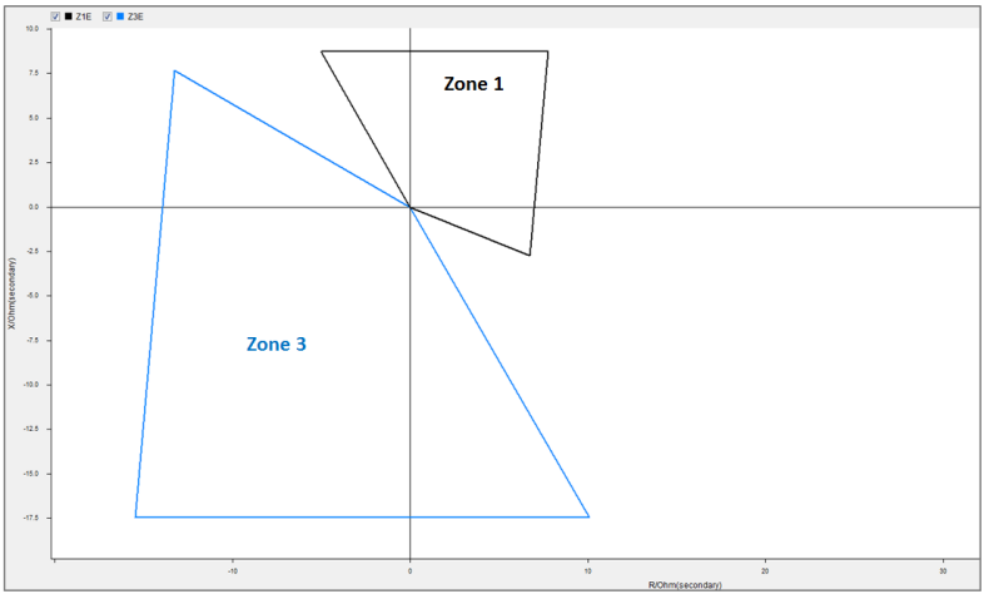

Figure 3.7 Protection setting shape in impedance plane

4 Simulation of the Dynamic Conditions

Various dynamic conditions are simulated according to the IEC 60255-121 standard to represent the disturbance conditions that might occur in power system. It is necessary to study the characteristics of various dynamic conditions to have an idea about their effect on the operations of distance protection. The dynamic conditions are simulated through variation of fault parameters and network configurations. Seven dynamic conditions with total 890 test cases are simulated. A detailed explanation for all the test cases is given in this chapter.

For each simulation case, the voltage and the current (both in secondary value) at the distance relay location will be calculated and stored.

4.1 Simulation with the decaying dc-offset

4.1.1 Introduction

The magnitude of decaying dc-offset in fault current is determined by the instant of fault occurrence (or the fault inception angle). Fault inception angle is the angle, on a fundamental frequency sine wave between the inception of the fault and the nearest preceding zero crossing with a positive derivative [1]. The relation between fault inception angle and decaying dc-offset in fault current can be explained using a simple switching of LR circuit as shown in Figure 4.1.

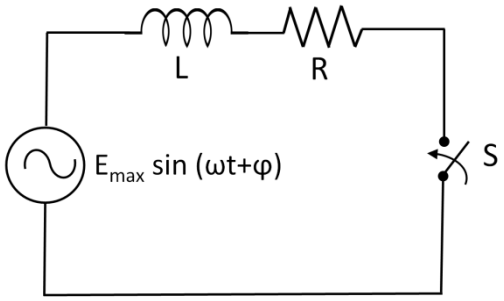

Figure 4.1 switching of an LR circuit

The current flowing in the circuit after the switch S closed is given by the following equation [12]:

$$i(t) = e^{-(R/L)t}\left\{-\frac{E_{max}}{\sqrt{R^2+\omega^2L^2}}sin\left[\varphi - tan^{-1}\left(\frac{\omega L}{R}\right)\right]\right\} + \frac{E_{max}}{\sqrt{R^2+\omega^2L^2}}sin\left[\omega\varphi - tan^{-1}\left(\frac{\omega L}{R}\right)\right] \quad (13)$$

From the equation, it can be seen that the current in the circuit consists of two parts. The first part of the equation represents the decaying dc-component, and the second part is the sinusoidal component with the frequency $(\omega/2\pi)$ Hz.

The decaying constant of dc component depends on the instant when the switch S closed and the ratio between R and L of the circuit. When the term $\left[\varphi - tan^{-1}\left(\frac{\omega L}{R}\right)\right] = 0°$ or an integer

times of π, the dc-component is zero, while when the term $\left[\varphi - tan^{-1}\left(\frac{\omega L}{R}\right)\right] = 90°$, the dc-component has the highest magnitude. Figure 4.2 shows the decaying dc-component for a three-phase fault.

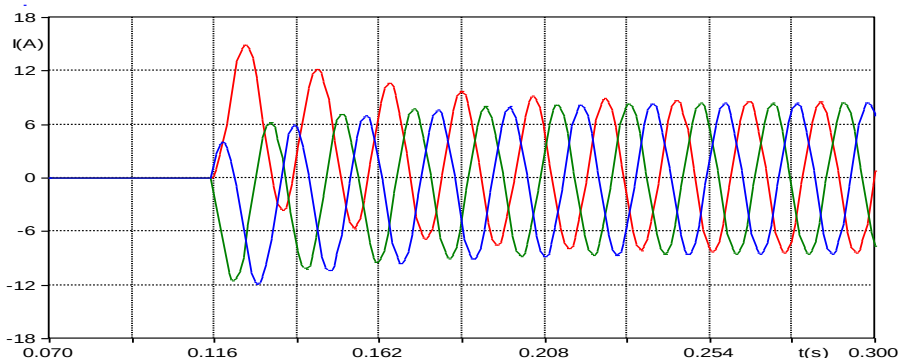

Figure 4.2 dc offset in fault current

To analyze the characteristic of the dc-offset, various faults with different inception angle are simulated. Four inception angles are used: 0°, 30°, 60°, and 90°. Two transmission networks from the IEC 60255-121 standard are applied in the simulation. The first network is a short transmission line with a length of 20 km. The second network is a long transmission network with a length of 100 km.

Both networks are radial feeder types with zero load transfer as shown in Figure 4.3. The current transformer (CT) and voltage transformer (VT) are considered as ideal transformers. Furthermore, the transmission line capacitances are not considered in the simulation.

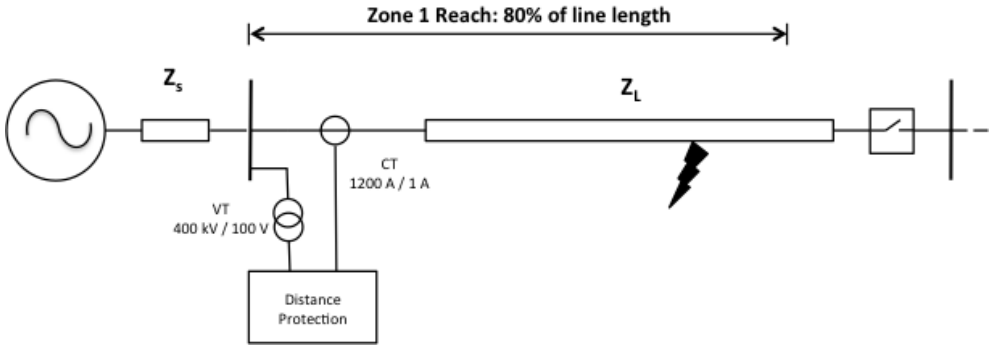

Figure 4.3 Transmission network with zero load transfer

Four fault types are also simulated. The fault types are single phase-to-ground (LN), phase-to-phase (LL), double phase-to-ground (LLN) and three-phase fault (LLL). Several fault positions as shown in Table 4 are also simulated. Fault positions are defined in the percentage of zone-1 reach impedance setting. Total 224 fault cases are simulated.

Table 4.1 Fault parameters of simulation with decaying dc-offset

Network length	Fault position (Percentage of zone 1 setting)	Fault type	Fault inception angle (°)
Short (20 km)	0, 50, 80, 90, 95, 105, and 110	AG, BC, BCG, and ABC	0, 30, 60, and 90
Long (100 km)	0, 50, 80, 90, 95, 105, and 110	AG, BC, BCG, and ABC	0, 30, 60, and 90

In practice, the operation of distance protection is not only affected by the fault parameters. However, it also influenced by the magnitude of the voltage measured at the relay location. During short circuit conditions, the voltage magnitude depends on the short circuit level of the system and the total impedance between the measurement transformers and the faulted point. The relation between the measured voltage at the relay location with the total impedance of the system can be explained in terms of source impedance ratio (SIR). Source impedance ratio is defined as the ratio between the impedance of power source and the impedance setting of distance protection as displayed in Figure 4.4.

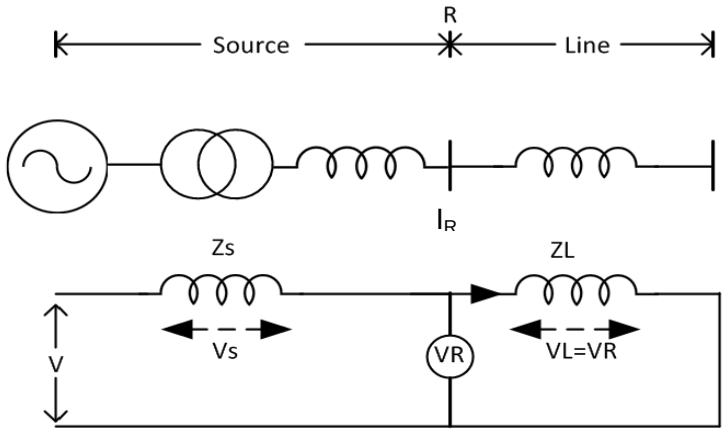

Figure 4.4 SIR effect on residual voltage measured by distance relay

Point R is the relay location, with the measured voltage (V_R) and current (I_R). Z_L and Z_s are the transmission line impedance and the source impedance, respectively. The measured voltage at the relay location (V_R) can be described as a function of the source impedance ratio ($\frac{Z_s}{Z_L}$) using the following equations:

$$V_R = I_R \cdot Z_L$$

Where,

$$I_R = \frac{V}{(Z_s + Z_L)}$$

Hence,

$$V_R = \frac{1}{\frac{Z_s}{Z_L} + 1} \cdot V \qquad (14)$$

Table 4.2 provides the voltages at the relay location for a range of source impedance ratios. As the source impedance ratio increases, the voltage measured by relay drops to very low values. The magnitude of the transient, in turn, remains constant as the dc offset in fault signal is a function of fault inception angle (independent from the source impedance ratio). This results in a disadvantageous transient to fundamental-frequency ratios that affect both the reach accuracy and the operating time of distance protections.

Table 4.2 measured voltage as function of source impedance ratio

Source impedance ratio	0.1	0.5	1	5	10	50
Measured voltage (pu)	0.91	0.67	0.5	0.17	0.09	0.02

In the simulation, two SIR values are applied for each network. For the short network, the SIR values used are 5 and 50. While for the long network, the SIR values are 0.2 and 10. Therefore, the total simulation cases with the decaying dc-offset are 448 cases.

4.1.2 The networks and component model

Power source

Two power source models can be used for protection relay studies: the ideal sources behind sub-transient reactance model and the detailed synchronous machine model. An ideal source model is used to represent big generators in an integrated system where the disturbance will not cause a significant frequency deviation. The detailed synchronous machine model is used for representing weak generators in an un-integrated system. In this thesis, the ideal source behind sub-transient reactance model will be used.

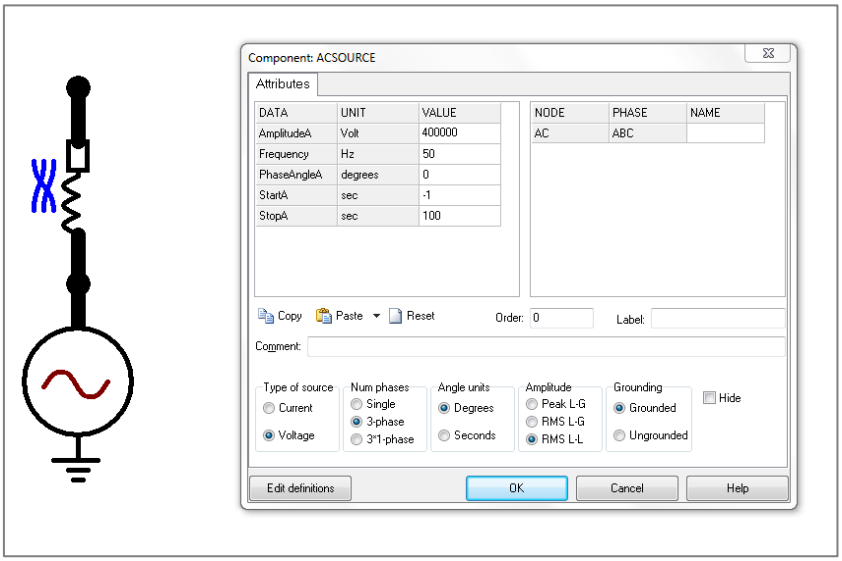

Figure 4.5 Power source model

The value of the sub-transient reactance of the model is varied to obtain the desired source impedance ratio as shown in Figure 4.5.

Transmission line

The transmission line defined in the standard has fixed and homogenous impedances over the frequency range as shown in Table 4.3. Moreover, the conductance (G) and capacitance (C) of the line are neglected.

Table 4.3 Network impedance values

	R_1	X_1	R_2	X_2	R_0	X_0
Values (Ω/km)	0.03184	j 0.3636	0.03184	j 0.3636	0.1274	j 1.4552

ATP-EMTP provides three transmission line models: *nominal pi, constant parameter distributed line,* and *frequency-dependent distributed line*. These models can be built using the LCC routine. The Frequency-dependent distributed parameter model is known to be the best model for electromagnetic transient simulations because of its wider frequency response compared to the other models. However, this model cannot represent the characteristic

described in the benchmark network because of the varying impedance values over various frequency ranges.

To accurately represent the benchmark network, the nominal Pi model given in Figure 4.6 is used. This model provides a more accurate network representation because it allows inputting the impedance parameter directly. This results in more accurate impedance values compared to the frequency-dependent models where the impedances are calculated based on the physical transmission parameters. Nominal Pi model can also be used to represent transmission line response over various frequency ranges if several cascaded sections are used in the simulation [4].

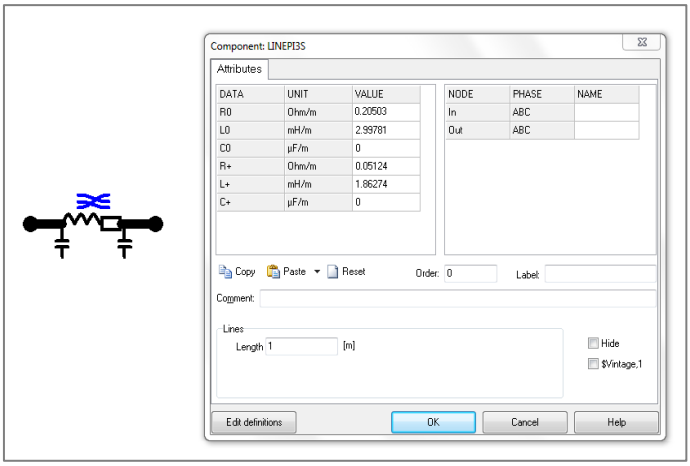

Figure 4.6 Transmission line model

Current and voltage transformers

The current transformer (CT) is considered as an ideal transformer, meaning that all the primary currents are transformed exactly to the secondary side without any errors. An ideal CT model assumes that there is no reluctance in the magnetic core and there is also no flux leakage in the circuit. The basic equation for an ideal CT is given by the following equation:

$$\frac{i_s}{i_p} = \frac{N_p}{N_s} = n \tag{15}$$

Where,
I_p is the primary current
I_s is the secondary current
n is the current transformer ratio

A CT model in ATP-EMTP is realized using the ideal transformer (TRAFO_I) and the linear component (RLC) as displayed in Figure 4.7. The ratio of the CT is 1200/1 A.

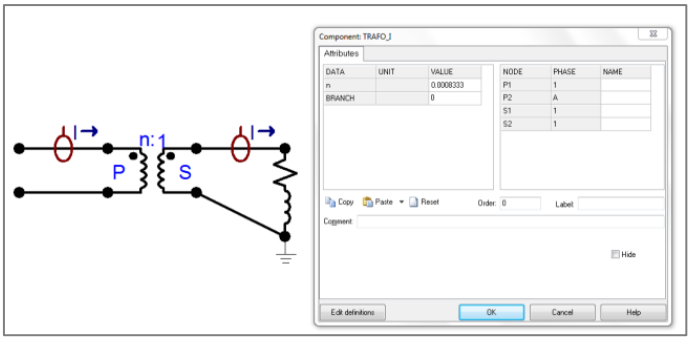

Figure 4.7 current transformer model

Similar to the CT model, the voltage transformer (VT) used in the network is also considered as an ideal transformer. The VT ratio is 400 kV / 100 V. Basic equation for an ideal VT is given by the following equation:

$$\frac{V_p}{V_s} = \frac{N_p}{N_s} = n \tag{16}$$

Where,
V_p is the primary voltage
V_s is the secondary current
n is the voltage transformer ratio

The VT model in ATP-EMTP is developed using the ideal transformer (TRAFO_I) and the linear component (RLC) as shown in Figure 4.8.

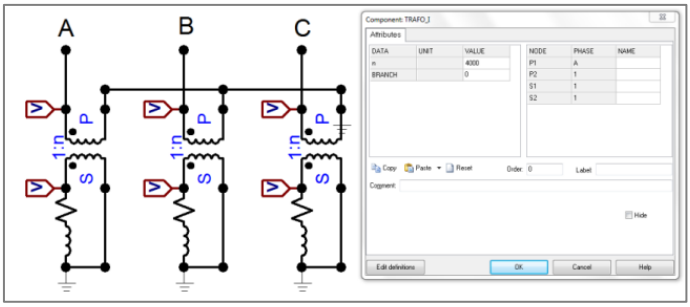

Figure 4.8 Three-phase voltage transformer model

Circuit Breaker

There are three switch models available in ATP-EMTP: time controlled switch, statistics switch, and TACS. To model the three-phase circuit breaker (CB), the time controlled switch (SWIT_3XT) is used in this thesis as shown in Figure 4.9.

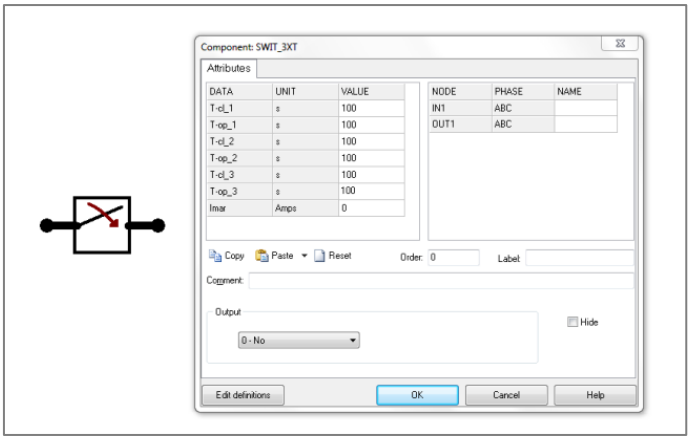

Figure 4.9 Three-phase circuit breaker model

Fault model

The faults are modeled using the time-controlled single-phase switches. There are four fault types utilized in the test cases as shown in Figure 4.10.

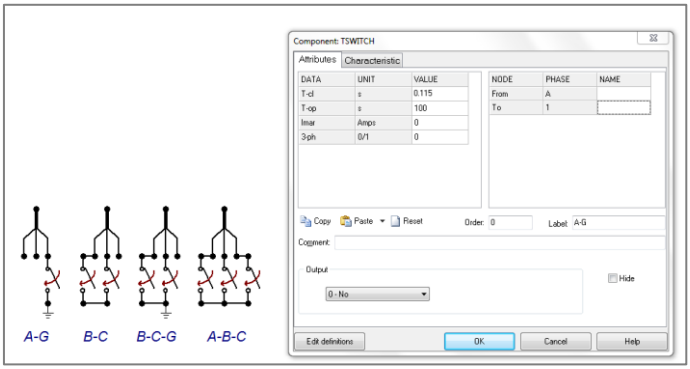

Figure 4.10 Faults model

The closing time of the switches is controlled to obtain the desired fault inception angles. The voltage waveforms of four different inception angles are shown in Figure 4.11.

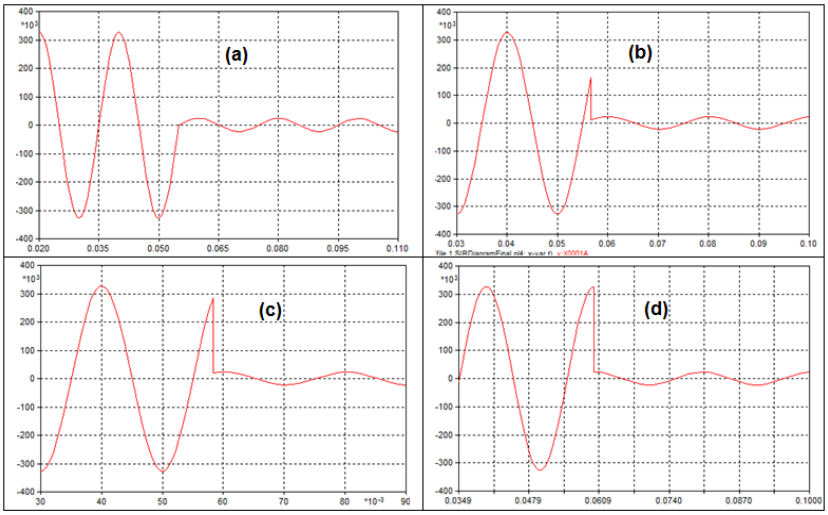

Figure 4.11 Voltages for various fault inception angles: (a) 0°, (b) 30°, (c) 60°, and (d) 90°

The power system components are modeled with reference to [4]. Finally, the benchmark network model in ATP-EMTP is shown in Figure 4.12.

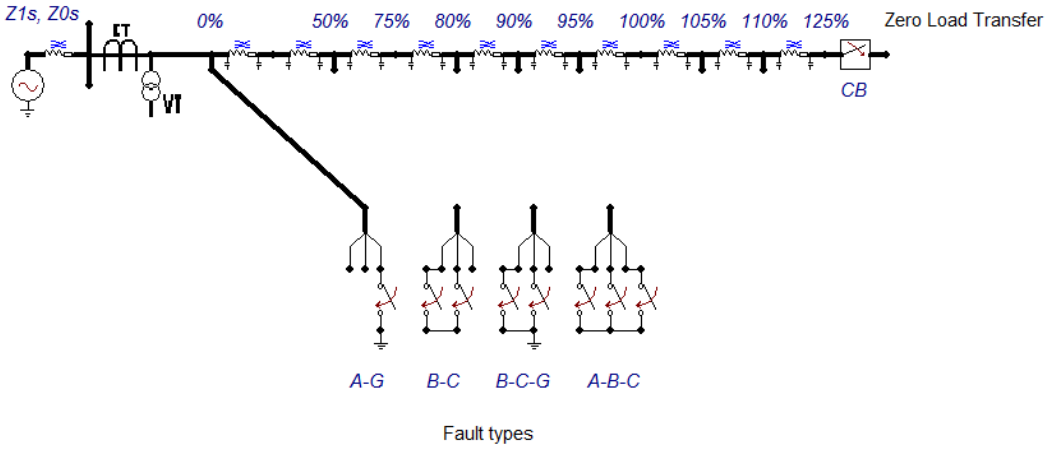

Figure 4.12 Short transmission network model

4.1.3 Analysis of the simulation result

This section describes the simulation results of ATP-EMTP. For each case, the total simulation time is 300 ms, with pre-fault duration around 100 ms, and the solution time step 5 µs.

Varying the fault inception angle

The simulated fault currents (secondary value) for an AG fault with different fault inception angles are shown in Figure 4.13. The faults are located at 50% of the zone 1 impedance setting. The results indicate that when the faults occur at around 100 ms, the current in phase A jumps from zero to its peak values and then decreases gradually until it reaches the nominal fault current.

The peak of the current varies with the fault inception angle. In this case, the fault inception angle 0° generates the highest peak of 7.47 A. While the other inception angles produce a relatively lower peak currents (30° = 7.02 A; 60° = 5.73 A; 90 ° = 4.47 A). It is also shown that the decaying time the of dc-component is around five cycles (100 ms) for all the fault inception angles.

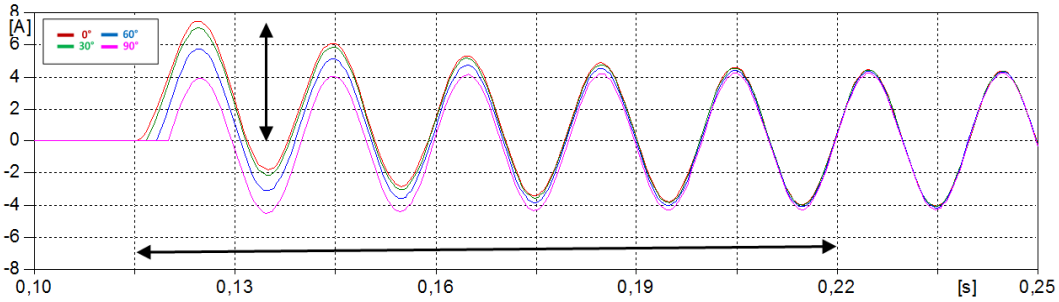

Figure 4.13 Fault current with variation of fault inception angle

Analysis using the impedance (R-X) plane shows the effect of decaying dc-offset to the impedance trajectory as illustrated in figure 4.14. The decaying dc-offset in the fault current seems to shift the trajectory of the impedance. In this case, the highest dc-offset (fault

inception angle 0°) causes the impedance to shifted more to the right side in the impedance plane.

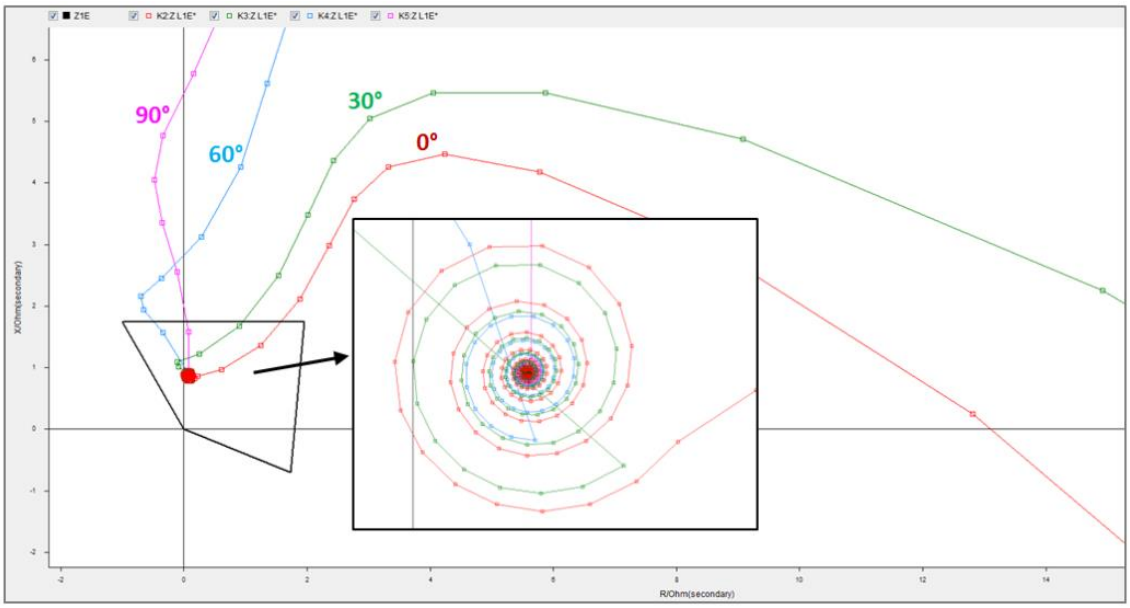

Figure 4.14 Fault impedance trajectory with variation of fault inception angle

Varying the fault type

The voltages and currents for different fault types are shown in the following figures. All the faults are located at 95% of the zone 1 impedance setting. Once the faults are initiated at around 100 ms, the currents in the faulted phase(s) jump to their peak values. In contrary with the current, the voltage in the faulted phase(s) rapidly drop to much lower values.

Single phase-to-ground faults (LN) are classified as unsymmetrical faults. LN faults are characterized by a sudden drop in the faulted-phase voltage and an increase in the healthy-phases voltages after the fault inception. For an AG Fault, the voltage in phase A decreases while the voltages in phase B and C increase as shown in Figure 4.15.

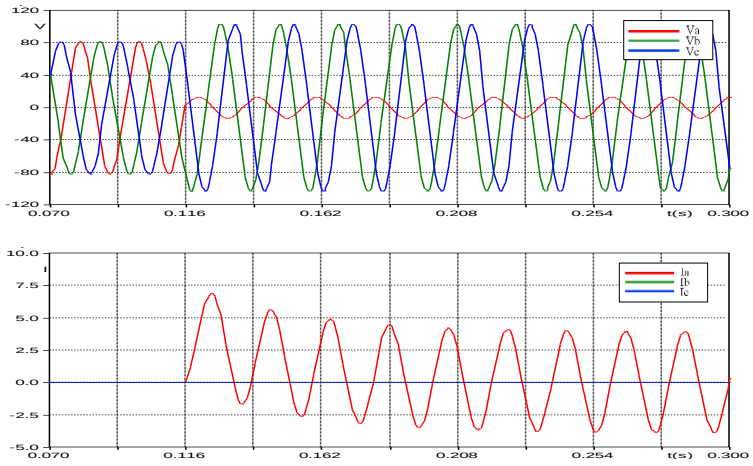

Figure 4.15 Voltages and currents (secondary value) for LN fault

Phase-to-phase (LL) and double-phase-to-ground (LLN) faults are also classified as unsymmetrical faults. These faults are characterized by a rapid voltage decrease and a current increase on the faulted phases after the fault initiation. Moreover, the fault currents at both

phases are 180° apart. The main difference between LL and LLN faults lies in the voltage of the healthy phase. For double-phase-to-ground faults, the voltage in the healthy phase is increased, while for phase-to-phase faults, it remains the same with the pre-fault voltage. The characteristics of LL and LLN faults are shown in Figure 4.16 and 4.17.

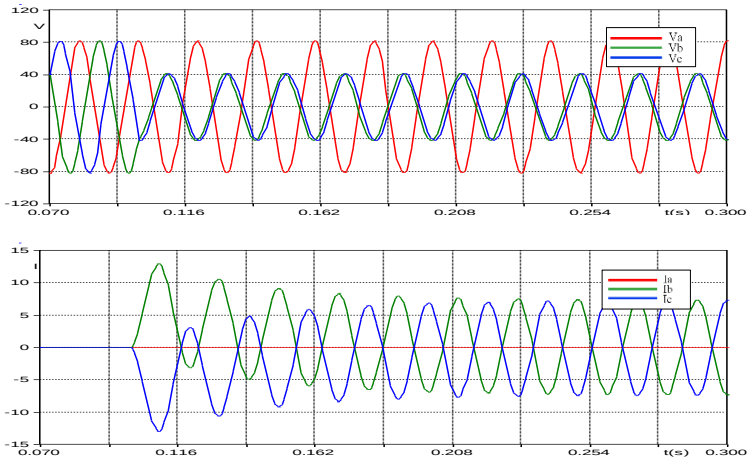

Figure 4.16 Voltages and currents (secondary value) for LL fault

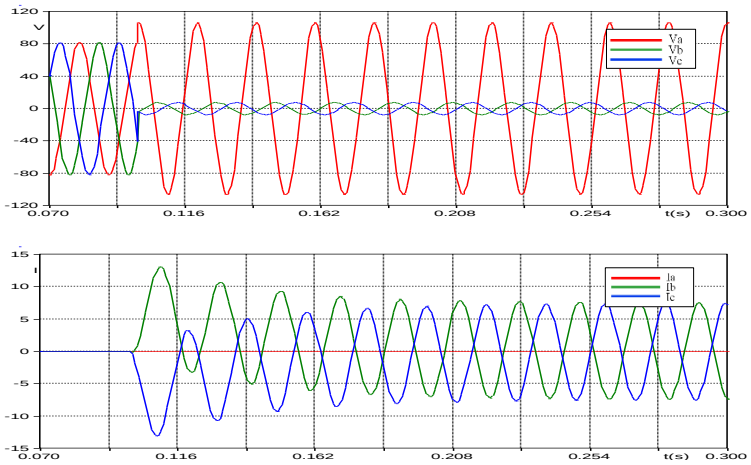

Figure 4.17 Voltages and currents (secondary value) for LLN fault

The last fault type is the three-phase (LLL) fault. Three-phase faults are classified as symmetrical faults. It characterizes by a sudden drop of the voltages and a rapid increase of the currents in all the three phases. The voltages and currents of a three-phase fault are displayed in Figure 4.18.

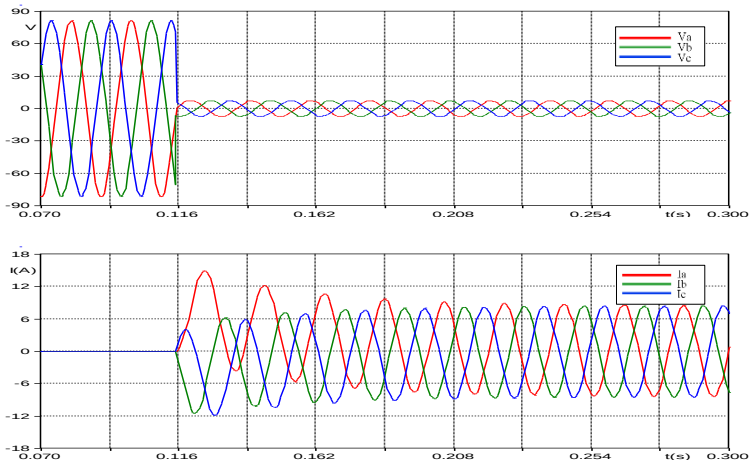

Figure 4.18 Voltages and currents (secondary value) for LLL fault

Varying the source impedance ratio

The voltages and currents of an AG fault with different SIR values are shown in Figure 4.19. It can be seen that an increase in the SIR value results in smaller voltages and currents at the location of the relay. In this case, with the SIR 5, the peak fault current is around 7.47 A. While for the SIR 50, the peak fault current is only 0.81 A. Furthermore, the magnitude of fault current affects the voltage measured by the relay. In the case of SIR 5, the peak voltage is around 7.42 V, while for the SIR 50, the voltage is as low as 0.84 V.

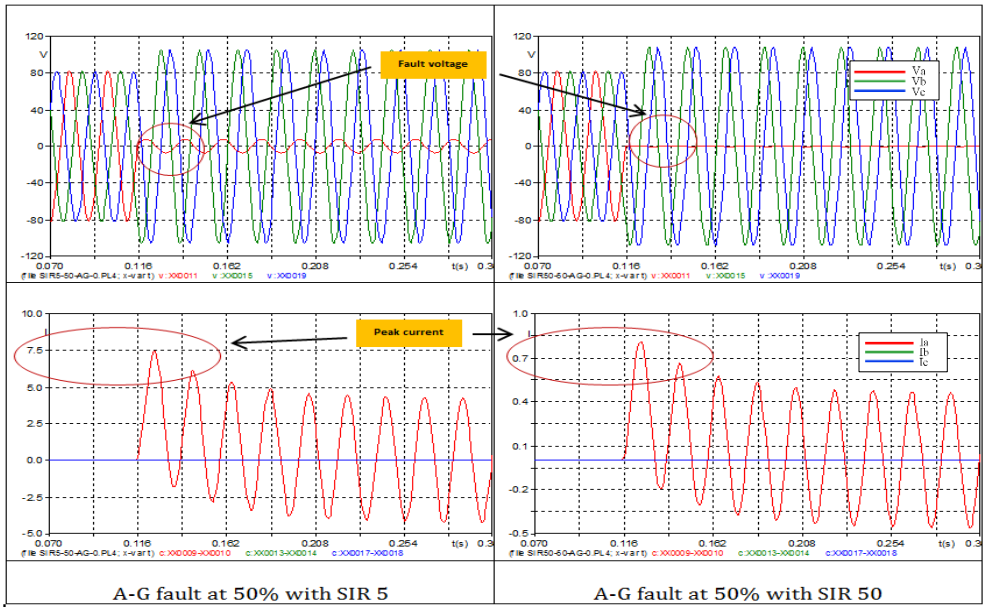

Figure 4.19 Voltages and currents (secondary value) with different SIR values

4.2 Simulation with the CVT transient

4.2.1 Introduction

Capacitive voltage transformer (CVT) is the most widely used of voltage transformer in high voltage (HV) and extra high voltage (EHV) networks. The CVT provides economic advantages compared to the other VT types, especially for EHV application. However, besides its

economic advantages, the CVT could produce a transient error during fault conditions. The transient error is caused by the energy stored in the capacitor stacks that cannot be dissipated instantaneously when the faults occur. The magnitude of transient error of CVT is determined by several factors such as [5]:

- The sum of the stack capacitances
- The shape and parameters of the ferroresonance suppression circuits
- CVT burden
- Fault inception angle

The voltage at the secondary side of CVT contains noise from the harmonics and the transient error. The secondary voltage of CVT can be explained by the following equation [5]:

$$v_{(t)} = v_{CVT(t)} + V_1 cos(\omega_1 t + \varphi_1) + v_{noise(t)} \quad (17)$$

Where,
V_{CVT} is the CVT-induced transient
V_1 and φ_1 are the phasor magnitude and the phase angle of fundamental frequency
V_{noise} is the high-frequency noise (including harmonics and decaying high frequency-oscillatory components)

The CVT-induced transient is a combination of one oscillatory decaying component and two aperiodically decaying dc components as explained in the following equations [5]:

$$v_{CVT(t)} = A_1 \cos(\omega_0 t + \varphi_0)\, exp\left(-\frac{t}{T_k}\right) + \sum_{k=2}^{3} A_k exp\left(-\frac{t}{T_k}\right) \quad (18)$$

The comparison of the magnitude of fundamental frequency component with the CVT-induced transients is shown in Figure 4.20.

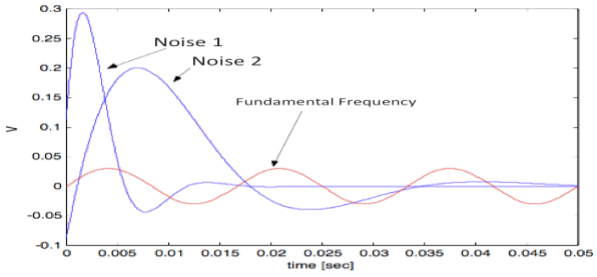

Figure 4.20 60 Hz signals with two oscillatory decaying components [5]

To study the characteristic of the CVT-induced transient, a CVT model is developed in ATP-EMTP. The CVT model is then added to the short network from the previous simulation. To obtained different transient characteristics, four fault inception angles are simulated. The summary of the fault parameters used in the simulation is shown in Table 4.4. Total 224 test cases are performed in the simulation.

Table 4.4 Parameter variation of CVT transient test case

Network length	SIR	Fault position (Percentage of zone-1 setting)	Fault type	Fault inception angle (°)
Short (20 km)	5 and 50	0, 50, 80, 90, 95, 105, and 110	AG, BC, BCG, and ABC	0, 30, 60, and 90

4.2.2 The CVT model

A CVT can be represented by the simplified mathematical model as shown in Figure 4.21. All the parameters in this model are referred to the primary values.

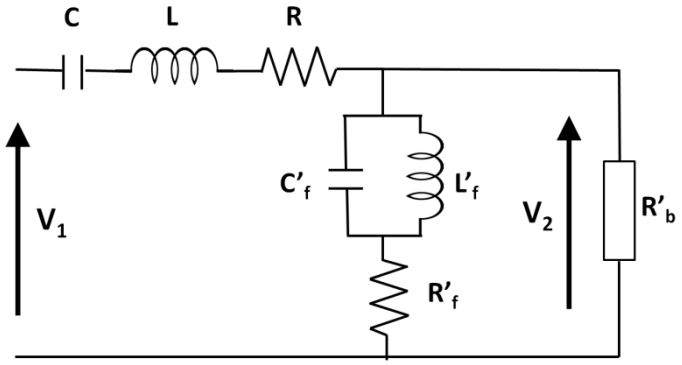

Figure 4.21 Simplified model of CVT

Where,
R and L are the resistance and inductance of the compensating reactor
C is the stack capacitance
R_f', L_f', and C_f' are the resistance, inductance, and capacitance of the ferroresonance circuit
R_b' is the burden

The transfer function of the model is given in Equation (19) [5]:

$$\frac{V_1(s)}{V_2(s)} = \frac{A_3S^3 + A_2S^2 + A_1S}{B_4S^4 + B_3S^3 + B_2S^2 + B_1S + B_0} \quad (19)$$

Where,

$$A_1 = R_f R_b C$$
$$A_2 = L_f R_b C$$
$$A_3 = L_f C_f R_f R_b C$$
$$B_0 = R_f + R_b$$
$$B_1 = RCB_0 + L_f + A_1$$
$$B_2 = LCB_0 + RCL_f + L_f C_f B_0 + A_2$$
$$B_3 = LCL_f + RCL_f C_f B_0 + A_3$$
$$B_4 = L_f C_f B_0 + LC$$

The CVT model in the simulation is based on the CVT equivalent circuit in the IEC 60255-121 standard. The equivalent circuit and the component parameters are shown in Figure 4.22.

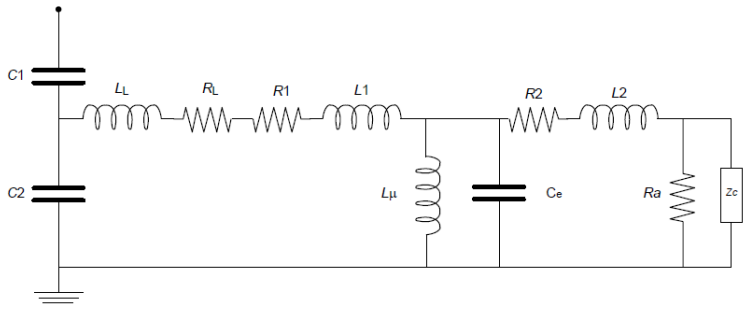

Vpri	400000	V	**Ra**	177700	Ω
Vsec	100	V	**LL**	107	H
C1	4210	pF	**L1**	5	H
C2	80000	pF	**L2**	8	H
Ce	0	pF	**Lμ**	177820	H
RL	650	Ω	**Zc**	80/1840	VA/ kΩ
R1	1550	Ω	**Load PF**	1	
R2	2700	Ω			

Figure 4.22 CVT equivalent circuit and parameters [1]

The CVT model as illustrated in figure 4.23 is developed using several component models that are available in the ATP-EMTP, including capacitance (CAP_RS), Inductance (IND_RP), resistance, Transformer (TRAFO_I), and splitter.

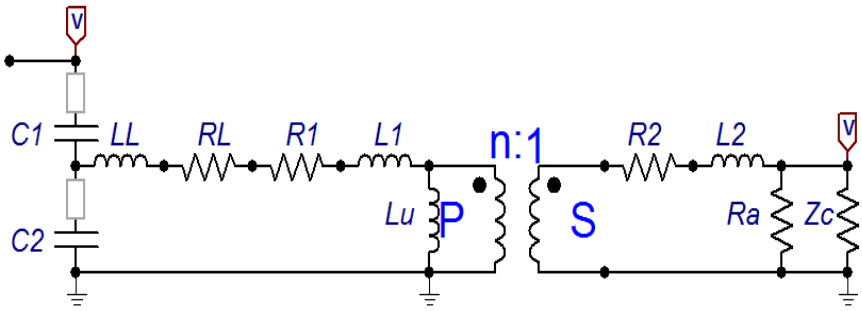

Figure 4.23 Capacitive voltage transformer model

To validate its transient characteristic, the model is tested using the transient response test in the *IEC 61869-5 standard (Additional requirement for capacitive voltage transformer)*. The tests are performed by short-circuiting the high voltage source at the actual primary voltage Vp and then record the secondary voltage response of the CVT. The tests are conducted at the peak and the zero passage of the primary voltage as shown in Figure 4.24.

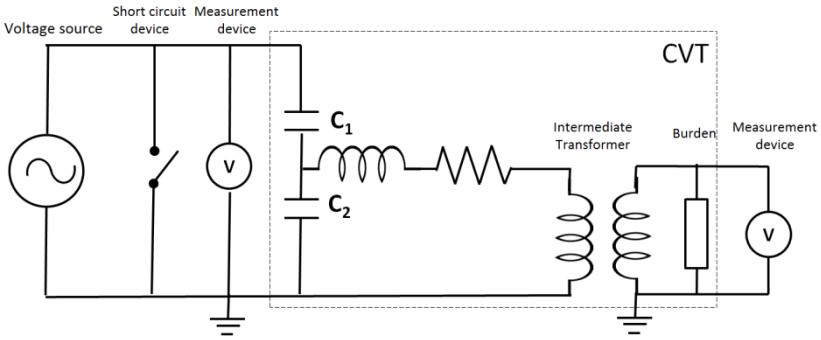

Figure 4.24 CVT Transient response test

The transient response of the model is then compared with the CVT transient waveforms in [1] as displayed in Figure 4.25. For a short circuit at the zero crossing of the primary voltage, the secondary voltage is damped aperiodically (top right figure), this response is similar to the blue signal in the reference waveforms (left figure) from the standard.

Moreover, for a short circuit at the peak of the primary voltage, the secondary voltage is damped periodically (bottom right figure), and this response is also similar to the red signal in the reference waveforms (left figure). Therefore, it is shown that the transient responses of the CVT model are correct for both test conditions.

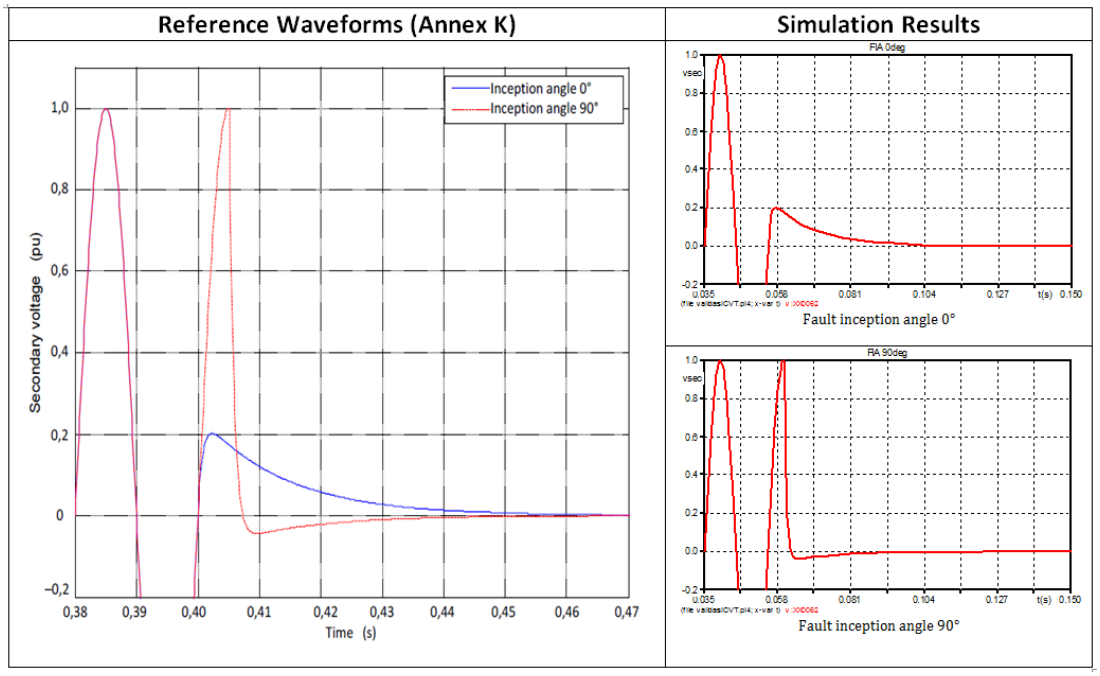

Figure 4.25 Comparison of CVT transient responses

After the CVT model has been validated, the network model is built in ATP-EMTP as shown in Figure 4.26.

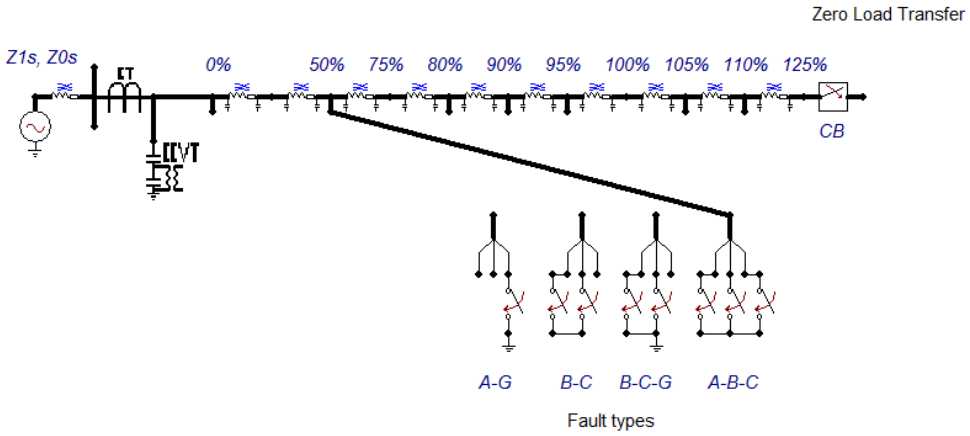

Figure 4.26 Short transmission network with CVT model

4.2.3 Analysis of the simulation result

Similar to the previous simulation, the total simulation time is 300 ms with pre-fault duration around 100 ms, and solution time step 5 µs. The comparison of the transient response of VT and CVT are highlighted in this section.

The fault voltages (secondary value) for an ABC fault with the VT and the CVT are shown in Figure 4.27, 4.28, and 4.29.The fault is located at 50% of the zone 1 impedance setting. Once the fault is initiated at around 100 ms, the secondary voltages of the VT drop rapidly into a much smaller fault voltages. In this case, the fault voltage is around 7.38 V (peak). However, in the case of the network with CVT, the secondary voltages are not instantly dropped into the fault voltages. It can be observed that the voltages are gradually decreased for two cycles (40 ms) until they reach the nominal fault voltages. The simulation also shows that the shape of the transient waveform is different for various fault inception angles (0° and 90°).

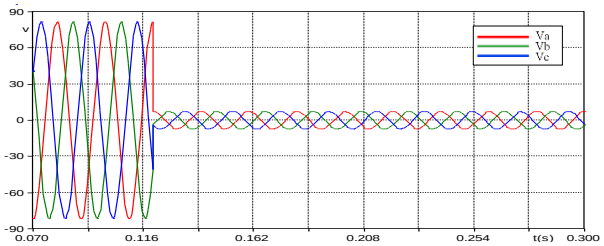

Figure 4.27 Secondary voltage using VT

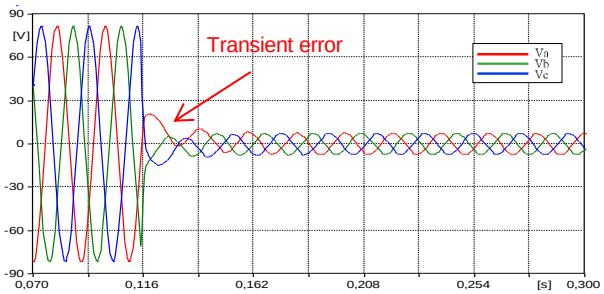

Figure 4.28 Secondary voltage using CVT (inception angle 0°)

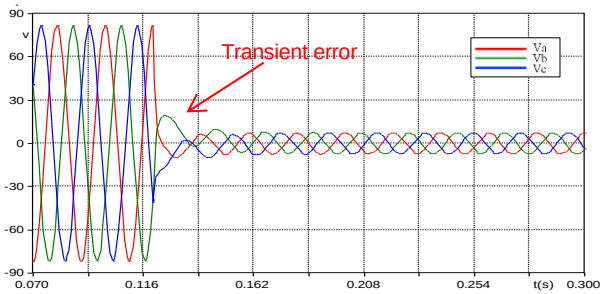

Figure 4.29 Secondary voltage using CVT (inception angle 90°)

An analysis using the impedance (R-X) plane shows the influence of the CVT transient error to the fault impedance trajectory as illustrated in figure 4.30. Due to the voltage error, the measured impedances for the first two cycles (40 ms) will be different. The CVT transient error seems to alter the impedance shape and enlarge the spiral diameter of the trajectory in the impedance plane. Moreover, the shape of the transient waveforms also causes the trajectory to shift more to the left side of the impedance plane.

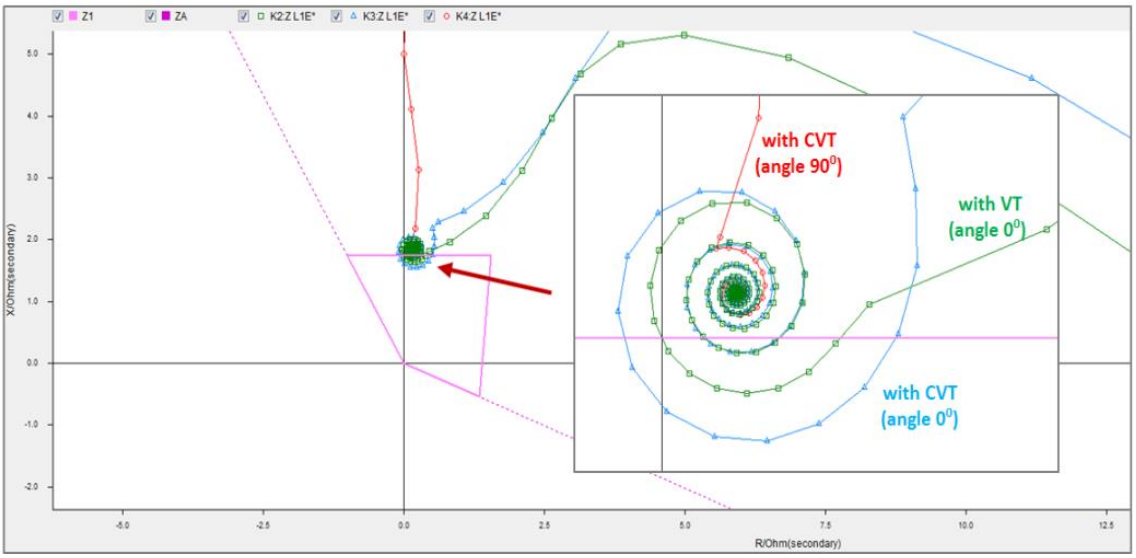

Figure 4.30 Impedance trajectory for LN fault with and without CVT

.

4.3 Simulations with the superimposed harmonics

4.3.1 Introduction

The constant developments of non-linear components in the power system levels are the main source of the harmonics. At the transmission system level, the non-linear components can be found in the HVDC converter, wind generators, FACTS, and static VAR compensators. These components generate a high level of harmonics in the transmission line that can affect the performance of electrical equipment.

The harmonic components in power system can be described as the sinusoidal components of a periodic waveform that have frequencies equal to an integer multiple of the fundamental frequency of the system. The distorted waveforms can be expressed as the superposition of the fundamental frequency waveform with the other harmonic waveforms. Figure 4.31 shows a typically distorted waveform of the six-pulse converters used in HVDC.

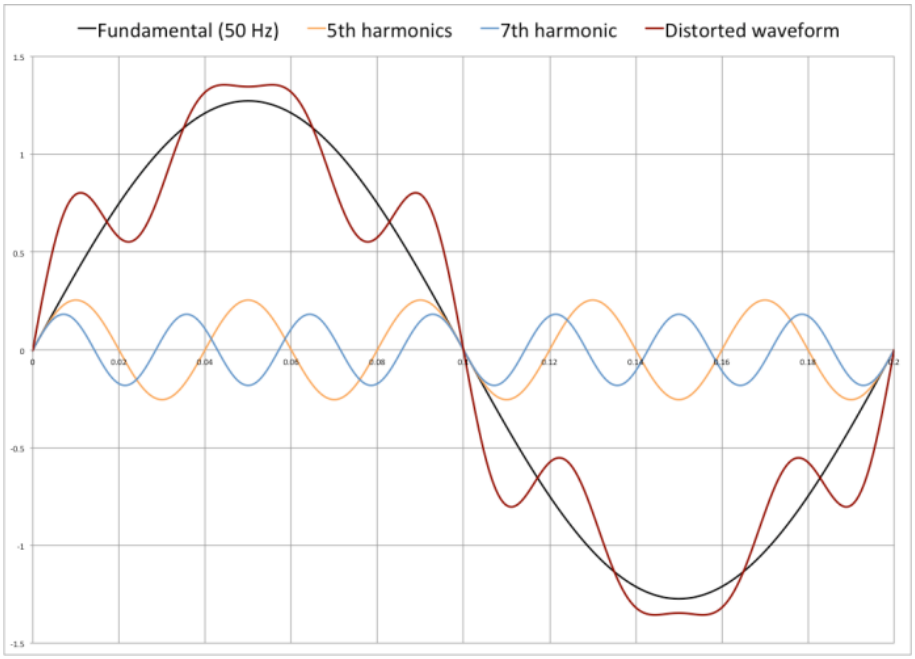

Figure 4.31 Distorted waveforms contain harmonics

Harmonics order in the voltage (or current) can be expressed by the following equations:

$$V_{Ah} = V_h sin(h\omega_0 t + \theta_h) \tag{20}$$

$$V_{Bh} = V_h sin\left(h\omega_0 t - \frac{2h\pi}{3} + \theta_h\right) \tag{21}$$

$$V_{Ch} = V_h sin\left(h\omega_0 t + \frac{2h\pi}{3} + \theta_h\right) \tag{22}$$

Where,
h is the harmonic order

The influence of the harmonics on the distance relay is not well documented because of the various operating principle used in each of the relay design. The electromechanical and static

relays tend to be affected by the harmonics. However, the microprocessor-based distance relays, which extract the fundamental frequency from the distorted waveforms using both digital and analog filters are relatively unaffected by the harmonics [6].

To study the characteristics of the harmonics in power system, superimposed harmonics in voltage and current during fault will be simulated. Transmission networks used in the simulations are based on transient oscillation benchmark network of [1].

The network is a radial feeder network with zero load transfer as shown in Fig. 4.32. Two source capacitance values are used: 4.31 and 8.93 µF. Moreover, the current transformer (CT) and the voltage transformer (VT) used in the network are considered as ideal transformers. In the simulation, the superimposed harmonics are generated through oscillations between the source capacitance and the transmission line inductance during the faults.

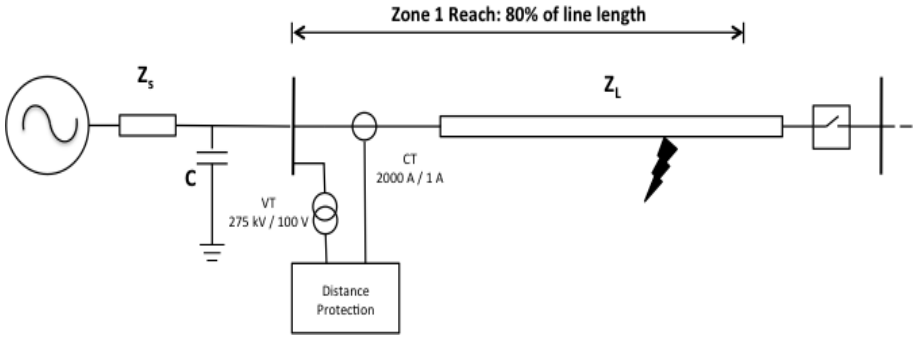

Figure 4.32 Transmission network with source capacitance

To vary the harmonics order and total harmonic distortion (THD), two different values of source capacitance will be used. In addition, various fault positions and fault types will also be applied in the simulation. The simulation parameters are shown in Table 4.5. Total simulations performed for the superimposed harmonics are 24 cases.

Table 4.5 Parameter variation of superimposed harmonics test case

Capacitance Value (µF)	Fault position (Percentage of zone 1 setting)	Fault type	Fault inception angle (°)
4.31	80, 90, 95, 105, 110, and 125	AG and ABC	90
8.93	80, 90, 95, 105, 110, and 125	AG and ABC	90

4.3.2 The network and component models

Source capacitance model

The source capacitance is modeled using the three-phase RLC symmetrical PI-equivalent component (LINEPI3S) as shown in Figure 4.33.

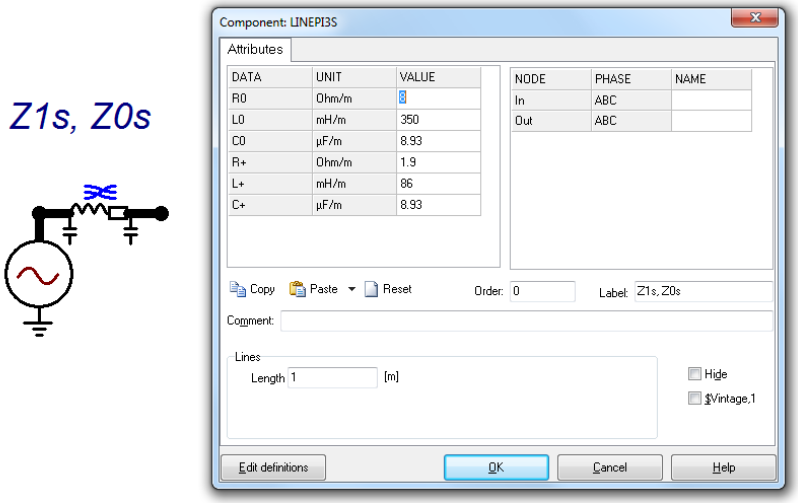

Figure 4.33 Source capacitance model

After the capacitance has been modeled, the transient oscillations network as illustrated in figure 4.34 is developed in the ATP-EMTP.

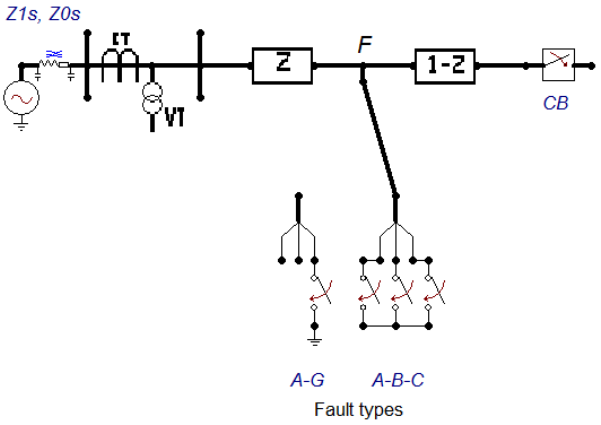

Figure 4.34 Transient oscillation network model

4.3.3 Analysis of simulation result

This section describes the simulation results of ATP-EMTP. For each case, the total simulation time used is 350 ms, with pre-fault duration around 100 ms, and solution time step 5 µs. The voltage and current for ABC fault at 95% of zone 1 setting are shown in Figure 4.35.

It can be seen that once the fault is initiated at around 100 ms, the voltages on three phases suddenly drops from nominal voltage into the fault voltage. Moreover, because of the LC oscillations during the fault, the voltage and current waveforms are highly distorted with the harmonics. For each simulation result, the harmonics content in the signals can be analyzed by using the Fourier analysis. For the case of ABC fault at 95% of the zone 1 impedance setting, the 9^{th} and 10^{th} harmonics have the highest magnitude as shown in Figure 4.36.

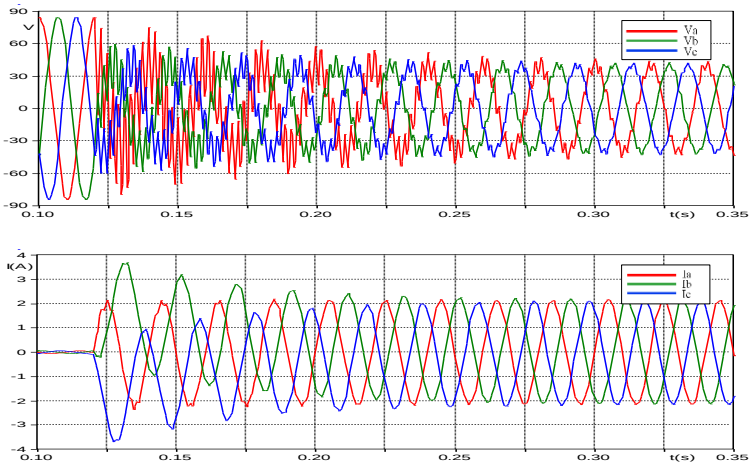

Figure 4.35 Voltages and currents (secondary value) for LLL fault with C=4.31 µF

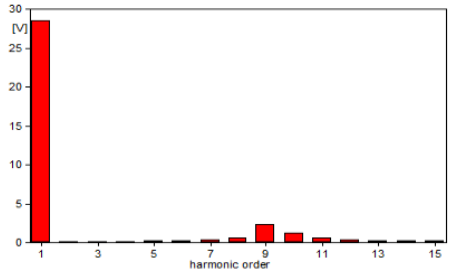

Figure 4.36 Harmonics content for LLL fault with C=4.31 µF

By replacing the source capacitance to 8.93 µF, the superimposed harmonics in fault signals are different from the previous results. The harmonics magnitudes after decomposition using the Fourier analysis are shown in Figure 4.37. In this case, the 7th harmonics has the highest magnitude.

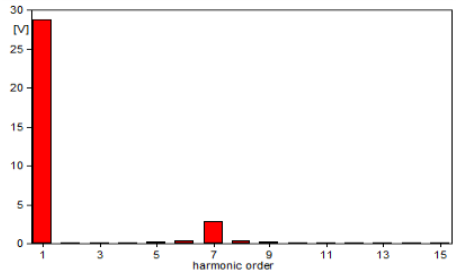

Figure 4.37 Harmonics content for LLL fault with C=8.93 µF

The fault voltage and current for an AG fault at 80% of the zone 1 impedance setting are shown in Figure 4.39, and its harmonics contents are shown in Figure 4.39. In this case, once the fault is initiated at around 100 ms, the voltage on phase A drops rapidly, while the current sharply increases to the nominal fault current. It can be seen that the voltage and the current waveforms are also highly distorted with the harmonics. In this case, the results of Fourier analysis show that the 7th harmonics has the highest magnitude.

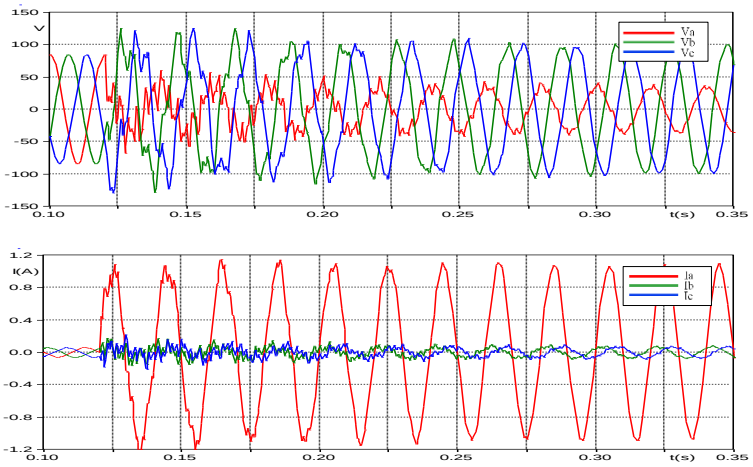

Figure 4.38 Voltages and currents (secondary value) for LN fault with C=4.31 µF

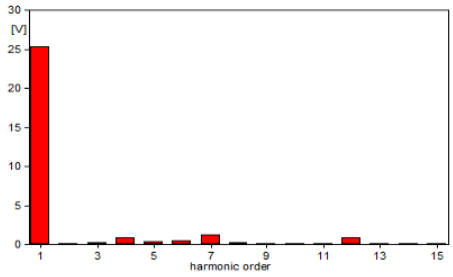

Figure 4.39 Harmonics content for LN fault with C=4.31 µF

The complete simulation results are presented in Table 4.6. It shows the highest harmonics order and the total harmonic distortion (THD) for all fault positions and capacitance values.

Table 4.6 Superimposed harmonic simulation results

Source capacitance (µF)	Fault type	Fault position (% of zone 1 setting)	Harmonics Order	THD (%)
4.31	ABC	80	10th	11.49
		90	10th	10.14
		95	9th	9.57
		105	9th	8.77
		110	9th	8.36
		125	8th	7.40
	AG	80	7th	6.98
		90	7th	5.77
		95	6th and 7th	5.58
		105	6th	5.00
		110	6th	5.18
		125	6th	4.41
8.93	ABC	80	7th	11.57
		90	7th	10.42
		95	7th	9.92
		105	7th	8.76
		110	7th	8.37
		125	6th	7.40
	AG	80	5th	7.66
		90	5th	6.74
		95	5th	6.71
		105	5th	5.69
		110	5th	5.73
		125	3rd and 5th	4.74

4.4 Simulations with the off-nominal frequency

4.4.1 Introduction

The Numerical distance relays are designed to operate at the nominal frequency of 50 Hz or 60 Hz. The digital filter used in the relay such as the discrete Fourier transform (DFT) operates correctly at the nominal power frequency. However, a significant frequency deviation of power system could happen during the emergency states when a considerable amount of generation and load are connected or disconnected to the system. During this period, the impedance measurement might become inaccurate due to an error in the sampling process. The effect of the frequency deviation on the sampling error of numerical relays is illustrated in Figure 4.40.

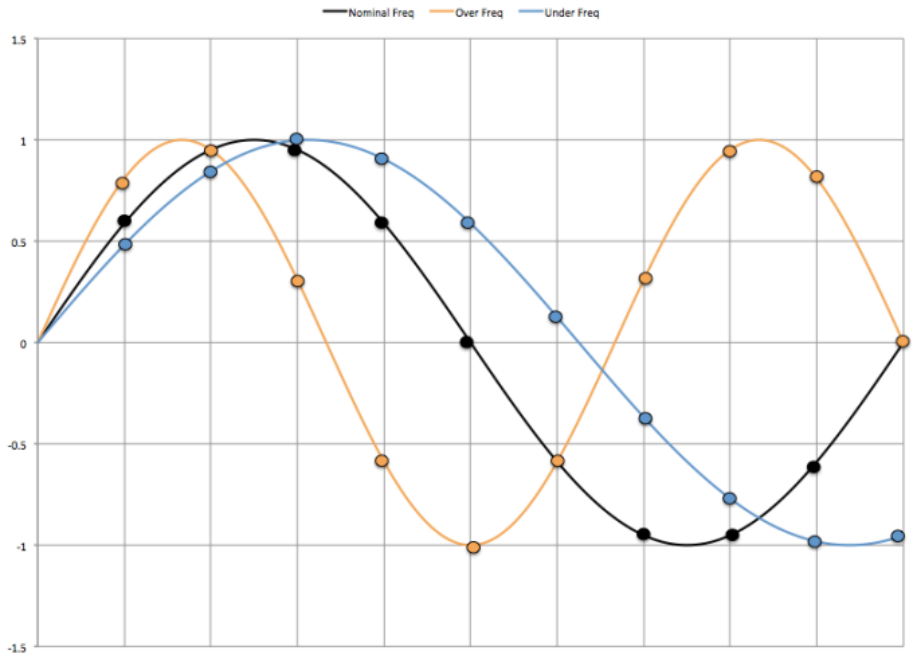

Figure 4.40 Frequency deviation effects on relay sampling error

In the case of 10 samples per cycle used in the relay ($T_{sampling}$ = 2 ms for the 50 Hz systems), both an increase and a decrease in the system frequency will cause the incorrect measurement of the rms value. Ideally, the rms values are calculated in each cycle of the waveforms. An increase in frequency will cause the rms value to be calculated based on the wave fragments shorter than one cycle. On the other hand, a decrease in frequency will cause the rms value to be calculated using the wave fragments longer than one cycle waveforms. These conditions could lead to an error when averaging the rms values from all the samples.

To study the effects of frequency deviation on distance relay performance (especially on the numerical type), the voltage and the current with off-nominal frequencies during fault will be simulated. The transmission network used in the simulation is similar to the short transmission network in the decaying dc-offset case. In this case, the frequency of the voltage source will be varied to simulate the off-nominal frequency conditions. In the simulation, the system frequencies will be set to the maximum and the minimum allowable frequency of the relay, 51 Hz, and 49 Hz (for 50 Hz system), respectively. The simulation parameters are shown in Table 4.7.

Table 4.7 Parameter variation of transient frequency deviation test case

Frequency (Hz)	Fault position (Percentage of zone-1 setting)	Fault type	Fault inception angle (°)
49	-0, 0, 50, 80, 90, 95, 105, 110	A-G	0 and 90
50	-0, 0, 50, 80, 90, 95, 105, 110	A-G	0 and 90
51	-0, 0, 50, 80, 90, 95, 105, 110	A-G	0 and 90

4.4.2 The network model

The network model used for the frequency deviation test is similar to the short transmission network of the decaying dc-offset case. However, an additional bus was added to the network to simulate the reverse fault condition (-0%). The network model built in ATP-EMTP is shown in Figure 4.42.

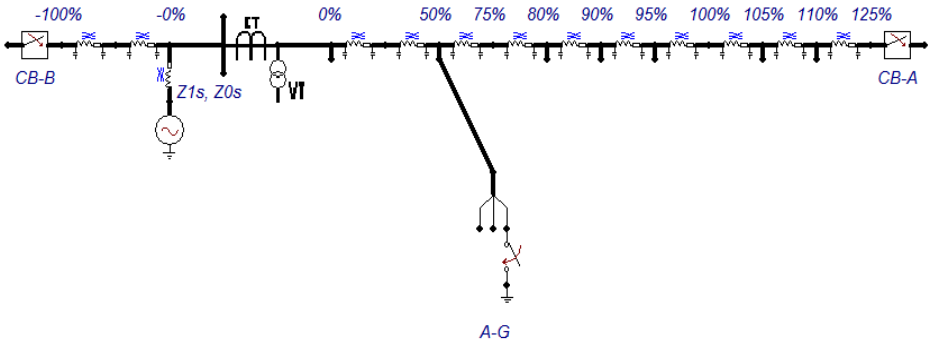

Figure 4.41 Transient frequency deviation network

4.4.3 Analysis of the simulation result

The total simulation time used is 300 ms, with pre-fault duration around 100 ms, and solution time step 5 µs. The voltage and the current for an AG fault located at 80% of the zone 1 impedance setting are shown in Figure 4.42 and 4.43.

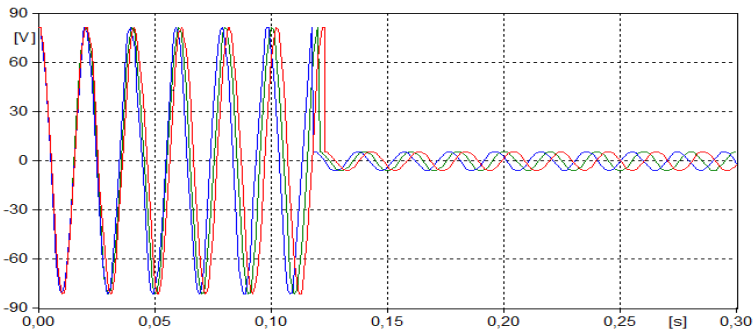

Figure 4.42 Secondary voltages for system frequency of 49, 50, and 51

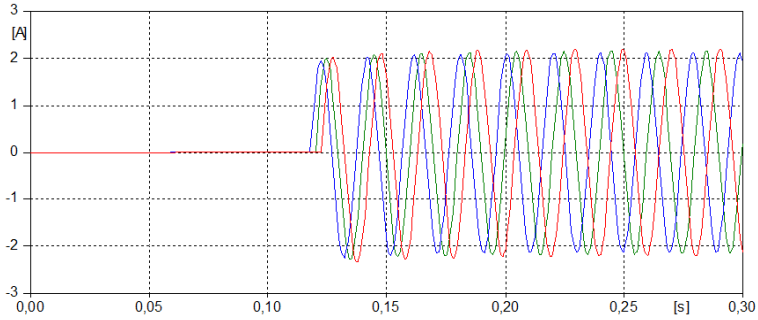

Figure 4.43 Secondary currents for system frequency of 49, 50, and 51

An analysis using the impedance (R-X) plane shows the influence of system frequency to fault impedance trajectory as illustrated in figure 4.44. The example is shown for a LN fault (with inception angle 0^{o}) located at 105% of the zone 1 impedance setting. It is shown that the frequency of power system seems to alter the shape and the position of the impedance trajectory. In this case, for the 49 Hz systems (red), the spiral trajectory will enter the tripping zone 4 times, while for the 50 Hz (green) and the 51 Hz (blue) systems, the spiral trajectories enter the tripping zone two times and one time, respectively.

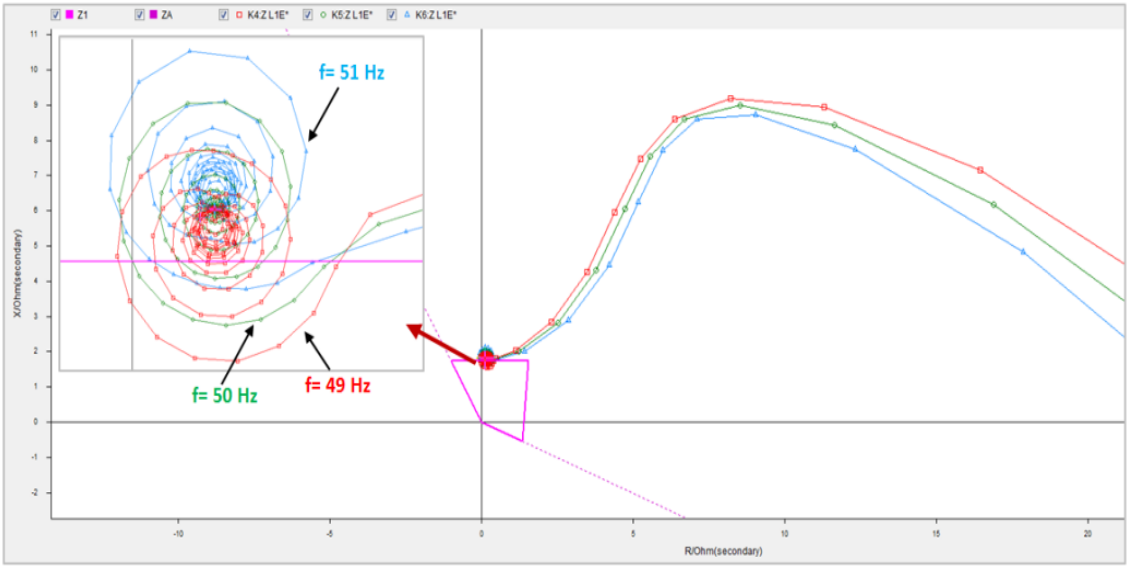

Figure 4.44 Impedance trajectories for different system frequency

Depending on the protection functions and the logics applied in the distance relay, the spiral trajectories that enter the tripping zone might cause the distance relay to operate, even though the fault point is located outside of the tripping zone. In other words, it might cause an overreach of the distance relay.

4.5 Simulations with the fault resistance and remote in-feed current

4.5.1 Introduction

Distance relay differentiates the load and the fault conditions by estimating both the magnitudes and the phase angle of the impedance. The relay operates if the estimated impedance falls inside the tripping characteristic as shown in Figure 4.45. Therefore, it is

essential to ensure that the maximum load of the system (the smallest impedance) is always located on the outside of the tripping characteristic. The figure also shows that the higher the fault resistance, the more difficult for distance relays to differentiate between load and fault conditions as the fault impedance angle becomes smaller.

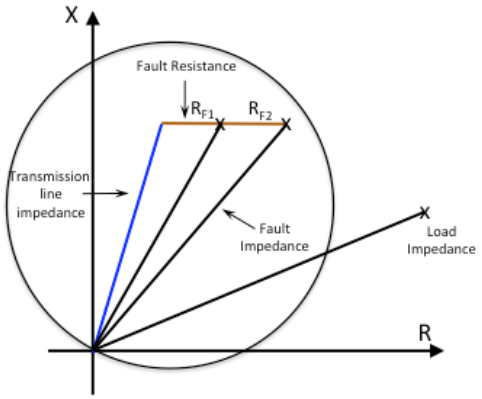

Figure 4.45 Load and fault impedance on RX-plane

The fault resistances are usually high in case of ground faults caused by the flashover on the string insulators of the transmission tower. The fault loop of the ground faults usually consists of the arc resistance, the tower footing resistance, and the tower resistance. The total resistance value can vary from less than few ohms to several hundred ohms. However, this is not the case for the other fault types where the fault resistance values are usually much smaller.

The combined effects of load current and fault resistance could also lead to an incorrect operation if the fault resistance value is too large. In this case, the relay could trip for an external fault (lack of security), or not trip for a fault inside the protection zone (lack of dependability). Figure 4.46 shows the effect of load current and fault resistance on the measured impedance in distance relay.

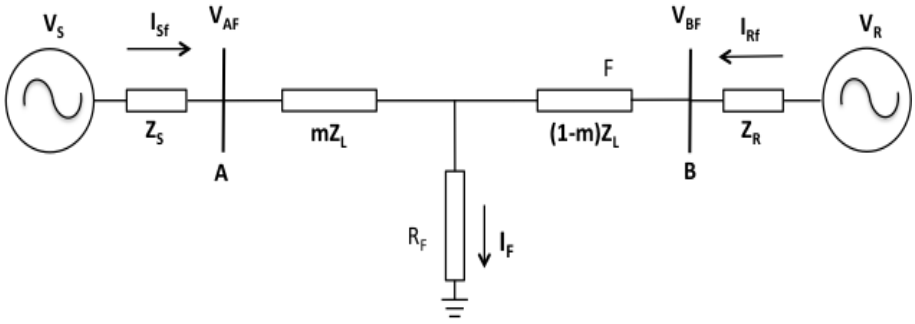

Figure 4.46 Effect of load and fault resistance on the measured impedance

Two voltage sources are connected by a transmission line through bus A and B. The source impedances are represented by Z_S and Z_R; the transmission line is represented by Z_L, and the fault resistance by R_f.

The impedance measured by the relay at bus A (Z_A) is given by the following equations:

$$Z_A = \frac{V_{Af}}{I_{Sf}} = \frac{mZ_L \times I_{Sf} + R_f I_f}{I_{Sf}} \quad (23)$$

$$Z_A = mZ_L + R_f k_s \tag{24}$$

Where,
m is the distance of fault to bus A
V_{af} is the voltage at bus A
I_{sf} is the current from bus A
I_f is the total fault current
k_s is the ratio of total fault current and current at relay location ($\frac{I_f}{I_{Sf}}$)

The ratio k_s describes the effect of the remote in-feed current to the fault impedance measured by the distance relays. In general, the value of k_s is *greater* than 1, which means that the remote in-feed will amplify the fault resistance value as seen by the relay. However, if the ratio k_s is a complex number (I_f and I_{sf} is not in phase), it may also alter the apparent impedance angle, which causes incorrect operation for the faults located outside of the protection zone. The effect of the remote in-feed and fault resistance in the impedance plane is shown in Figure 4.47.

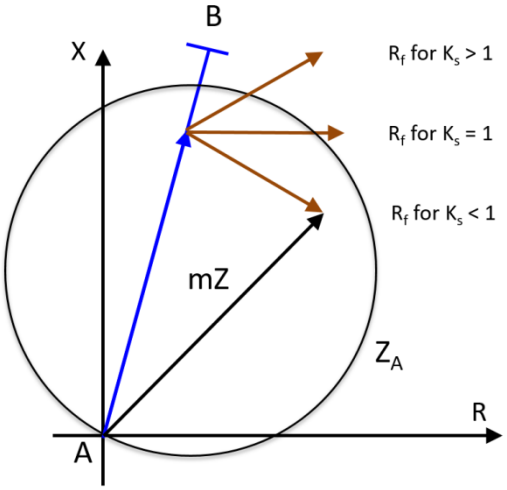

Figure 4.47 Combination effects of fault resistance and remote in-feed

In this section, the operation problems of distance protection associated with the fault resistance and the remote in-feed are analyzed. Two simulation cases are performed: the fault with resistance, and the combination of remote in-feed with fault resistance. The fault resistance used in the simulations are 10 Ω for the LN faults and 5 Ω for the LL & LLN faults. The test cases are simulated on the long and the short transmission networks. Several fault locations along the transmission network are defined to assess both the security and the dependability of distance protection. Moreover, four fault types are simulated (LN, LL, LLN, and LLL). In summary, total 88 simulation cases are performed in this section as shown in Table 4.8.

Table 4.8 Simulation parameters for fault with resistance

Case	Fault position (Percentage of network length)	Fault type	Fault inception angle (°)	Total
Without pre-fault current	-0, +0, 70,90	A-G, A-B, A-B-G, A-B-C	45	28
With pre-fault current	-0, +0, 50, 70, 100	A-G, A-B, A-B-C	45	60

4.5.2 The network and component models

The transmission networks used in the simulations are based on the single line double in-feed benchmark network in the IEC 60255-121 standard. In this network, the CT and VT are considered as ideal transformers, and the transmission line capacitances are neglected. There are two types of source impedance used in the simulations:

- Homogenous source – S1 ($Z_1 = Z_0 = 1+j30\ \Omega$)
- Non-homogenous source – S2 ($Z_1 = 1+j7\ \Omega$; $Z_0 = 1+j21\ \Omega$)

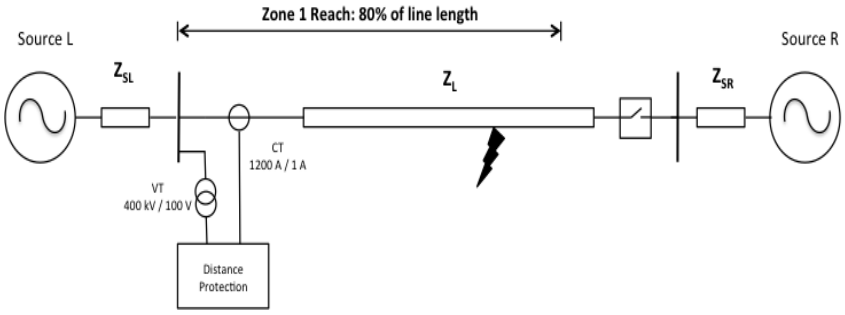

Figure 4.48 Double in-feed transmission network

The fault resistances are modeled using the time-controlled single-phase switches and the single-phase resistances. The closing time of the switches is controlled to obtain the fault inception angles 45°. The fault models in ATP-EMTP are shown in Figure 4.49.

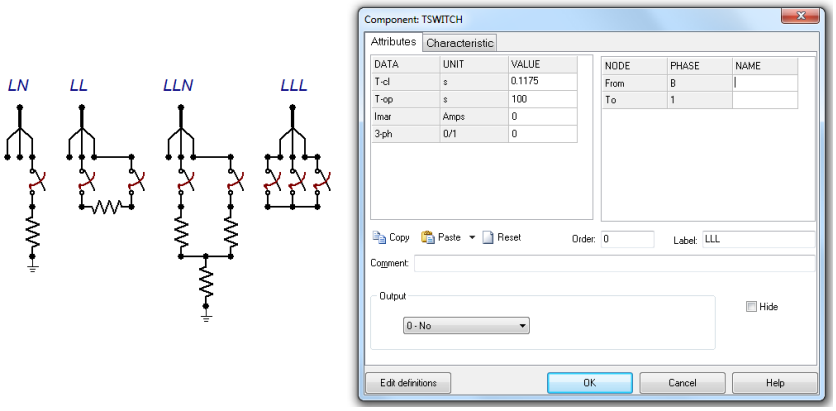

Figure 4.49 Models of fault with resistance

Two load conditions are considered in the simulation:

- Exporting load 830 MVA (source L to R)
- Importing load 830 MVA (Source R to L)

The load current is simulated by adjusting the initial angle of the source that sends the power to lead the other source. Furthermore, the remote CB behaviors in the simulations are defined as follow:

- For faults in zone 1 (80% of the line), the breaker will open 60 ms after the fault inception (20 ms relay tripping time + 40 ms breaker opening time).
- For faults in zone 2 (>80% of the line), the breaker will open 300 ms after the fault inception.

Finally, a network model in ATP-EMTP is shown in Figure 4.50.

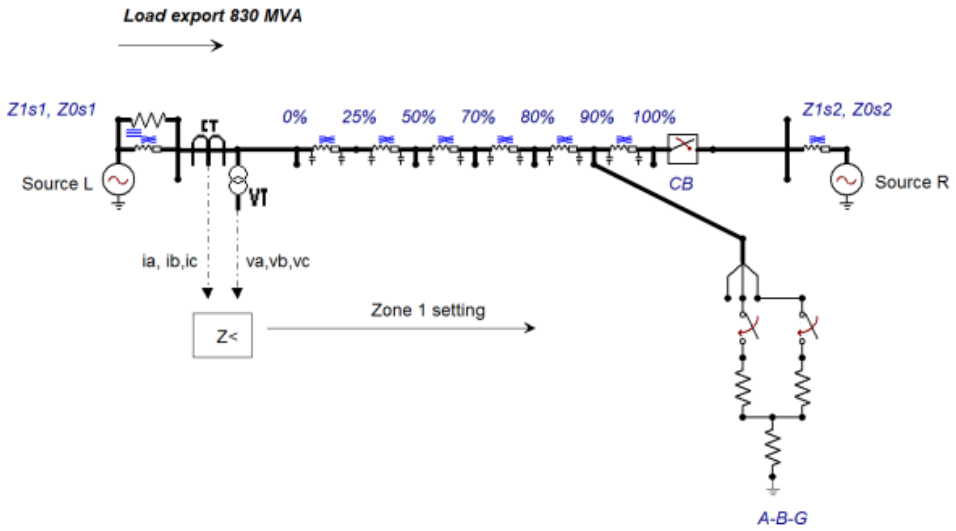

Figure 4.50 Double in-feed short transmission network model

4.5.3 Analysis of the simulation result

This section presents some of the simulation results, including the impedance analysis in RX-plane. For each simulation, the total time is 800 ms, with pre-fault duration around 100 ms, and solution time step 5 µs. The voltage and the current of an AG fault located at 70% of the transmission line length are shown in figure 4.51. In this case, no pre-fault loads are applied in the simulation.

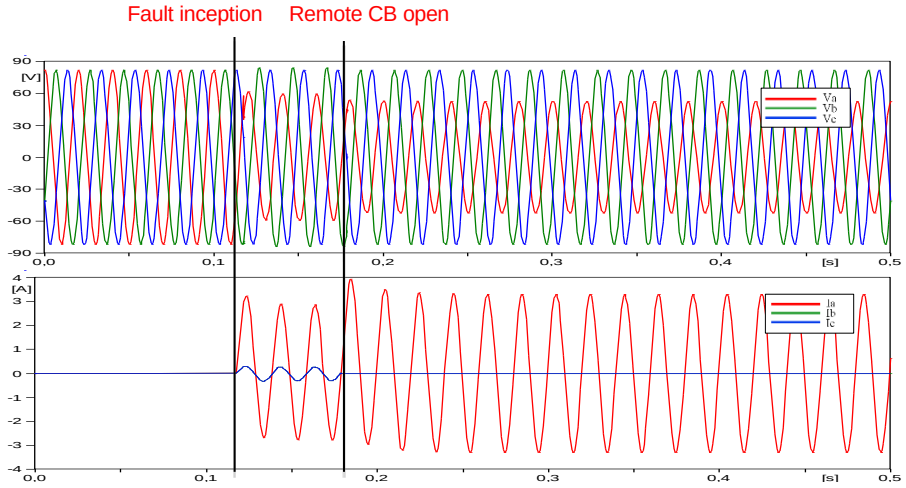

Figure 4.51 Secondary voltages and currents for AG fault at 70% (case 1)

When the fault is initiated at around 100 ms, the phase A current (measured at bus L) jumps from zero to its maximum peak value. At the same time, low magnitude fault currents are starting to flow on the healthy phases (B and C) due to the fault contribution from the remote-end generator (source R). Moreover, the phase A voltage suddenly drops to a much lower fault voltage.

Three cycles (60 ms) later, the CB at bus R will open the three poles to isolate the fault. In this state, the fault currents from source R are eliminated. It can be seen in the figure that there is no current flowing in the healthy phases after the CB R open. In this state, the current of phase A (measured at bus L) suddenly jumps to a higher value because all the fault currents are now being supplied by the source L. The peak value of the current jumps from 3.18 A to 3.89 A, and the voltages remain at the same value.

The voltage and the current for the same fault with exporting load are shown in Figure 4.52. Before the fault initiation, it can be seen that pre-fault currents are already flowing in the network with a magnitude of 1.41 A (peak).

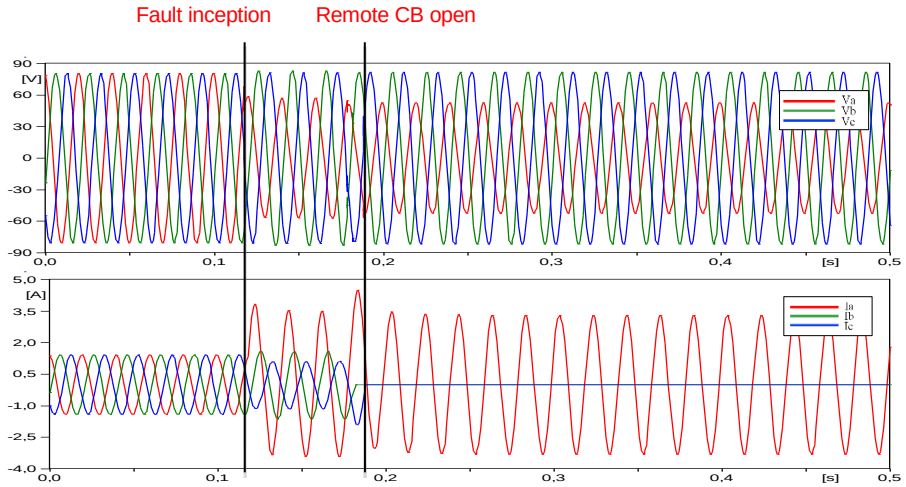

Figure 4.52 Secondary voltages and currents for AG fault at 70% (case 2)

Once the fault is initiated, the current instantly jumps into a higher short circuit current (3.82 A). Similar to case 1, the fault current in the healthy phases (B and C) are also flowing. However, in this case, the currents are not in phase due to the load effects. When the CB at bus R opens the three phases, similar characteristic with the previous test case are also observed: the phase A current jumps while the currents at the healthy phases are eliminated.

The similar characteristic can be analyzed in the case of the importing load as shown in Figure 4.53. However, in this case, the currents have an opposite polarity compared to the exporting load case.

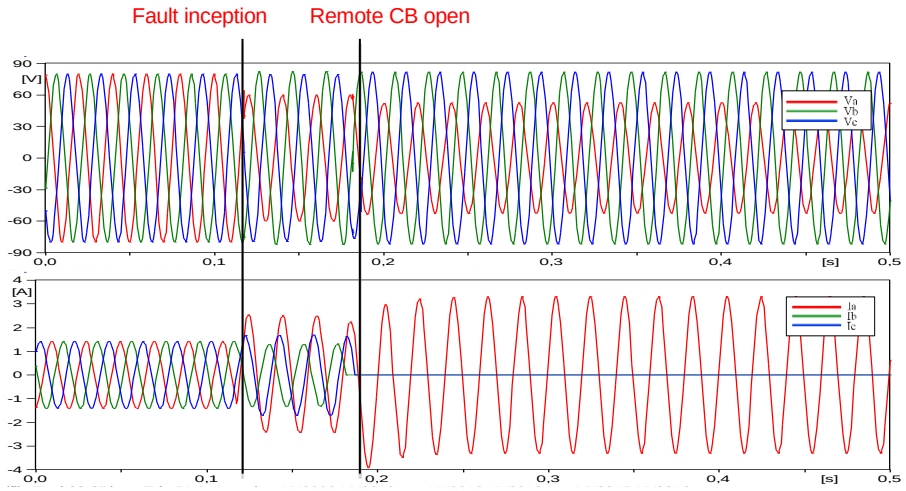

Figure 4.53 Secondary voltages and currents for AG fault at 70% (case 3)

An analysis using the impedance (R-X) plane shows the influence of remote in-feed on the fault impedance trajectory as illustrated in figure 4.54. the pre-fault load seems to cause the impedance trajectory to shift downward or upward in the impedance plane. In the case of the exporting load (source L to R), the trajectory is shifted downward. While for the importing load (source R to L), the trajectory is shifted upward. However, several cycles after the fault inception, the impedance values for all the three cases converge to the same final impedance.

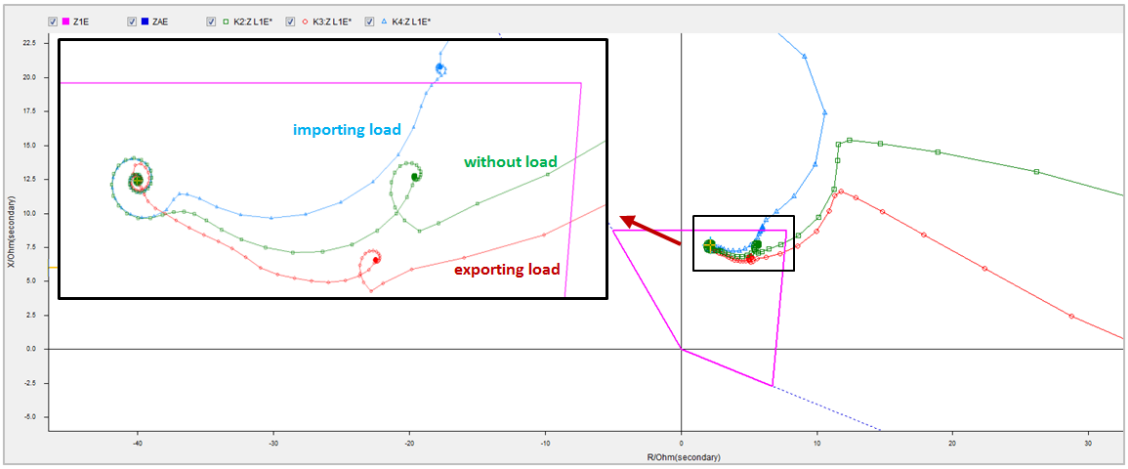

Figure 4.54 Impedance trajectories of AG fault

Further analysis of the impedance trajectory shows that depending on the pre-fault load direction, the shifted impedance trajectory during the first few cycle might cause underreach or overreach of the distance relay. The importing load will probably cause the relay to underreach as the measured impedance is higher than the actual impedance. While, the exporting load conditions might cause the relay to overreach as the measured impedance is lower than the real impedance.

4.6 Simulations of the parallel transmission line application

4.6.1 Introduction

Parallel transmission lines are widely used because they can provide a reliable and secure electrical energy transport compared to the single transmission lines. However, the different network configurations and operation modes in the parallel lines result in a more complex protection challenge for the distance protection. Some special conditions also need to be considered in the protection design, including the evolving fault and the current reversal.

Evolving faults

An evolving fault is a fault that starts with a single-phase-to-ground fault and turns into a multi-phases fault shortly after the first fault inception. When the evolving fault occurs, the distance relay must be able to detect the fault correctly and operate quickly without an additional time delay. The operation time delay can arise because of the change of the measured fault impedance during the fault. The phase selection algorithms used in the relay need to perform quickly to ensure a fast tripping and correct operation for evolving faults. In some situations, the first faults can also evolve from one line to the other line to form a cross-country fault.

A cross-country fault is multiple faults that occur on the transmission line at the same time but at different locations. For example, an AG fault at line 1 takes place at the same time with a

BG fault at line 2 as displayed in Figure 4.55. Cross-country faults often lead to an incorrect phase tripping and a selectivity problem in distance relays.

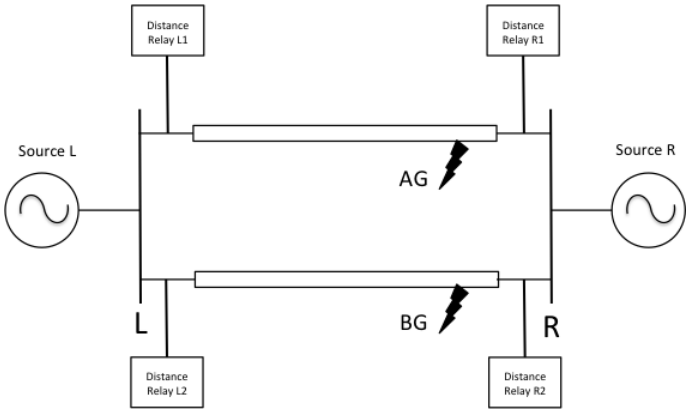

Figure 4.55 Cross-country fault

For faults located close to bus R, the distance relays R1 and R2 are normally able to detect the correct fault type. In this case, relay R1 will detect an AG fault, while relay R2 will detect a BG fault. However, this is not the case with the relays at bus L. Both distance relay L1 and L2 can detect the faults as the ABG fault due to the same electrical point in the system as seen by the relays.

Current reversal

Current reversal conditions might occur on the parallel transmission line with power sources at the both ends of the circuit. Current reversal is a case when the current direction in the healthy line suddenly change for a short period during the fault clearing of the faulted line. This condition leads to an unwanted tripping of distance relays on the healthy line. Figure 4.57 and 4.58 explain how current reversal occurs in parallel transmission lines.

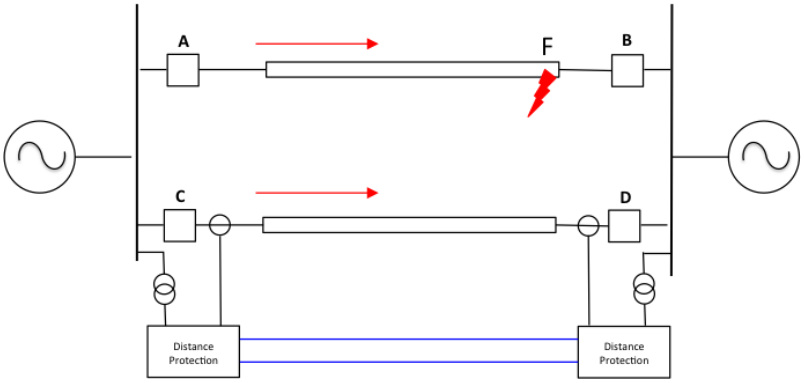

Figure 4.56 Current reversal consideration in parallel line

When a fault near the circuit breaker (CB) B occurs (location F), the distance relay at CB B will clear the fault faster than the relay at CB A. However, before CB B opens, relay C will also detect this fault as a zone 2 fault and send a trip signal to distance relay D. At the same time, the reverse element of relay D also detect the fault and blocks the trip operation of both CB C and D.

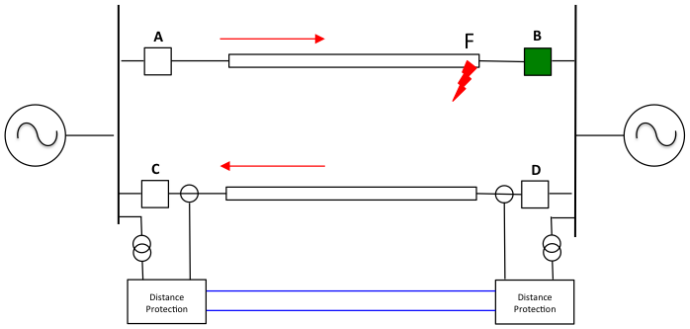

Figure 4.57 Reverse direction of current at healthy line

When CB B opens, the zone 2 protection of relay C begins to reset, while the forward element of relay D picks up due to the reverse in current direction. If the pickup time of relay D is faster than the reset time of relay C, both relay C and D will pickup at the same time and will cause the line between CB C and D to trip. The conditions usually happen when the transfer trip function is used in the protection scheme.

In this section, the performance of distance relay for evolving faults and current reversal conditions are analyzed. The simulations are performed on a long parallel transmission network (100 km). The evolving faults are simulated by varying the initiation time of the first and the second faults. The time differences between fault initiation are: 10 ms, 30 ms, and 200 ms. Two fault locations inside the protection zone 1 are also considered in the simulation: 0% and 70% of the transmission line length. In summary, total 41 cases are simulated for the evolving faults. Furthermore, one current reversal condition is also simulated. A detailed explanation on how to simulate the current reversal in ATP-EMTP is given in the next section.

4.6.2 The network model

The transmission networks used in the simulations are according to the parallel line double in-feed benchmark network in the IEC 60255-121 standard. In this network, The CT and VT are considered as ideal transformers, and the transmission line capacitances are neglected. Two types of source impedance are used:

- Homogenous source – S1 ($Z_1 = Z_0 = 1+j30\ \Omega$)
- Non-homogenous source – S2 ($Z_1 = 1+j7\ \Omega$; $Z_0 = 1+j21\ \Omega$)

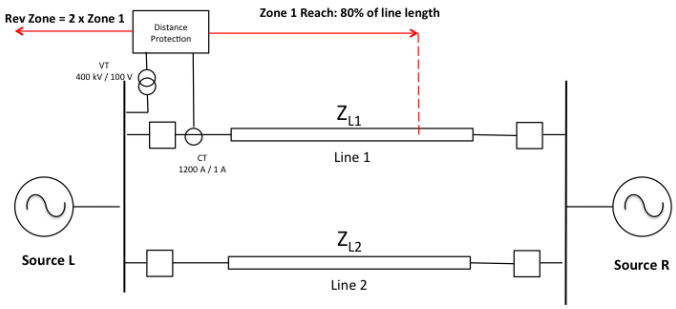

Figure 4.58 Parallel transmission network [1]

In the simulation, the behaviour of the remote and parallel CBs are defined as follow:

- For faults located inside the zone 1 setting (80% of the line), the CBs will open 60 ms after the fault inception (20 ms relay tripping time + 40 ms breaker opening time).
- For faults located outside the zone 1 (>80% of the line), the CBs will open 300 ms after the fault inception.

The parallel network model built in ATP-EMTP is shown in Figure 4.59.

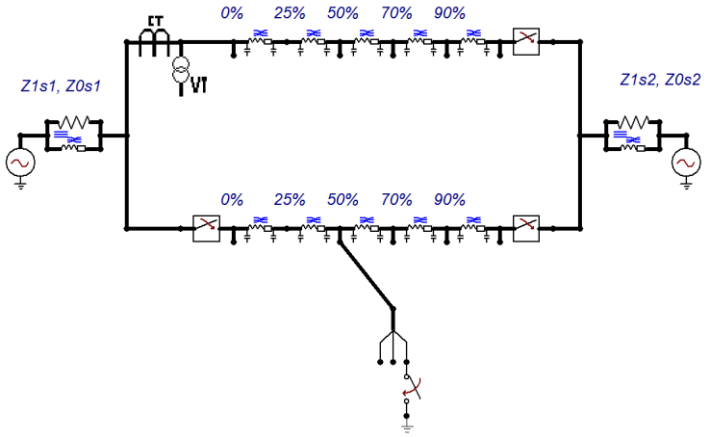

Figure 4.59 Parallel network model

Simulation sequence for the current reversal condition is based on [1]. The simulation sequence in ATP-EMTP is described as follow:

1. The pre-fault load is simulated for both lines (each at 450 MVA). The load current is simulated by setting the initial angle of the source L to13º and the initial angle of source R to 0º.
2. A single phase-to-ground fault (AG) is initiated in Line 2. The AG fault is location at 0% of the transmission line length.
3. The left side CB on Line 2 opens 60 ms after the fault initiation.
4. The right side CB on Line 2 opens 300 ms after the fault initiation.
5. The load continues to flow in line 1 (900 MVA).

For the evolving faults cases, two fault models are considered in the simulations [1]:

1. Evolving faults only in Line 1
   In this case, two fault models are built: AG-to-ABG and AG-to-ABC. The closing time of each switch phase (A, B, and C) is varied to obtain the desired fault characteristic.
2. Evolving faults in Line 1 and 2 (cross-country fault)
   In this case, two faults occur at the same time in the network with different fault type at each of the lines. The closing times of the faults are varied to obtain different fault characteristics.

4.6.3 Analysis of the simulation result

The total simulation time used is 800 ms, with pre-fault duration around 100 ms, and solution time step 5 µs. The voltage and the current during current reversal are shown in Figure 4.60. It can be seen that once the AG fault (at line 2) is initiated at around 100 ms, the phase A voltage suddenly drops to zero, while the phase A current increases to the maximum fault current. The opening of left side at line 2 affects the fault currents as can be seen in the discontinuity of the shape of the current waveforms in all three phases.

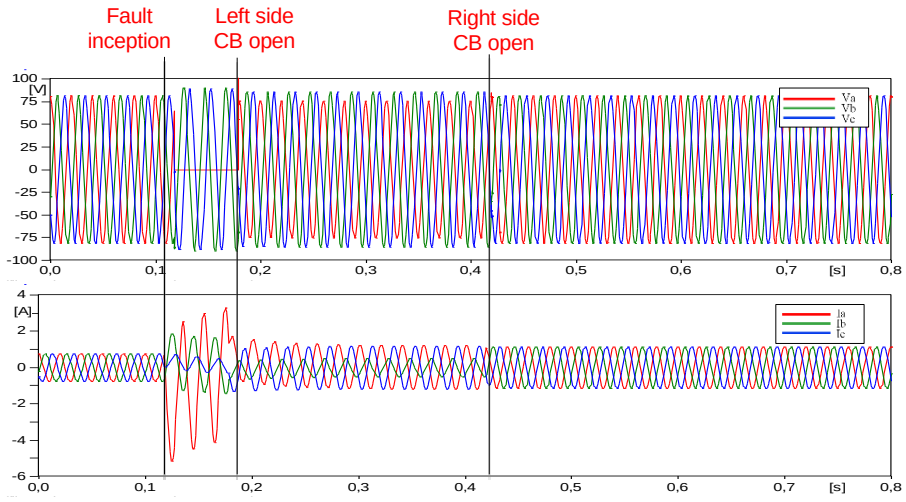

Figure 4.60 Secondary voltages and currents for current reversal in parallel line

Further analysis using the impedance plane shows the impedance trajectory during current reversal as illustrated in figure 4.61. During the first three cycles (when the fault is occurring at line 2), the impedance trajectory is located in the reverse protection zone (zone 3). Further on, after the left side CB at line 2 opens, the impedance moves towards the forward zone. However, the trajectory of the impedance does not enter the zone 1 protection.

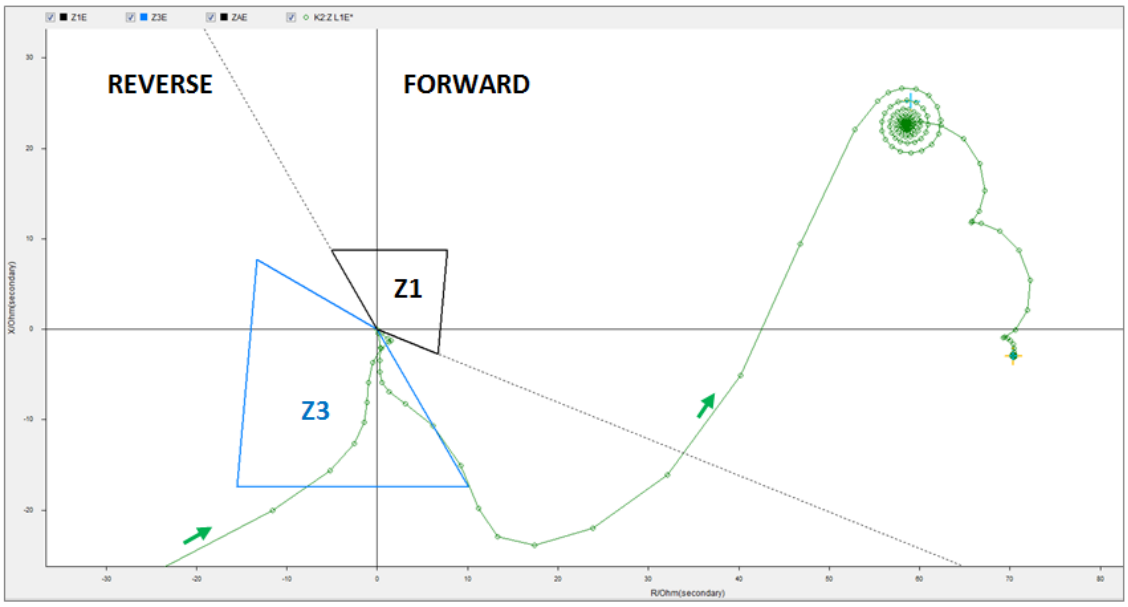

Figure 4.61 Impedance trajectories of A-E loop for current reversal test

The shape of the voltage and the current for an AG fault that evolve to an ABC fault at line 1 are shown in Figure 4.62. It can be seen that after the fault initiation, the phase A current jumps from zero to the maximum peak value and 1.5 cycles (30 ms) later, the currents are starting to flow in the other two phases (B and C) as the ABC fault is initiated.

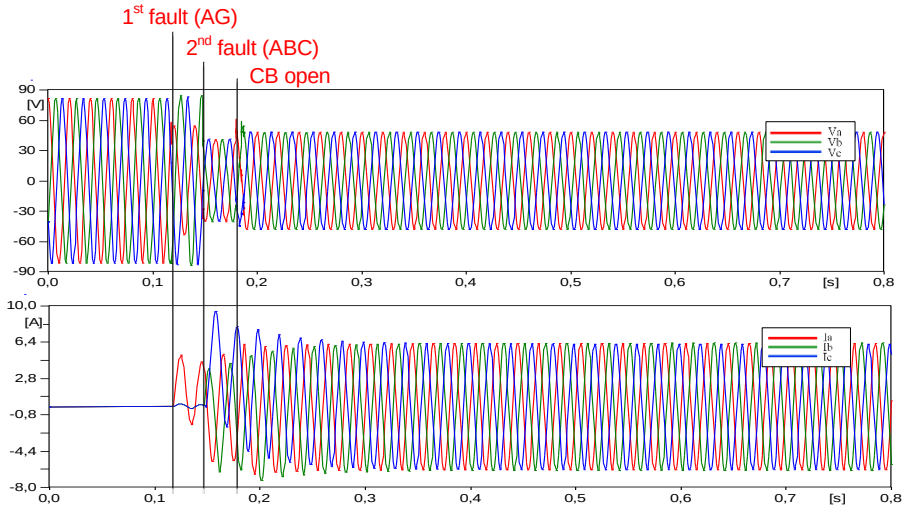

Figure 4.62 Fault signals of AG fault evolves to ABC fault (time difference 30 ms)

An analysis using the impedance plane shows the impedance trajectory of the evolving fault. Because of the shape of the voltage and current, the measured impedances for each phase are different both in its shape and direction as observed in the impedance plane. However, all the impedances of three phases enter the zone 1 characteristic and converge into the impedance value after some time.

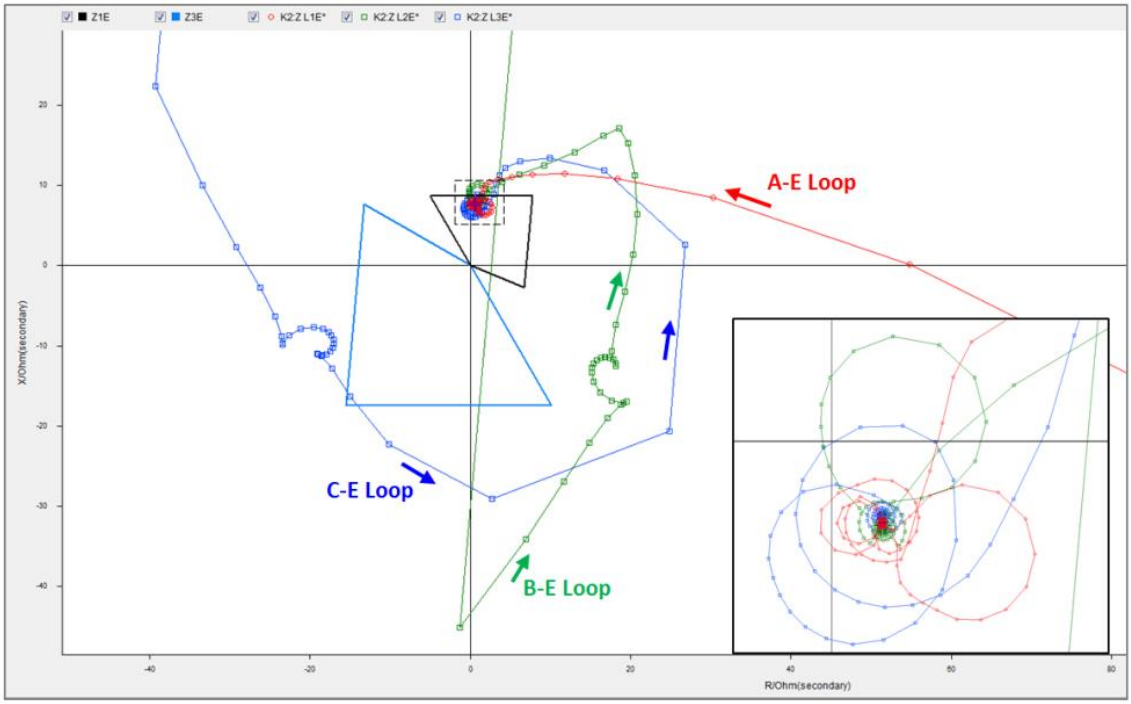

Figure 4.63 Impedance trajectories AG fault evolves to ABC fault (time difference 30 ms)

Figure 4.64 shows the voltage and current of a cross-country fault. In this case, an AG fault located at line 1 is followed by a BG fault at line 2 after 30 ms.

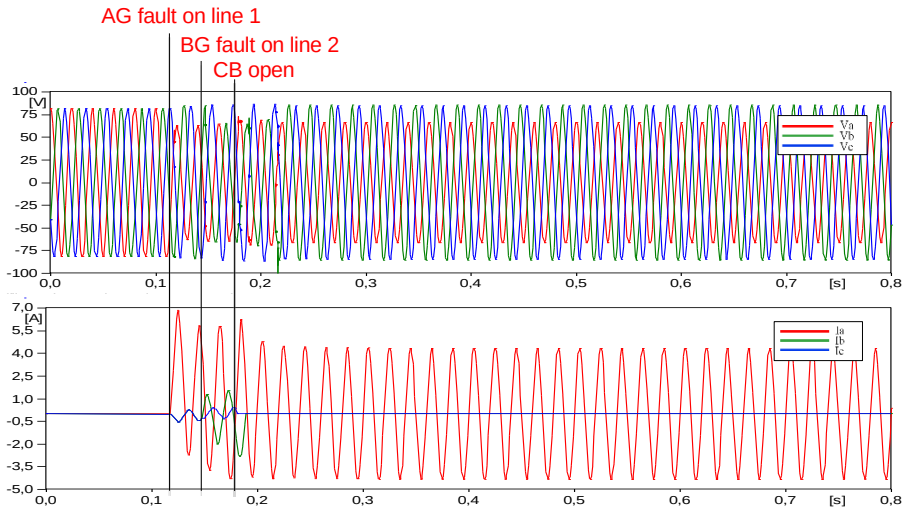

Figure 4.64 Fault signals of AG fault at line 1 followed by BG fault at line 2 (time difference 30 ms)

An analysis using the impedance (R-X) plane shows the impedance trajectory of the fault as shown in Figure 4.65. In this case, the AE loop is the only impedance loop that enters the zone 1 characteristic.

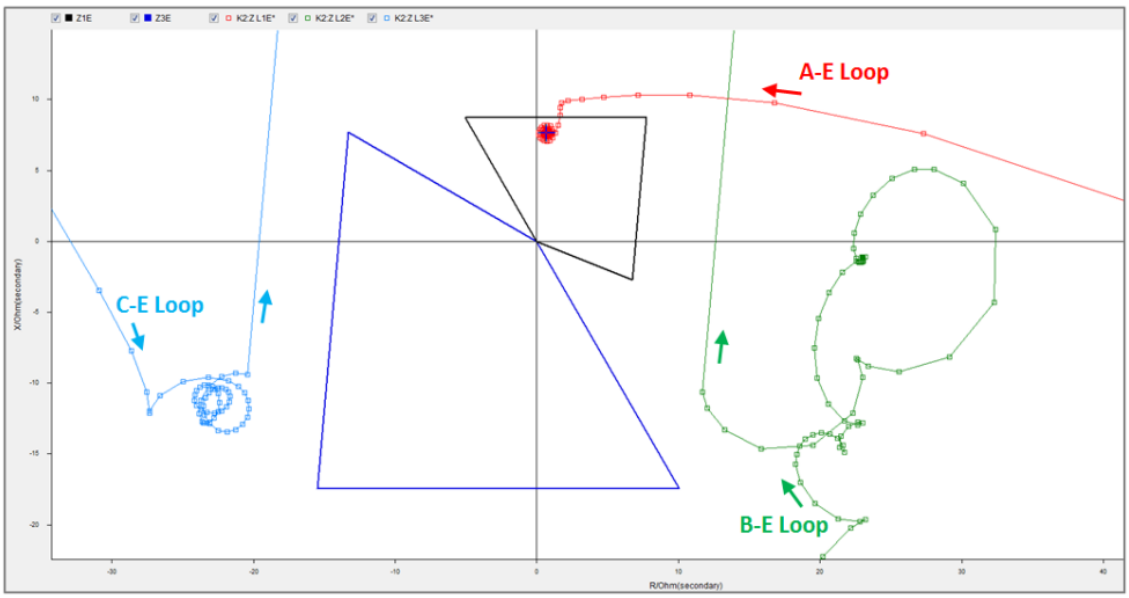

Figure 4.65 Impedance trajectories of AG fault on line 1 evolves to BG fault on line 2 (time difference 30 ms)

4.7 Simulations with the fault arc

4.7.1 Introduction

Most of the faults in overhead transmission lines are single phase-to-ground faults with arcing. Arcing faults are typically caused by lightning strikes that create a flashover on the surface of the string insulators. There are two types of arc on the transmission line: the primary arc and the secondary arc. The primary arc happens during the fault period and is preserved by the high fault current. The primary arc is only removed when the CB isolates the faulty phase. The secondary arc starts when the CB has cleared the faulty phase. In general, the secondary arc

has a much lower current compared with the primary arc, and is removed when the arc path inside the circuit breaker becomes too long to sustain the current flow.

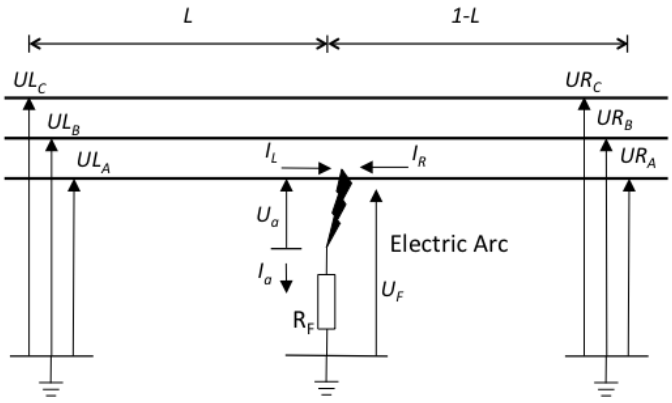

Figure 4.66 Equivalent circuit of single line to ground fault with arc

The arcing fault in transmission network has a non-linear resistance due to the varying arc length. The non-linear resistance causes the voltage and current of the arc to vary non-linearly during the faults. The voltage and current waveforms of a real arc are shown in Figure 4.67 [24].

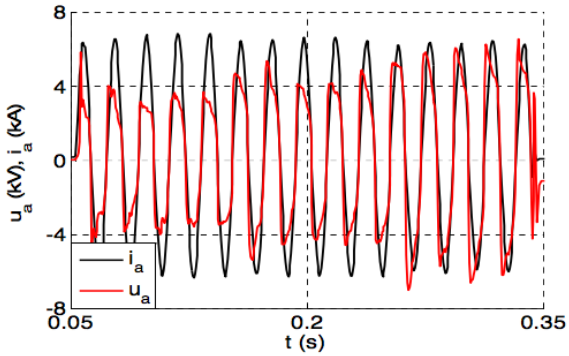

Figure 4.67 Voltage and current waveform of arc [24]

The resistance of arcing faults can be calculated using the following equation [9]:

$$R_A = \frac{2\sqrt{2}}{\pi} \cdot \frac{E_A L}{I} \tag{25}$$

Where,
R_A = Arc resistance (Ω)
L = Arc length (m)
I = Arc current (A)
E_A = $950 + \frac{5000}{I}$ (V/m)

An arcing fault creates operation problems of distance relay because it affects the measured impedance by the relay. The most critical situation for the operation of distance relay arises when an arcing fault occurs near the end of the impedance reach setting (for example 80% of the transmission line). In this case, there are high possibilities that the distance relay mis-

operates and causes an overreach or underreach operation due to the non-linear resistive components.

In this section, the performance of distance relay under arcing faults is studied using a series of test cases. The simulations are performed on the short transmission line with double in-feed. The arc model used in the simulation is developed by [10]. The detail explanation about the arc model is given in the next section. Several arcing faults located near the zone 1 impedance setting are defined to test both the security and the dependability of distance relay. In summary, total 18 test cases are performed in the simulation as shown in Table 4.9.

Table 4.9 Fault parameters for arc fault test

Case	Fault position (Percentage of network length)	Fault type	Fault inception angle (°)	Total
Security test	85,90	A-G	45	9
Dependability test	75, 80	AG	45	9

4.7.2 The arc model

The arc model in ATP-EMTP is developed by [10] and is based on a mathematical model by Kizilcay and Pniok [11]. The model consists of the primary and the secondary arc. The equations for the primary can be described as follow:

$$\frac{dg}{dt} = \frac{1}{\tau_0} G \tag{26}$$

$$G = \frac{i_{arc}}{(u_0 + r_0 |i_{arc}|) \cdot l_0} \tag{27}$$

Where,
G = stationary arc conductance
g = time varying arc conductance
τ_0 = initial time constant of the arc
u_0 = characteristic arc voltage (V/cm)
r_0 = characteristic arc resistance (mΩ/cm)
i_{arc} = arc current
l_0 = initial arc length (cm)

The secondary arc starts after the CB clears the faulty phase. The secondary arc is explained by the following equations:

$$\frac{dg}{dt} = \frac{1}{\tau} (G - g) \tag{28}$$

$$G = \frac{i_{arc}}{(u_0 + r_0 |i_{arc}|) \cdot l_{arc}} \tag{29}$$

$$l_{arc} = (v_l \cdot t + 1) \cdot l_0 \tag{30}$$

$$\tau = \tau_0 - v_\tau \cdot (l_{arc} - l_0) \tag{31}$$

The secondary arc extinction limit is defined by:

$$\frac{g_{min}}{l_{arc}} = 0.25\ \mu mho/cm$$
$$\frac{max\left\{\frac{d\tau}{dt}\right\}}{l_{arc}} = 64\ k\Omega/(s.cm)$$

Based on the equations for primary and secondary arcs, the complete arcing fault model is developed using the MODELS language in ATP-EMTP as displayed in Figure 4.68 [10]:

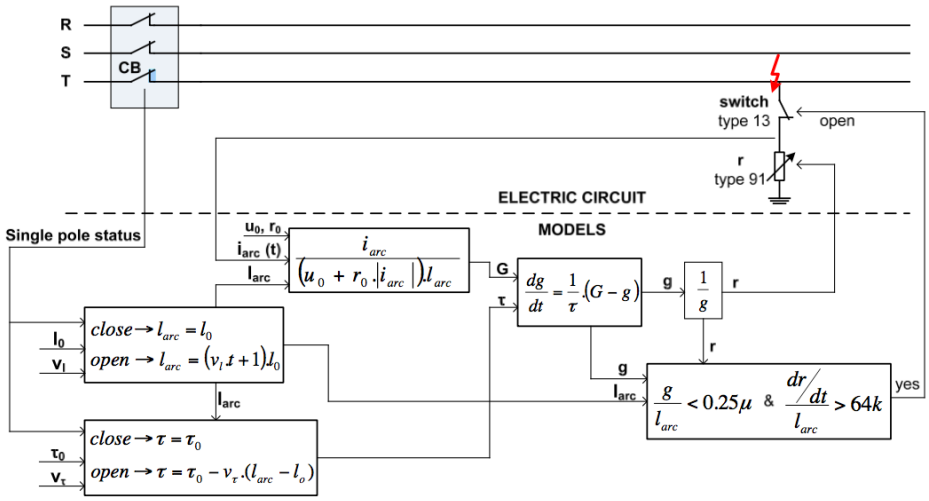

Figure 4.68 Fault arc models in ATP-EMTP [10]

Network model with an additional arc is built in ATP-EMTP as shown in Figure 4.69. In the simulation, the fault inception angle is set to 45°.

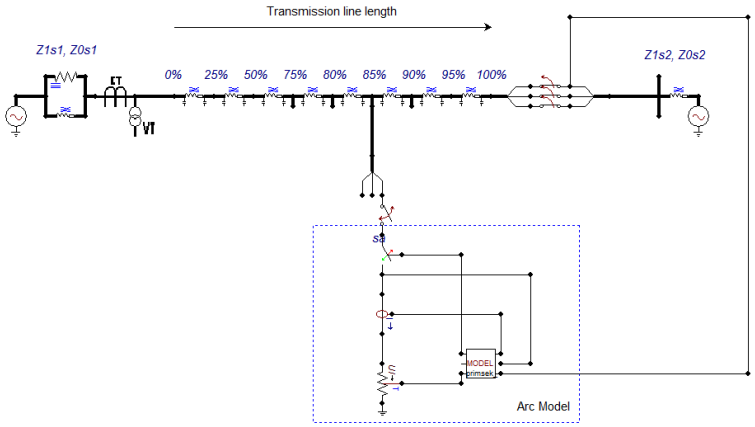

Figure 4.69 Transmission network with fault arc model in ATP-EMTP

4.7.3 Analysis of the simulation results

The essential characteristics of an arcing fault are shown in Figure 4.71. It can be observed that the voltage, current, and conductance of the arc are different for various arc stages. The arc voltage during the primary arc period represents the short circuit voltage of the system. It can be seen that the voltage during this period is much smaller than the nominal voltage. Moreover, the primary arc occurs for 60 ms and extinguished after the remote-end CB clears

the faulty phase. As soon as the remote-end CB opens, the secondary arc stage begins. In this period, the arc voltage increases because of the decreased arc current.

Further analysis shows that due to the lower resistance during the primary arc period, the current in this stage is much higher compared to the current of the secondary arc. The other characteristic of an arcing fault is the time-varying conductance. It can be seen that the conductance values are varying in time. As a result, the arc produces harmonics components that can alter the shape of the voltage.

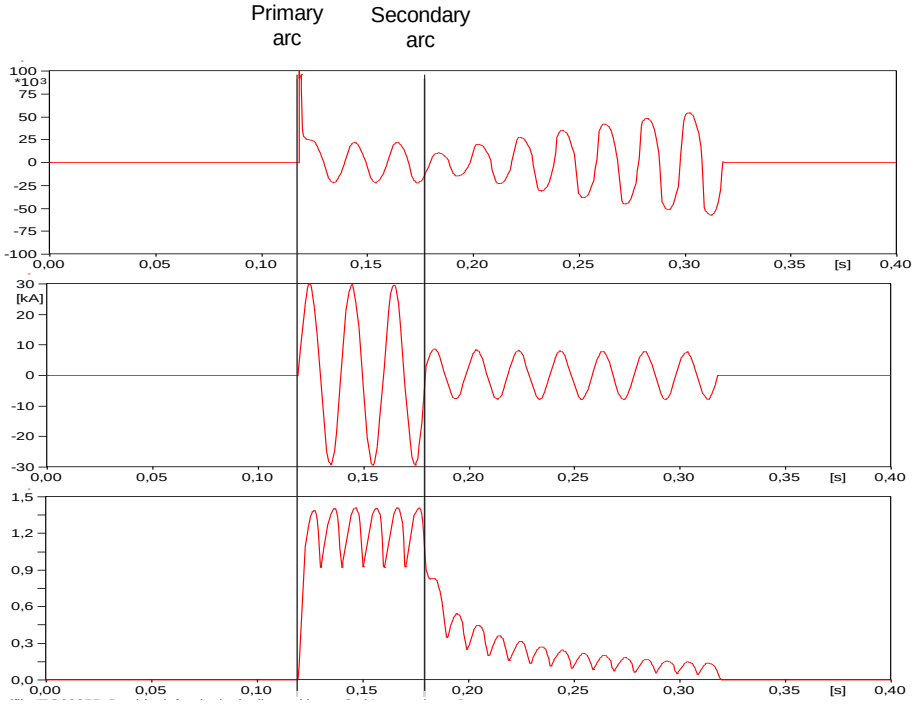

Figure 4.70 Arc voltage, current, and conductance of the arc

The critical stage of distance relay operation is when the primary arc occurs. During this period the relay must detect the fault and send a signal to open the circuit breaker. The shape of the voltages and currents measured by distance relay during an arcing fault are shown in Figure 4.72. When an AG fault is initiated at around 100 ms, the phase A current jumps from the load current the peak fault current, while the phase A voltage suddenly drops to a much smaller magnitude.

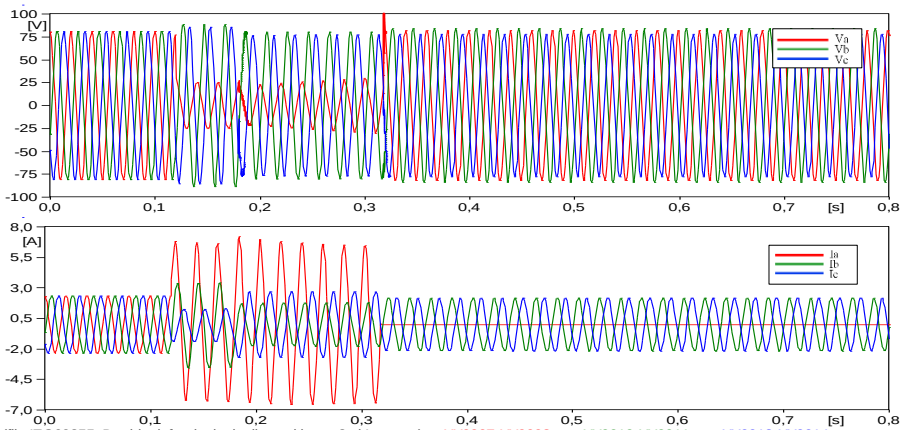

Figure 4.71 Secondary voltage and current for AG fault at 75% of transmission length

The analysis using impedance (R-X) plane shows the time varying impedance during arcing faults. In both the exporting and the importing load cases, the impedance trajectories enter the protection zone after the fault initiation. However, the trajectory is slightly tilted upward and moves to the outside of zone 1 characteristic in the case of importing load, while for the exporting load, the trajectory lies in the reactance line setting. Due to the time varying resistance of arcing faults, it can be observed that the fault trajectory has the “curl” shape in the impedance plane.

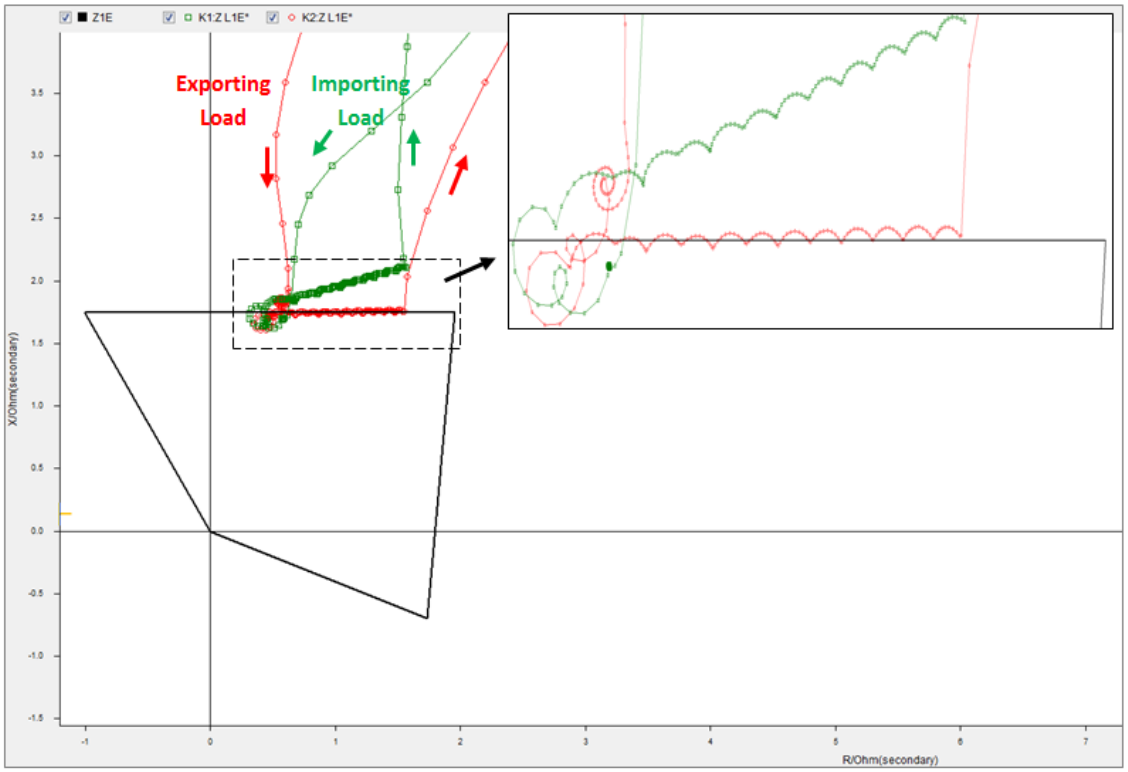

Figure 4.72 Impedance trajectory A-E loop for AG fault at 80% of transmission length

5 Dynamic Test Results

5.1 Introduction

The dynamic tests are performed based on the test methodology described in Chapter 3. For all the test cases, the voltage and current from the simulation results of chapter 4 are injected into physical distance relays. Total 5898 test shots are performed. For each test shots, distance protection response such as tripping time is recorded in the test library.

Two distance protections from the different manufacturers are tested: distance relay M and N. Both distance relays are numerical relays used for protection of HV and EHV transmission line. Distance relay M has six protection zones, which can be set to forward, reverse, and non-directional. It uses 32-bit microprocessors with highly integrated components and 20 samplings per power frequency cycle. The shortest tripping time is 17 ms for 50 Hz systems.

Distance relay N is used for the protection, control, and monitoring of HV overhead lines and cables in solidly earth networks. It has five protection zones with fully independent measurements and settings. Relay N has a sampling frequency of 5000 Hz at 50 Hz systems and a typical operating time of 25 ms.

5.2 Test with decaying dc-offset

Test results for decaying dc-offset are presented in the source impedance ratio (SIR) diagram. In the SIR diagram, the average operating times for four fault types (LN, LL, LLN, and LLL) are shown as a function of the fault position and the source impedance ratio.

Figure 5.1 and 5.2 show the average operating time of relay M and N for LN faults. It can be seen that as the fault distance increases, the average operating times of both relays are delayed. This characteristic is similar for the short and the long transmission networks. In the case of relay M, the tripping times for the faults located at 0% of the zone 1 setting are constant at 20 ms for all the SIR values. While, for the same fault location, the tripping time of relay N is gradually delayed with the increasing of SIR values.

In figure 5.1, it is shown that the operating times of relay M are sharply increased for the faults located at more than 80% of the zone 1 setting. Furthermore, in the case of SIR 50, the operating time is significantly delayed for faults located after 50% of the zone 1 setting. The operating time delay is due to the lower fault current and voltage measured by the relay. In general, relay M has a fast operating time for faults located at 0% of the zone 1 setting and a significant operating delay for faults located beyond 50% of zone 1 setting.

Similar operating delay characteristic can be observed for relay N in Figure 5.2. However, relay N seems to have a *less steep* operating delay compared to the relay M. The same significant delay is found on relay N for the SIR 50. In this case, the operating time is significantly delayed for faults located beyond 80% of the zone 1 setting. Moreover, the operating time for the SIR 50 can be delayed up to 52 ms for faults located at 95% of the zone 1 setting.

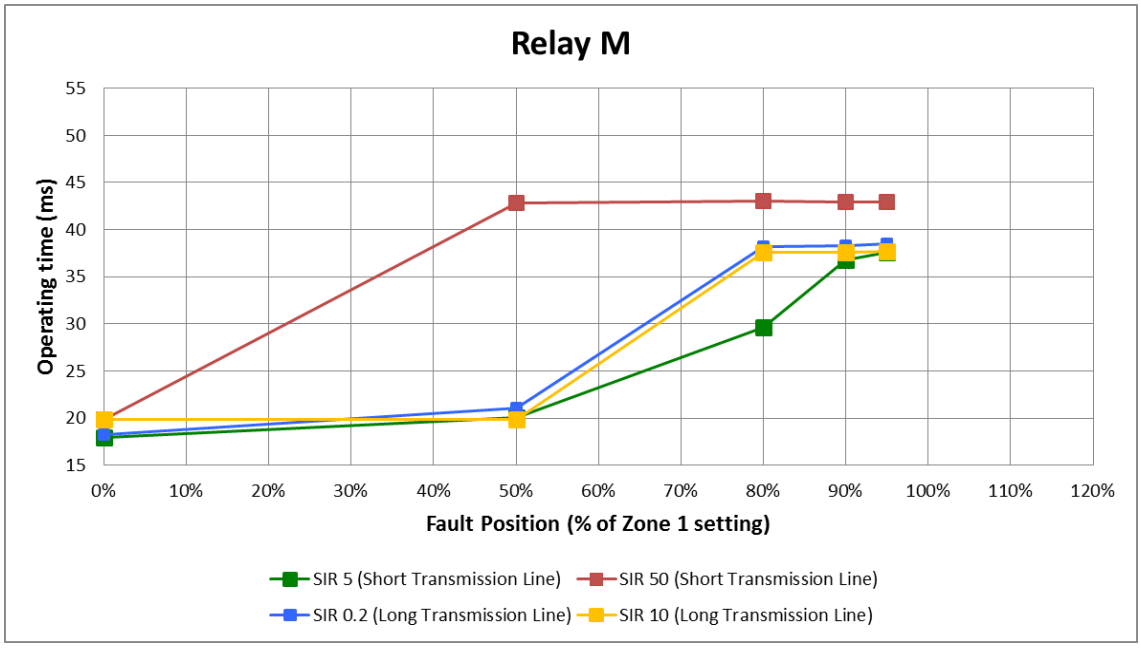

Figure 5.1 Average operating time for LN fault - Relay M

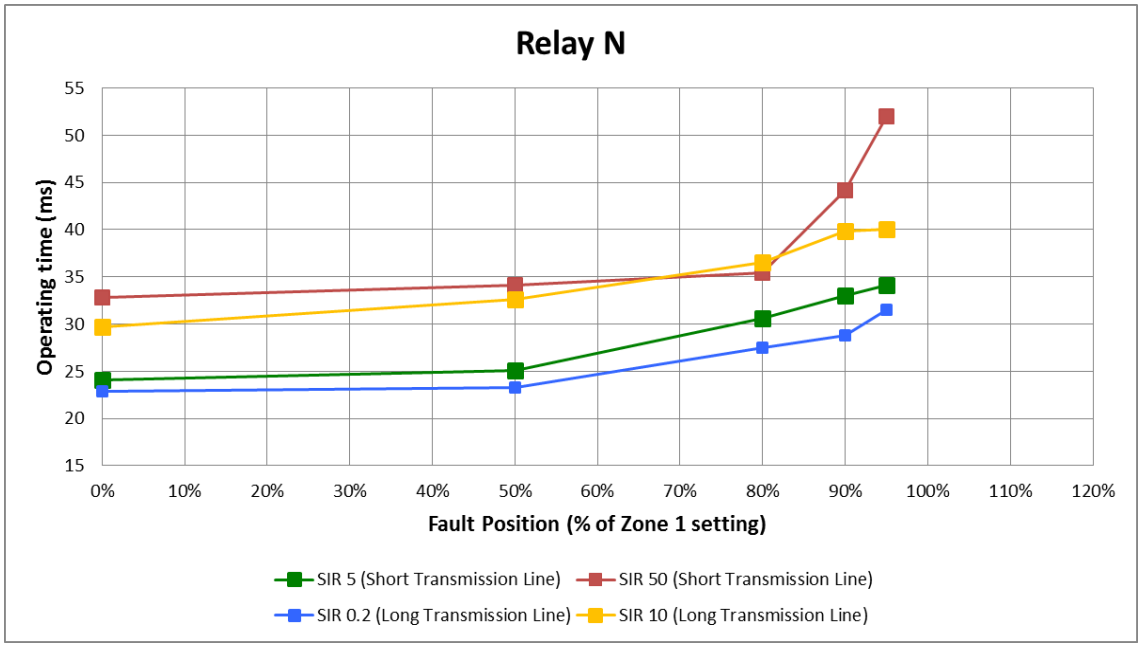

Figure 5.2 Average operating time for LN fault - Relay N

Figure 5.3 illustrates the average operating time of relay M for LL faults. The operating time characteristic is relatively similar with the LN faults. However, in the case of LL faults, the operating times for the faults located at 0% of the zone 1 setting are varied with different SIR values. It is also seen that for the faults beyond 50% of the zone 1 setting, the operating time can be delayed up to 20 ms. Furthermore, it is seen that the operating times for faults located at 50% of the zone 1 setting are slightly faster than the faults at 0% of zone 1 setting.

In the case of relay N, the operating time for the SIR 10 is slightly slower than the SIR 50 for the faults located at 0% to 90% of the zone 1 setting as shown in figure 5.4. In general, relay N also has a *less steep* delay characteristic for LL faults compared to the relay M.

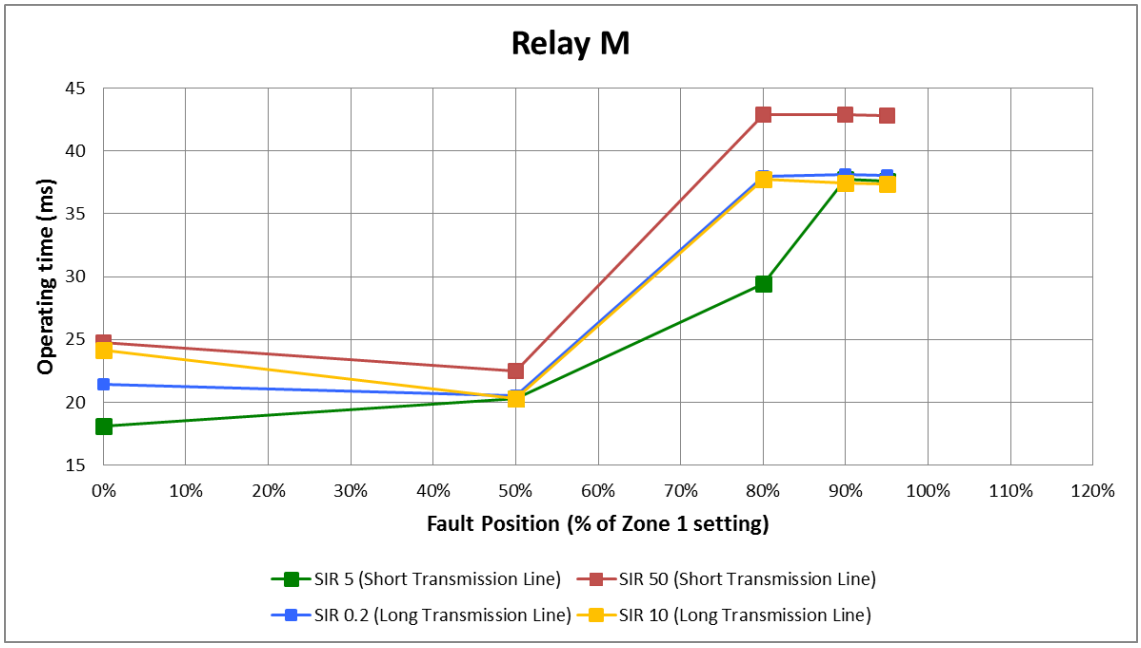

Figure 5.3 Average operating time for LL fault - Relay M

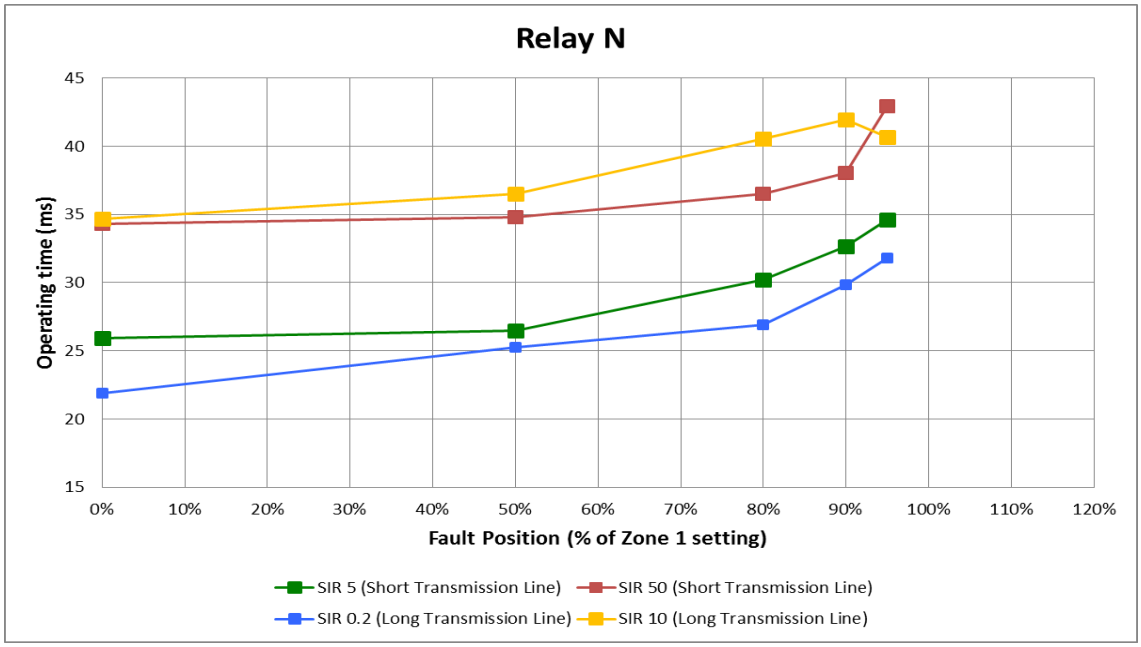

Figure 5.4 Average operating time for LL fault - Relay N

The operating time of relay M and relay N for LLN faults are illustrated in Figure 5.5 and Figure 5.6, respectively. For the relay M, a significant time delay can be observed for faults located at 80% of the zone 1 setting. In this case, the operating time is delayed up to more than three cycles (60 ms) for the SIR 50. For the other SIR values, the delays are found to be less than one cycle (20 ms). In the case of relay N, it is found that the tripping time characteristic is relatively similar with the previous faults (LN and LL).

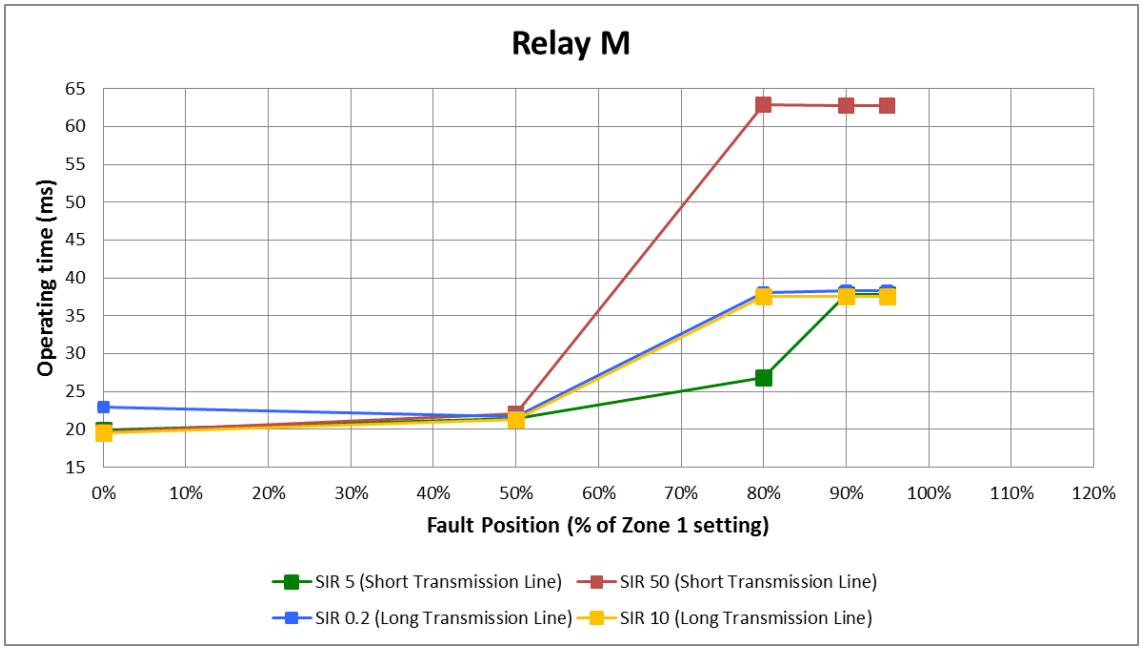

Figure 5.5 Average operating time for LLN fault - Relay M

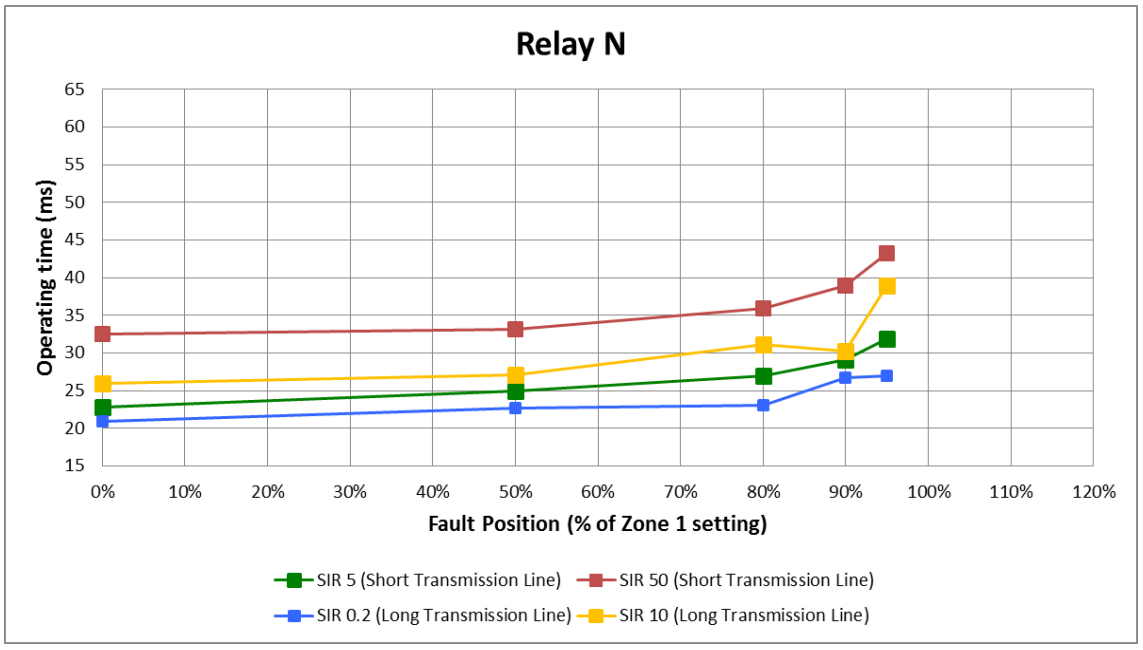

Figure 5.6 Average operating time for LLN fault - Relay N

Figure 5.7 shows the operating time of relay M for three-phase faults. For the faults located at 0% of the zone 1 setting, relay M operates slower for the SIR 0.2 compared to the other SIR values. However, for the faults in the middle of zone 1 setting (50%), it can be observed that the operating time are relatively stable for all SIR values. In this case, the operating time is in the range of 20 – 25 ms. The graphs also show the delayed tripping time for the faults located beyond 80% of the zone 1setting for all the SIR values.

The operating time characteristic of relay N during LLL faults is illustrated in Figure 5.8. The graph shows the delayed operating time especially for the SIR 50. It is seen that for the faults located at 95% of the zone 1 setting, the operating time is delayed up to 49 ms. However, the

characteristic seems to be different for the other SIR values as the delays are found to be less than 10 ms.

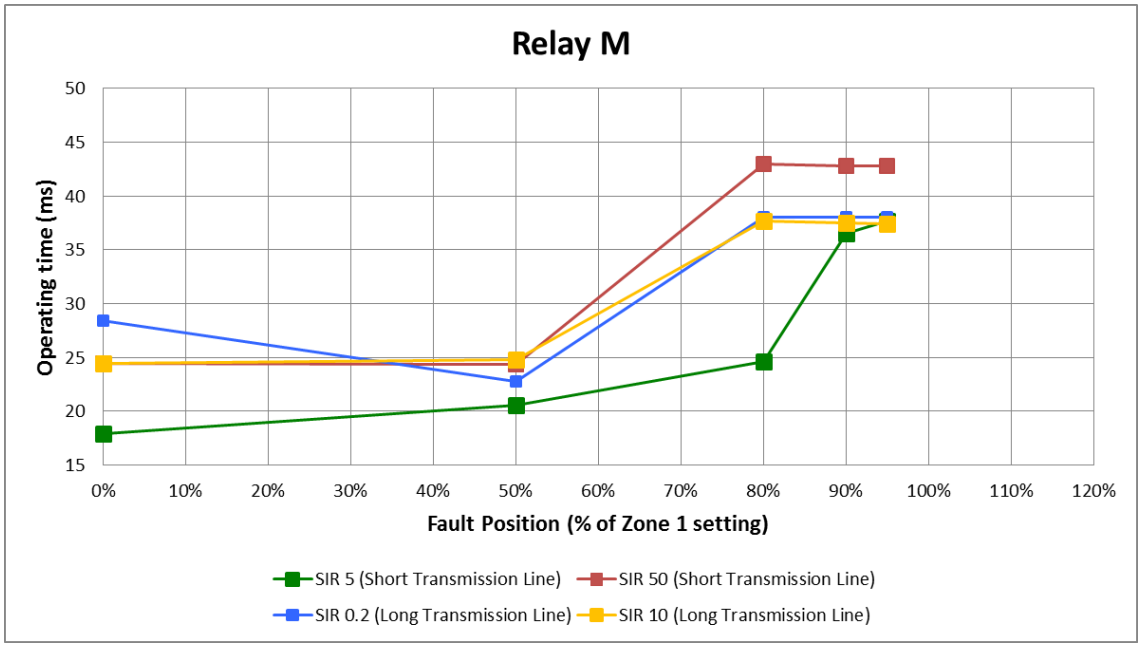

Figure 5.7 Average operating time for LLL fault - Relay M

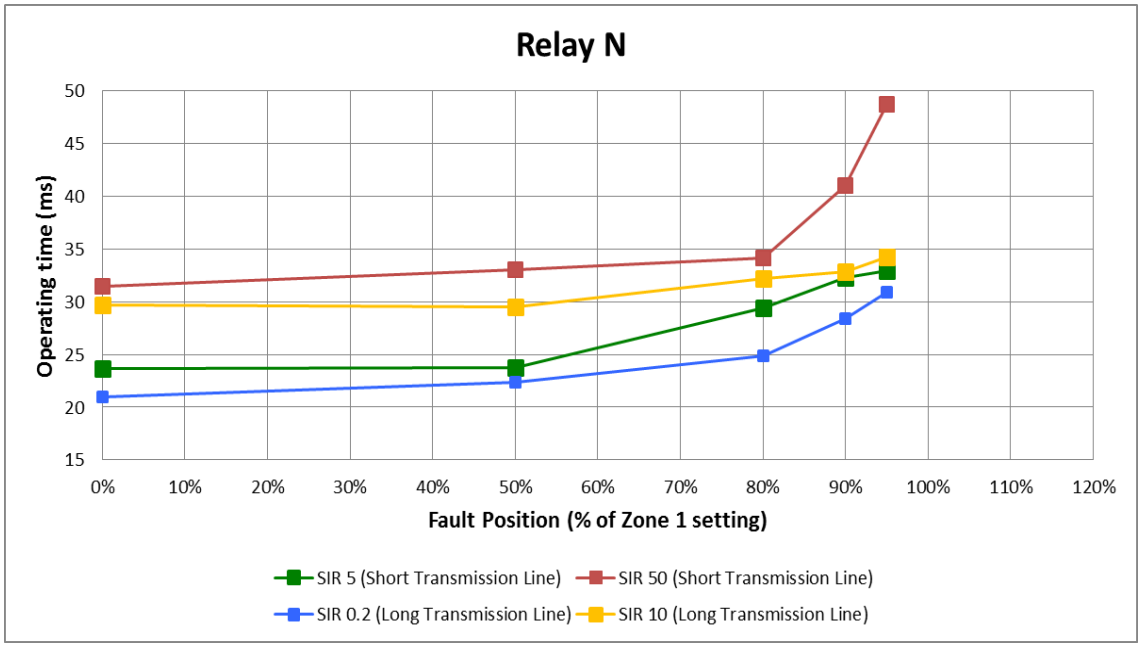

Figure 5.8 Average operating time for LLL fault - Relay N

Results Discussion

Based on the test results, some interesting findings regarding distance relay performance are presented as follow:

Faults located close to distance relay vs faults at the end of zone-1 reach

The tripping times for the faults located at the end of zone-1 setting (95%) are much slower compared to the faults close to the distance relay (0%). Test results show the average tripping time difference of 18.9 ms and 10.1 ms, for relay M and N, respectively. Furthermore, the maximum tripping time difference can be up to 43.2 ms for Relay M and 19.2 ms for Relay N.

High source impedance ratio (SIR)

Both distance relays operate slower in the system with very high source impedance ratio (SIR). This characteristic is particularly true for faults that occur at the end of zone-1 reach (95%). The average tripping time for the systems with low source impedance ratio (0.2, 5, and 10) are: 30.2 ms for relay M and 31.3 ms for relay N. However, when applied to the systems with high source impedance ratio (50), both distance relays operate much slower: 38.7 ms for Relay M and 38.2 ms for Relay N.

Types of the fault

Test results show that the fault types do not have major effects on the tripping time. The average tripping times for each fault types are summarized below:

Fault type	Relay M	Relay N
LN fault	32 ms	32.9 ms
LL fault	31.6 ms	33.3 ms
LLN fault	34.3 ms	29.7 ms
LLL fault	32.1 ms	30.8 ms

Transient overreach

In terms of the reach accuracy, both distance relays have no transient overreach issues. The test results show that both distance relays do not trip for the faults located outside of the protection zone (105% and 110% of the zone-1 setting).

5.3 Test with CVT transient

The test results for the transient error of CVT are also presented in the SIR diagram. The average operating time of distance relay is shown as a function of the fault position, the fault type, and the source impedance ratio.

Figure 5.9 illustrates the operating time of relay M with the CVT. It is seen that relay M operates much faster for the network with SIR 5, and this characteristic applies for all the fault types. In the case of faults located at 0% of the zone 1 setting, the operating time for the SIR 5 is around one cycle (20 ms), while for the SIR 50, the operating time is delayed up to two cycles (40 ms). Also, it can be observed that for the LLN faults with SIR 50, relay M is significantly delayed for the faults located beyond 80% of the zone 1 setting. In this case, the operating time is delayed up to more than three cycles (60 ms). Moreover, relay M seems to have a problem to operate fast for the LL faults located at 95% of the zone 1 setting.

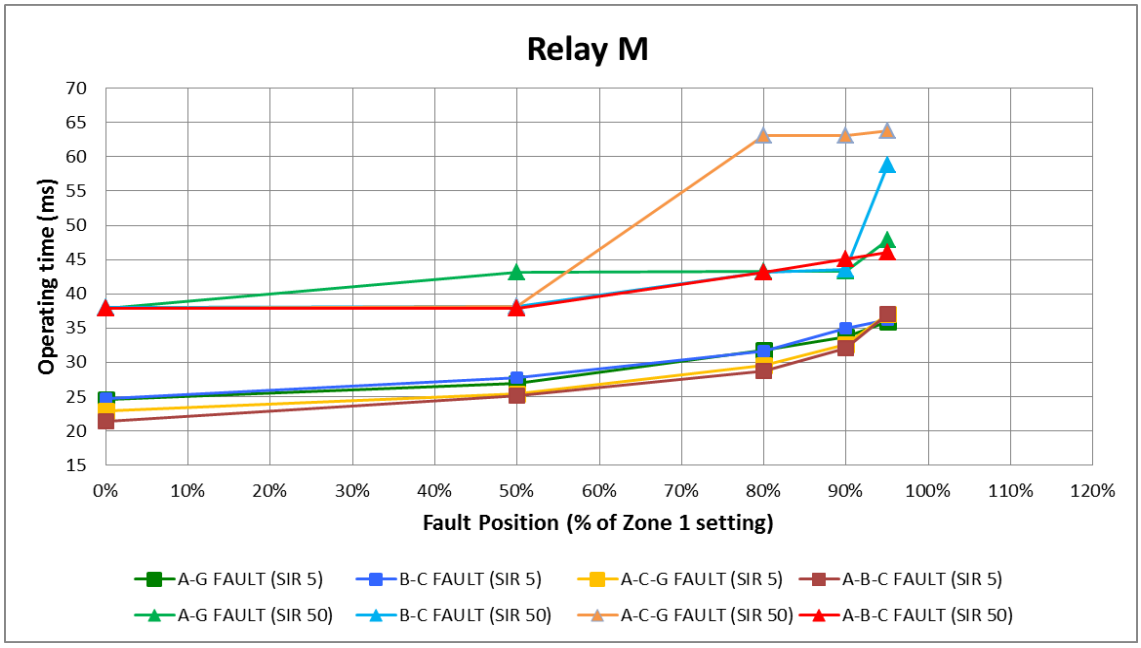

Figure 5.9 Average operating time with CVT - Relay M

The operating time of relay N with the CVT is shown in Figure 5.10. The graphs show the similar delay characteristic with relay M. For the faults located at 0% of the zone 1 setting, relay N trips after 25 ms for the SIR 5, and around 45 ms for the SIR 50. However, for the faults located at 95% of the zone 1 setting, the operating time are delayed up to more than 60 ms for the SIR 50, while for the SIR 5 the tripping times are slightly delayed to 30 ms.

To sum up, the CVT transient causes a significant time delay for both relays, especially for the system with SIR 50. The operating time delay applies for all the fault types.

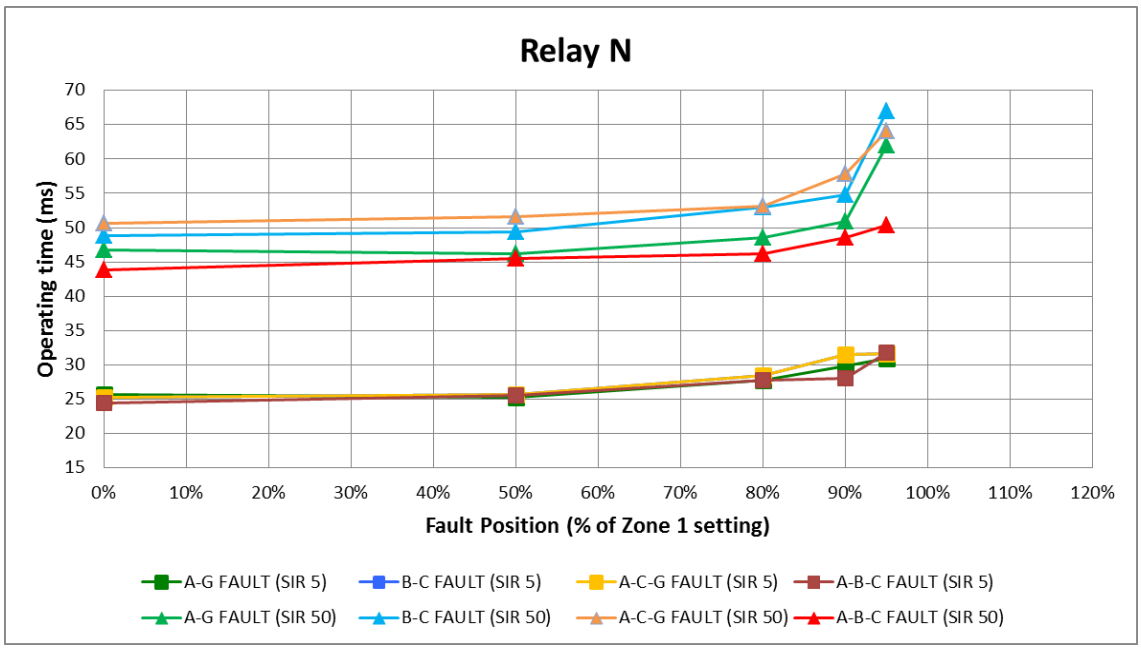

Figure 5.10 Average operating time with CVT - Relay N

Results Discussion

The performance of distance relay with the CVT can be summarized as follow:

Operating time for fault located close to relay location (with high SIR)

The CVT transient seems to cause significant tripping delays for both distance relays. In the case of high SIR (50), the average tripping times for the faults close to the relay location are 30.6 ms for relay M and 36.3 ms for relay N. The tripping times are much slower compared to the average tripping time without the CVT, which is found to be 20.33 ms for relay M and 28.4 ms for relay N.

Types of the fault

Similar to the previous test results, the fault types do not have major effects on the tripping of the relay. However, in the case of the CVT, the average tripping times for each fault types are slightly slower compared to the test cases without the CVT.

Fault type	Relay M	Relay N
LN fault	36.9 ms	39.4 ms
LL fault	37.7 ms	41.6 ms
LLN fault	41.4 ms	42 ms
LLL fault	35.4 ms	37.2 ms

Transient overreach

In terms of the reach accuracy, both distance relays have no transient overreach issues caused by the CVT. The test results show that the relays did not trip for faults located on the outside of zone 1 setting.

5.4 Test with superimposed harmonics

Figure 5.11 shows the average operating time of relay M for faults with superimposed harmonics. The voltage and current superimposed with harmonics order from the fifth to tenth harmonics are injected into the relay.

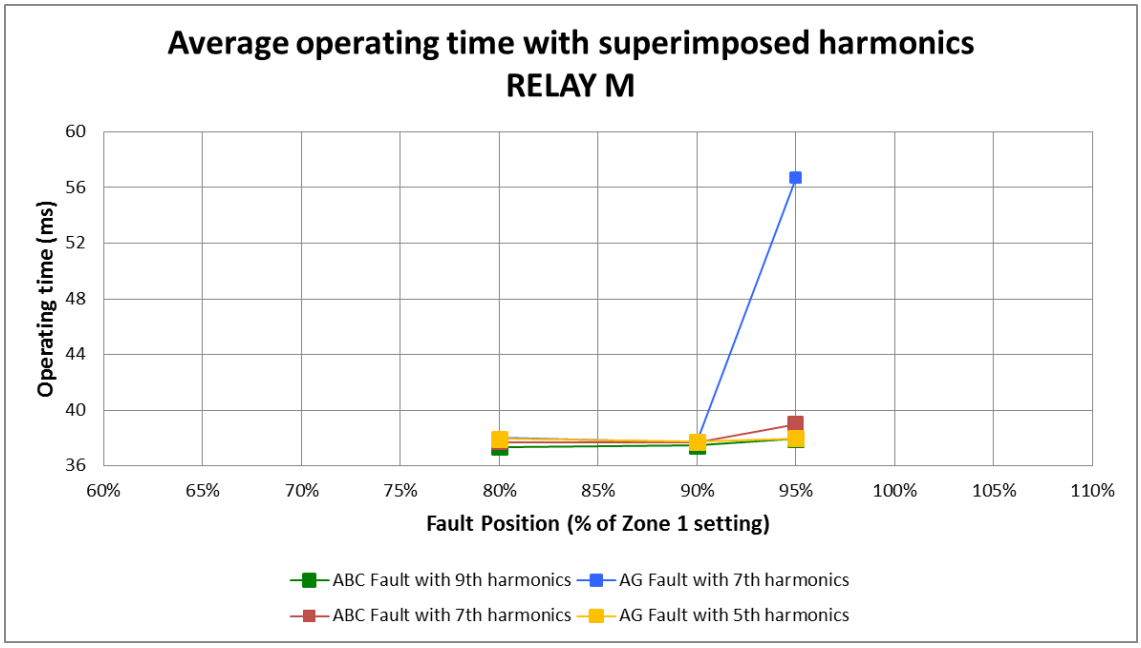

Figure 5.11 Average operating time with superimposed harmonics

Results Discussion

Delay in tripping time

Compared to the previous cases where there is no superimposed harmonics in the voltage and current signals, the tripping time of the relay is relatively similar and there is no significant time delay found. Moreover, the average tripping time with superimposed harmonics is 38.3 ms.

However, this is not the case when relay M was tested using LN faults with seventh harmonics. It is shown that the seventh harmonics seems to cause a significant time delay of around one cycle. The average tripping time for LN faults with the seventh harmonic is 56.7 ms.

Transient overreach

The accuracy of relay M is not affected by the superimposed harmonics as there was no transient overreach found in the test. The digital filtering used in relay M seems to be able to extract the fundamental frequency component correctly from the distorted waveforms. However, the filtering process produces a significant operating time delay for the seventh harmonics.

5.5 Test with transient frequency deviation

The average operating time of relay M with the transient frequency deviation is illustrated in Figure 5.12. For all the frequency variations, relay M trips less than one cycle in the case of faults located at 0% of the zone 1 setting. Moreover, the operating times are delayed up to around 35 ms for the faults at 95% of zone 1 setting, and the delay characteristic applies for all the system frequencies.

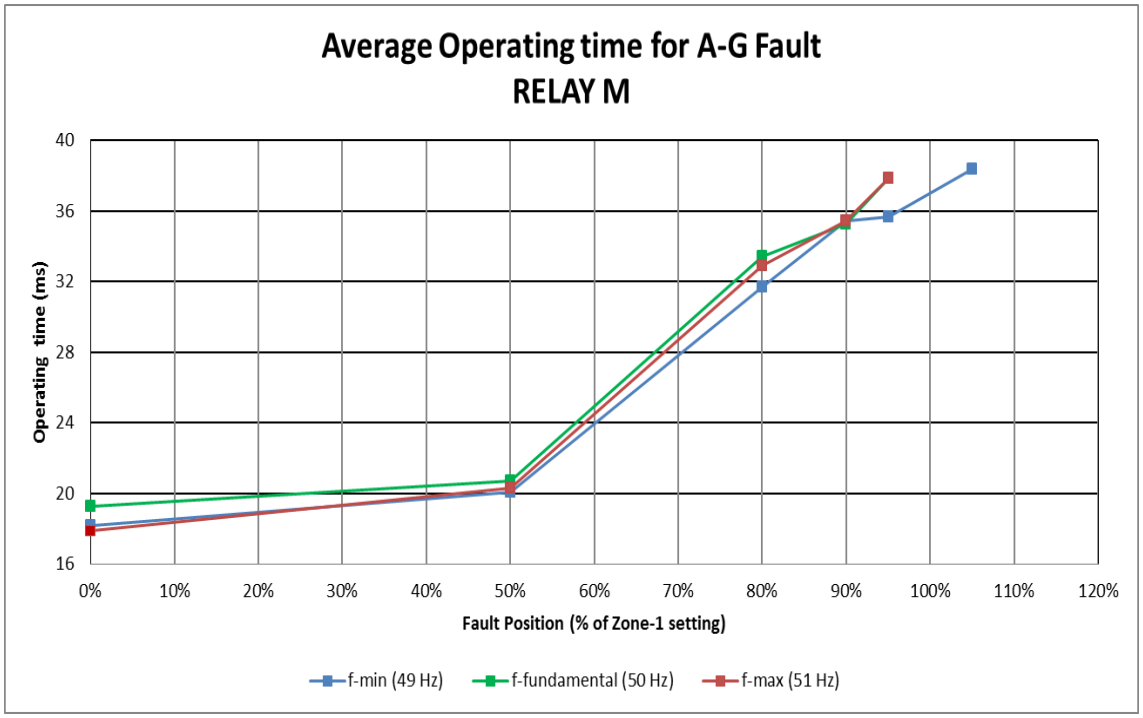

Figure 5.12 Average operating time with transient frequency deviation

Results Discussion

Delay in tripping time

The frequency deviation has negligible effects on the operating time of Relay M. It is found that the maximum time delay caused by the off-nominal frequency conditions is only 0.2 ms.

Transient overreach

The frequency of the system seems to affect the accuracy of relay M. From the test results, it is shown that relay M trips for faults located at 105% of zone 1 setting (overreach). The overreach happens when the minimum frequency (49 Hz) is applied to the relay.

5.6 Test with fault resistance and remote in-feed

Distance relay response to fault resistance (without pre-fault load)

Test results for the fault resistance (without pre-fault load) are presented in Table 5.1. The table compares the tripping time of relay M and N for various system parameters such as fault type, fault location, and network length. In this test, the impedance setting of zone 1 is set to protect from 0% to 80% of the transmission line length.

In the case of the long transmission line (fault no. 1 - 16), both distance relays M and N can detect the faults and operate correctly according to the zone 1 criteria. It can be seen that both relays correctly operate for the faults located inside of the zone 1 (i.e. 0% and 70% of transmission line length). On the other hand, the relays do not operate for the faults located outside of the zone 1 (i.e. -0% and 80%). Moreover, it is shown that for several faults, the operating times of relay N are delayed up to more than four cycles (80 ms), while the relay M shows relatively faster operating time (less than three cycles) for all the faults.

Table 5.1 Test result of fault resistance without pre-fault load

Fault no.	Fault Type	Fault location	Line Type	Zone 1 Criteria	Operating time (ms)	
					Relay M	Relay N
1	A-G	70%	Long	Trip	37,4	87,4
2	A-G	90%	Long	No Trip	-	-
3	A-B	70%	Long	Trip	37,4	86,3
4	A-B	90%	Long	No Trip	-	-
5	A-B-G	70%	Long	Trip	47,5	85,5
6	A-B-G	90%	Long	No Trip	-	-
7	A-B-C	-0%	Long	No Trip	-	-
8	A-B-C	+0%	Long	Trip	17,7	25
9	A-G	70%	Long	Trip	48,1	88
10	A-G	90%	Long	No Trip	-	-
11	A-B	70%	Long	Trip	38,7	28,9
12	A-B	90%	Long	No Trip	-	-
13	A-B-G	70%	Long	Trip	48,2	29,7
14	A-B-G	90%	Long	No Trip	-	-
15	A-B-C	-0%	Long	No Trip	-	-
16	A-B-C	+0%	Long	Trip	28	20,4
17	A-G	70%	Short	Trip	117,9	86,7
18	A-G	90%	Short	No Trip	-	-
19	A-B	70%	Short	Trip	117,9	88,2
20	A-B	90%	Short	No Trip	-	-
21	A-B-G	70%	Short	Trip	117,9	-
22	A-B-G	90%	Short	No Trip	-	-
23	A-G	70%	Short	Trip	117,9	83,5
24	A-G	90%	Short	No Trip	-	-
25	A-B	70%	Short	Trip	37,7	32,2
26	A-B	90%	Short	No Trip	-	-
27	A-B-G	70%	Short	Trip	48	30,3
28	A-B-G	90%	Short	No Trip	-	-

Furthermore, distance relay M and N have problems to operate fast enough in the case of short transmission networks (fault no. 17 – 28). It can be seen that the tripping times are delayed up to more than four cycles (80 ms) for the relay N and almost six cycles (120 ms) for the relay M. It is also observed that in the test case 21 (LLN faults at 70% of the transmission length), relay N fails to operate for a fault located inside the protection zone.

It can be concluded that relay M operates satisfactory only for the long transmission network, while for the short network, its operating times are delayed up to six cycles (120 ms). On the other hand, relay N seems to have a problem to operate quickly for both the short and the long transmission networks.

Distance relay response to fault resistance (with pre-fault exporting load)

The test results for fault resistance with pre-fault exporting load are presented in Table 5.2. The pre-fault exporting load means that the load current flows from the source L to R (in Figure 4.8) or in the same direction with the fault current as seen by the distance relay.

Similar tripping characteristics are shown for the long transmission network (fault no. 29 – 43) compared with the cases without the pre-fault load. It can be observed that both the relays can detect the faults and operate correctly according to the zone 1 criteria. However, the operating time of relay N is also delayed up to four cycles (80 ms) for the long transmission network.

In the case of the short transmission network, relay M and N are significantly delayed in all the cases. It can be observed that the faults at 0% of transmission line length produce the slowest operating time, where both relays are delayed up to more than 15 cycles (300 ms).

Table 5.2 Test result of fault resistance with exporting pre-fault load

Fault no.	Fault Type	Fault location	Line Type	Load Direction	Zone 1 Criteria	Operating time (ms)	
						Relay M	Relay N
29	A-G	-0%	Long	Export	No Trip	-	-
30	A-G	+0%	Long	Export	Trip	47,8	20,1
31	A-G	50%	Long	Export	Trip	20,6	82,5
32	A-G	70%	Long	Export	Trip	38,3	82
33	A-G	100%	Long	Export	No Trip	-	-
34	A-B	-0%	Long	Export	No Trip	-	-
35	A-B	+0%	Long	Export	Trip	18,9	23,3
36	A-B	50%	Long	Export	Trip	27,5	82,3
37	A-B	70%	Long	Export	Trip	37,6	86,2
38	A-B	100%	Long	Export	No Trip	-	-
39	A-B-C	-0%	Long	Export	No Trip	-	-
40	A-B-C	+0%	Long	Export	Trip	18,9	20,7
41	A-B-C	50%	Long	Export	Trip	24,5	22,4
42	A-B-C	70%	Long	Export	Trip	37,8	28,4
43	A-B-C	100%	Long	Export	No Trip	-	-
44	A-G	-0%	Short	Export	No Trip	-	-
45	A-G	+0%	Short	Export	Trip	337,4	324,9
46	A-G	50%	Short	Export	Trip	112,9	86,4
47	A-G	70%	Short	Export	Trip	117,3	86,5
48	A-G	100%	Short	Export	No Trip	-	-
49	A-B	-0%	Short	Export	No Trip	-	-
50	A-B	+0%	Short	Export	Trip	335,6	322,1
51	A-B	50%	Short	Export	Trip	113	86
52	A-B	70%	Short	Export	Trip	116,8	88
53	A-B	100%	Short	Export	No Trip	-	-
54	A-B-C	-0%	Short	Export	No Trip	-	-
55	A-B-C	+0%	Short	Export	Trip	17,8	23,9
56	A-B-C	50%	Short	Export	Trip	24,3	25,8
57	A-B-C	70%	Short	Export	Trip	37,9	28,3
58	A-B-C	100%	Short	Export	No Trip	-	-

Distance relay response to fault resistance (with pre-fault importing load)

The pre-fault importing load means that the load current flows in the opposite direction with the fault current as seen by the distance relay, or the current flows from source R to L. Table 5.3 presents the test results of fault resistance with the pre-fault importing load.

Table 5.3 Test result of fault resistance with importing pre-fault load

Fault no.	Fault Type	Fault location	Line Type	Load Direction	Zone 1 Criteria	Operating time (ms)	
						Relay M	Relay N
59	A-G	-0%	Long	Import	No Trip	-	-
60	A-G	+0%	Long	Import	Trip	19	20,3
61	A-G	50%	Long	Import	Trip	48,2	92,8
62	A-G	70%	Long	Import	Trip	123,3	97
63	A-G	100%	Long	Import	No Trip	-	-
64	A-B	-0%	Long	Import	No Trip	-	-
65	A-B	+0%	Long	Import	Trip	19,3	25,5
66	A-B	50%	Long	Import	Trip	37,9	82,1
67	A-B	70%	Long	Import	Trip	38,3	86,7
68	A-B	100%	Long	Import	No Trip	-	-
69	A-B-C	-0%	Long	Import	No Trip	-	-
70	A-B-C	+0%	Long	Import	Trip	17,4	22,2
71	A-B-C	50%	Long	Import	Trip	25	21,2
72	A-B-C	70%	Long	Import	Trip	37,7	29,1
73	A-B-C	100%	Long	Import	No Trip	-	-
74	A-G	-0%	Short	Import	No Trip	-	-
75	A-G	+0%	Short	Import	Trip	344	336,5
76	A-G	50%	Short	Import	Trip	122,9	97,3
77	A-G	70%	Short	Import	Trip	126,9	95,7
78	A-G	100%	Short	Import	No Trip	-	-
79	A-B	-0%	Short	Import	No Trip	-	-
80	A-B	+0%	Short	Import	Trip	335	321
81	A-B	50%	Short	Import	Trip	113,1	87,3

82	A-B	70%	Short	Import	Trip	116,4	86,2
83	A-B	100%	Short	Import	No Trip	-	-
84	A-B-C	-0%	Short	Import	No Trip	-	-
85	A-B-C	+0%	Short	Import	Trip	17,3	24,2
86	A-B-C	50%	Short	Import	Trip	24,4	25,4
87	A-B-C	70%	Short	Import	Trip	37,7	33,6
88	A-B-C	100%	Short	Import	No Trip	-	-

The distance relay M and N fail to provide fast operating time for both the long and the short transmission networks. For the long transmission network, relay M trips after six cycles (120 ms), while relay N has a slightly faster operating time (less than 100 ms). Moreover, the slowest operating time for both relays is found when the LN and LL faults occur at 0% of the transmission line length. In this case, the operating time is delayed up to more than 15 cycles (300 ms).

To sum up, the distance relay M can detect faults with resistance in all load conditions. Relay M trips correctly for all the faults inside zone 1, and never trip for the faults outside the zone 1. However, its operating time seems to be delayed severely in the case of the short transmission network configuration. Meanwhile, relay N cannot provide fast tripping for both the short and the long transmission networks. The operating time of the relay is found to be delayed for almost all the faults. Furthermore, relay N also fails to detect one of the faults located inside the protection zone.

5.7 Test with parallel transmission line application

The test results of relay M are presented in Table 5.4. The table shows the relay operating time for three different conditions. The first condition is the current reversal. In this case, the change of current direction when faults occur in the reverse direction is tested. The relay is expected not to trip in this case.

The second condition is the evolving fault on line 1. In this case, LN faults evolve to LLN (or LLL) faults after several ms as indicated in the table. All faults occur inside the protection zone 1. The relay is expected to provide fast operating time for all the faults. The third condition is the cross-country faults. In this case, LN faults on line 1 (or line 2) are evolving into faults on different lines to produce the cross-country faults. Similar with the evolving fault on one line, the relay is expected to provide fast tripping for all the faults inside the protection zone.

Table 5.4 Test result of parallel transmission line

Fault no.	1st fault	1st fault on line	2nd fault	2nd fault on line	Time difference (ms)	Fault position	Zone 1 Criteria	Operating time (ms)
								Relay M
Current Reversal								
89	A-G	1	-	-	-	+0%	No Trip	-
Evolving fault on line 1								
90	A-G	1	A-B-G	1	10	+0%	Trip	18,9
91	A-G	1	A-B-G	1	30	+0%	Trip	18,5
92	A-G	1	A-B-G	1	200	+0%	Trip	19,1
93	A-G	1	A-B-G	1	10	70%	Trip	57
94	A-G	1	A-B-G	1	30	70%	Trip	36,9
95	A-G	1	A-B-C	1	10	+0%	Trip	17,3
96	A-G	1	A-B-C	1	30	+0%	Trip	18,6
97	A-G	1	A-B-C	1	200	+0%	Trip	18,6
98	A-G	1	A-B-C	1	10	70%	Trip	48,5
99	A-G	1	A-B-C	1	30	70%	Trip	37,9
Cross-country fault								
100	A-G	1	B-G	2	10	+0%	Trip	18,5
101	A-G	1	B-G	2	30	+0%	Trip	17,5

102	A-G	1	B-G	2	200	+0%	Trip	18,2
103	A-G	1	B-G	2	10	70%	Trip	43
104	A-G	1	B-G	2	30	70%	Trip	38,3
105	A-G	1	A-B-C	2	10	+0%	Trip	18,2
106	A-G	1	A-B-C	2	30	+0%	Trip	18,1
107	A-G	2	B-G	1	10	+0%	Trip	37,1
108	A-G	2	B-G	1	30	+0%	Trip	52,6
109	A-G	2	B-G	1	200	+0%	Trip	24,7
110	A-G	2	B-G	1	10	70%	Trip	37,3
111	A-G	2	B-G	1	30	70%	Trip	53,5
112	A-G	2	A-B-C	1	10	+0%	Trip	22,8
113	A-G	2	A-B-C	1	30	+0%	Trip	47,1
114	A-G	2	A-B-C	1	200	+0%	Trip	17,9
115	A-G	1	B-G	2	10	+0%	Trip	17,6
116	A-G	1	B-G	2	30	+0%	Trip	19,9
117	A-G	1	B-G	2	200	+0%	Trip	17,6
118	A-G	1	B-G	2	10	70%	Trip	46,8
119	A-G	1	B-G	2	30	70%	Trip	37,7
120	A-G	1	A-B-C	2	10	+0%	Trip	18,1
121	A-G	1	A-B-C	2	30	+0%	Trip	18,4
122	A-G	1	A-B-C	2	200	+0%	Trip	17,3
123	A-G	2	B-G	1	10	+0%	Trip	37,1
124	A-G	2	B-G	1	30	+0%	Trip	47,1
125	A-G	2	B-G	1	200	+0%	Trip	24,6
126	A-G	2	B-G	1	10	70%	Trip	38,8
127	A-G	2	B-G	1	30	70%	Trip	53,4
128	A-G	2	A-B-C	1	10	+0%	Trip	36,6
129	A-G	2	A-B-C	1	30	+0%	Trip	36,6
130	A-G	2	A-B-C	1	200	+0%	Trip	27,7

Relay M operates correctly for all the three conditions. It is found that the relay is not trip in the case of the current reversal, while it is able to provide fast tripping for evolving and cross-country faults. The results also indicate that the operating times of relay M are below three cycles (60 ms) for all the faults.

5.8 Test with fault arc

The test results of relay M in the case of arcing faults are presented in Table 5.5. The table shows the operating time of the relay for different fault locations. Two load conditions are considered in the test: the exporting and the importing load. The zone 1 reach impedance is set to cover 80% of the transmission line length. Therefore, relay M is expected to operate for faults located at 75% and 80%. On the other hand, relay M must not trip for faults located beyond 80% of the transmission line length.

Table 5.5 Test result of faults with arc

Fault no.	Load Direction	Fault location	Source L	Zone 1 Criteria	Operating time (ms)
					Relay M
1	Export	75%	Homogenous	Trip	48,8
2	Export	80%	Homogenous	Trip	48,7
3	Export	85%	Homogenous	No Trip	-
4	Export	90%	Homogenous	No Trip	-
5	Export	75%	Non-homogenous	Trip	49,4
6	Export	80%	Non-homogenous	Trip	49,3
7	Export	85%	Non-homogenous	No Trip	-
8	Export	90%	Non-homogenous	No Trip	-
9	Import	75%	Homogenous	Trip	99
10	Import	80%	Homogenous	Trip	108,1
11	Import	85%	Homogenous	No Trip	-
12	Import	90%	Homogenous	No Trip	-
13	Import	75%	Non-homogenous	Trip	49,7
14	Import	80%	Non-homogenous	Trip	108,6
15	Import	85%	Non-homogenous	No Trip	-
16	Import	90%	Non-homogenous	No Trip	-

To sum up, the test results indicate that relay M is able to operate correctly under arcing fault conditions. However, in the case of the importing loads (source R to L), the operating time of relay M is delayed up to 100 ms. This condition is not happening for exporting load conditions where relay M consistently trips below three cycles (60 ms).

6 Conclusions and Recommendations

6.1 Conclusions

This thesis presents the implementation of the dynamic testing according to the IEC 60255-121 standard. The testing tools are applied to assess the operation of distance protection during dynamic conditions. The first part of the study is related to the modeling and simulation of dynamic conditions in the power system. The networks and components are modeled and simulated in ATP-EMTP. The models are developed based on benchmark network defined by the standard. From the simulation results, it can be concluded that:

- The network and component models work appropriately based on the requirement of IEC 60255-121 standard.
- Decaying dc-offset on fault current alters the fault impedance trajectory. The higher the magnitude of dc-offset, the more impedance is shifted to the right of R-X plane.
- CVT transient causes impedance measurement error in the first three cycles after fault inception.
- The frequency of power system affects the shape and the diameter of the spiral trajectory of fault impedance.
- Fault resistance and pre-fault load cause impedance trajectory on the RX plane to shift downward or upward. Impedance trajectory is shifted downward for exporting load, and it shifted upward in the case of importing load.
- Voltage and current dynamics during an evolving fault (and cross-country fault) cause the shape and direction of the measured impedances vary for each phase. Moreover, during the current reversal conditions, the faulted phase impedance will enter the reverse zone of distance protection.
- Simulations performed for arcing faults show similar results with the fault resistance test cases. However, due to the time-varying resistance of the arcing fault, it is shown that the impedance trajectory has the *"curl"* shape that encroaches inside and outside of the distance protection zone.

The second part of the thesis is related to developing the test tools for performing the dynamic testing of distance relays. The test libraries are developed using the Omicron Control Center (OCC) Software. The protection setting of the distance relay is defined, and the hardware connection was established between the relay and the Omicron CMC 356. An Extensive testing was performed to study the influence of the transient on the performance of commercial distance relays. From the test results, it can be concluded that each distance relay has a relatively different dynamic performance. The characteristics are summarized as follow:

- The average operating time of distance relay M is faster than distance relay N for faults located close to the relay location.
  Relay M: 24.4 ms; Relay N: 31.1 ms
- The average operating time of distance relay M is slower than distance relay N for faults located close at the end of zone 1 setting.
  Relay M: 41.9 ms; Relay N: 36 ms
- High source impedance ratio (SIR) causes a delay in operating time of distance relay. The delay can be different for different relay manufacturers. In this case: Relay M: 8.5 ms; Relay N: 6.9 ms
- CVT transient also causes a delay in operating time of distance relay. In this case: Relay M: 6.9 ms; Relay N: 14.1 ms

- The types of the fault do not cause significant effect on average operating time and accuracy of distance relay as can be seen in the following table

Fault type	Relay M	Relay N
LN fault	32 ms	32.9 ms
LL fault	31.6 ms	33.3 ms
LLN fault	34.3 ms	29.7 ms
LLL fault	32.1 ms	30.8 ms

- Superimposed harmonics could cause an operating time delay in distance relay. In this case (relay M), the seventh harmonics causes almost one cycle delay for AG fault at 95% of zone 1 setting.
- Frequency deviation has no influence on the operating time of distance relay. However, relay M seems to have overreach problems when operating on the minimum frequency.
- Both distance relays appear to have problems to provide fast operation during faults with resistance and arc. This condition happens especially in the short line application. In the extreme cases, the operating time delay can be up to more than 15 cycles (300 ms).

6.2 Recommendation

The dynamic testing tools developed in this thesis can be used to assess the operation of numerical distance protection under different dynamic conditions. The network models built in this thesis are *open models*. The models can be modified or expanded to represent other dynamic conditions of interest such as transformer inrush current, series-compensated line, ferroresonance, and CT saturation. Further study using sensitivity analysis is also recommended to provide an in-depth analysis of each dynamic condition.

References

[1] IEC *60255-121* std. (2014). *Functional Requirements for Distance Protection.*

[2] Ziegler, G. (2011). *Numerical distance protection: Principles and Applications* (4th ed. ed.). Hoboken: John Wiley & Sons.

[3] Campos, J.T.L.S., Neves, W.L.A., & Costa, F. B. (2016). *The Effect of Fault Variables in the Performance of Quadrilateral and Mho Relays. Natal, Brazil: SBSE 2016.*

[4] IEEE Power System Relaying and Control Committee (PSRC). (2004). *EMTP Reference Models for Transmission Line Relay Testing.* WG D10 Report.

[5] Kasztenny, D., Sharples, V., Asaro, & Pozzuoli, M. (2000). *Distance Relays and Capacitive Voltage Transformers - Balancing Speed and Transient Overreach*. GEC, GER-3986.

[6] IEEE Power System Relaying and Control Committee (PSRC). (2003). *Protective Relaying and Power Quality*. WG Report.

[7] IEEE Power System Relaying and Control Committee (PSRC). (2013). *Distance Element Response to Distorted Waveforms.* Technical Report.

[8] Thiab, O. S., Nogal, L., & Rasolomampionona, D. (2016). *Evaluation of frequency deviations effects on performance of digital protection relays.* IEEE International Energy Conference (ENERGYCON), 1-6.

[9] Terzija, V., Koglin, H-J. (2004). *On the Modeling of Long Arc in Still Air and Arc Resistance Calculation*. IEEE Transaction on Power Delivery, 19, 3, 1012-1017.

[10] Wihartady, H., Popov, M., & van der Sluis, L. (2009). *Modeling of Short Circuit Arc in 150kV System and Its Influence on the Performance of Distance Protection*. Delft, The Netherlands: EEUG Meeting.

[11] Kizilcay, M., Pniok, T. (1991). *Digital Simulation of Fault Arcs in Power Systems*. European Transactions on Electrical Power (ETEP), 1, 1, 55-60.

[12] van der Sluis, L. (2001). *Transients in Power Systems.* Delft, The Netherlands: Wiley.

[13] Kezunovic, M., & Ren, J. (2008). *New test methodology for evaluating protective relay security and dependability.* IEEE PES General Meeting - Conversion and Delivery of Electrical Energy in the 21st Century, 1-6.

[14] de Clippelaar, S. (2015). *Improve Protection Relaying System Reliability by Dynamic Testing.* International Protection Testing Symposium.

[15] CIGRE (2000). Analysis and Guidelines for Testing Numerical Protection Schemes. WG Report 34.10

[16] Dommel, H. W. (1986). *Electromagnetic Transients Program: EMTP Theory Book.* Bonneville Power Administration

[17] Costa, F. B., Souza B. A., & Brito, N. S. D. (2012). *Effects of the Fault Inception Angle in Fault-induced Transients.* IET Generation, Transmission & Distribution, 6, 5, 463-471.

[18] IEC *61869-5 std.* (2011). *Additional Requirements for Capacitive Voltage Transformer.*

[19] IEEE std C37.113-2015. (2016). *IEEE Guide for Protective Relay Applications to Transmission Lines.*

[20] Alstom Grid. (2011). *Network Protection and Automation Guide.*

[21] Apostolov, A., Tholomier, D., Sambasivan, S., & Richards, S. (2007). *Protection of Double Circuit Transmission Lines.* 60th Annual Conference for Protective Relay Engineers, 85-101.

[22] Terzija, V., Radojevic, Z., & Djuric, M. (1996). *A New Approach for Arcing Faults Detection and Fault Distance Calculation in Spectral Domain*. Transmission and Distribution Conference Proceedings, 573-578.

[23] Taghizadeh, M., Sadeh, J., Bashir, M., & Kamyab, E. (2011). *Effect of single phase to ground fault with arc resistance on the performance of distance relay*. 10th International Conference on Environment and Electrical Engineering, 1-5.

[24] Terzija, V., Preston, G., Popov, M., & Terzija, N. (2011). *New Static "AirArc" EMTP Model of Long Arc in Free Air*. IEEE Transactions on Power Delivery, 26, 3, 1344-1353.

[25] Benmouyal, G., Zimmerman, K. (2010). *Experience With Subcycle Operating Time Distance Elements in Transmission Line Digital Relays*. 37th Annual Western Protective Relay Conference.

[26] Kennedy, J. M., Alexander, G. E., & Thorp, J. S. *Variable Digital Filter Response Time in a Digital Distance Relay*. GEC GER-3798

[27] IEEE Power System Relaying and Control Committee (PSRC). (2009). *Understanding Microprocessor-based Technology Applied to Relaying*. WG Report I-01

[28] IEEE std C37.90-2005. (2006). IEEE Standard for Relays and Relay Systems Associated with Electric Power Apparatus.

[29] Bonetti, A., Yalla, M. V. V. S., & Holst, S. (2016). *The IEC 60255-121:2014 standard and its impact on performance specification, testing and evaluation of distance protection relays.* IEEE/PES Transmission and Distribution Conference and Exposition (T&D), 1-6.

[30] Phadke, A. (2009). *Computer relaying for power systems* (2nd ed. ed.). Chichester, West Sussex: John Wiley & Sons.

Appendix

A. Reach impedance setting calculation

The procedure steps required to calculate the reach impedance of distance zone are given in the following.

- Define system data

Parameter	Value
Nominal phase-phase voltage	400 kV
System frequency	50 Hz
VT ratio	400 kV / 100 V
CT ratio	1200 A / 1 A
Line length short	20 km
long	100 km
Line positive-sequence impedance	0.03184 + j0.3636 Ω/km
Line zero-sequence impedance	0.12740 + j1.4552 Ω/km
Maximum fault resistance Ph-e	15 Ω
Maximum fault resistance Ph-Ph	10 Ω

- Define characteristic shape
  In this thesis, the characteristic shape is *quadrilateral* as it provides independent settings for impedance and resistance reach.
- Calculate line reactance per length unit (secondary value)

$$x'_{sec} = \frac{CT\ ratio}{VT\ ratio} \cdot x'_{pri} = \frac{\frac{1200}{1}}{\frac{400000}{100}} \cdot 0.3636 = 0.10908\ \Omega/\mathrm{km}$$

- Calculate impedance reach setting (X_1)
  $X(Z1) = 0.8 \cdot x'_{sec} \cdot line\ length$
  Short line = 0.8 · 0.10908 · 20 = **1.74528 Ω**
  Long line = 0.8 · 0.10908 · 100 = **8.7264 Ω**
- Define zero-sequence compensation factor (R_E/R_L) and (X_E/X_L)
  The zero-sequence compensation factor is applied, so that distance relay measures the distance to the fault of all fault based on positive-sequence impedance reach. The setting is applied as R_E/R_L and X_E/X_L from line impedance data as follow

$$\frac{R_E}{R_L} = \frac{1}{3} \cdot \left(\frac{R_0}{R_1} - 1\right) = \frac{1}{3} \cdot \left(\frac{0.1274}{0.03184} - 1\right) = 1.0004$$

$$\frac{X_E}{X_L} = \frac{1}{3} \cdot \left(\frac{X_0}{X_1} - 1\right) = \frac{1}{3} \cdot \left(\frac{1.4552}{0.3636} - 1\right) = 1.0007$$

- Calculate resistive setting (R_1) for Ph-Ph fault and Ph-e fault
  The criteria for resistive setting of quadrilateral protection zone is defined as

$$0.8 \cdot X(Z1) < R(Z1) < 2.5 \cdot X(Z1)$$

  The ph-ph resistive setting for the short line can be calculated as follow:

$$R(Z1)_{ph-ph} = \frac{120\% \cdot R_{max,pri} \cdot \frac{CT\ ratio}{VT\ ratio}}{2} = \frac{1.2\ \cdot 10 \cdot 0.3}{2} = \mathbf{1.8\ \Omega}$$

Notes:

- With additional 20% safety margin
- Division by factor of 2 because fault resistance appears in the loop measurement, while the setting is done as positive-sequence impedance.

Ph-e resistive setting is then calculated by

$$R(Z1)_{ph-e} = \frac{120\% \cdot R_{max,pri} \cdot \frac{CT\ ratio}{VT\ ratio}}{(1 + \frac{R_E}{R_L})} = \frac{1.2\ \cdot 15 \cdot 0.3}{(1 + 1.0004)} = \mathbf{2.6994\ \Omega}$$

Notes:

- Division by factor ($1+R_E/ R_L$) because fault resistance appears in the loop measurement, while the setting is done as positive-sequence impedance.

For long transmission line, the minimum criteria of resistive setting is not satisfied (R(Z1) < 0.8 X(Z1)), hence minimum resistive settings are used

$R(Z1)_{ph-ph} = R(Z1)_{ph-e} = 0.8 \cdot X(Z1) = 0.8 \cdot 8.7264 = \mathbf{6.98112\ \Omega}$

- Calculate characteristic angle

Characteristic angle setting is calculated from the positive sequence line impedance data.

$$Char.angle = arctan\left(\frac{X_L}{R_L}\right) = arctan\ \left(\frac{0.3636}{0.03184}\right) = \mathbf{85}°$$

B. Test sequence

B.1 Decaying dc-offset

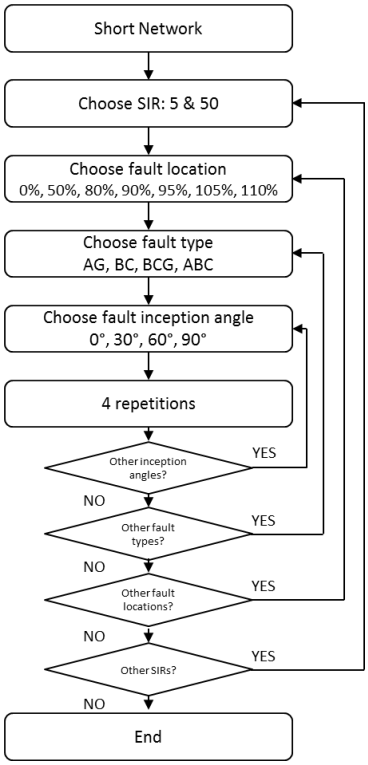

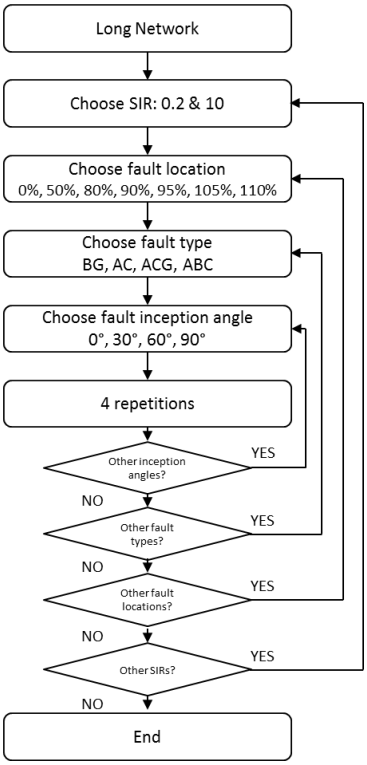

B.2 CVT transient

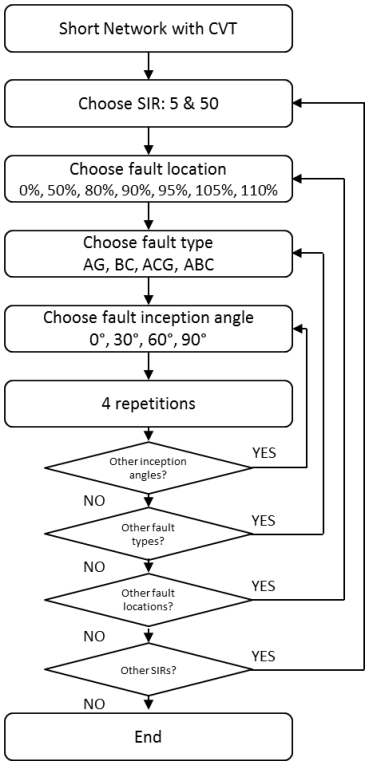

B.3 Superimposed harmonics

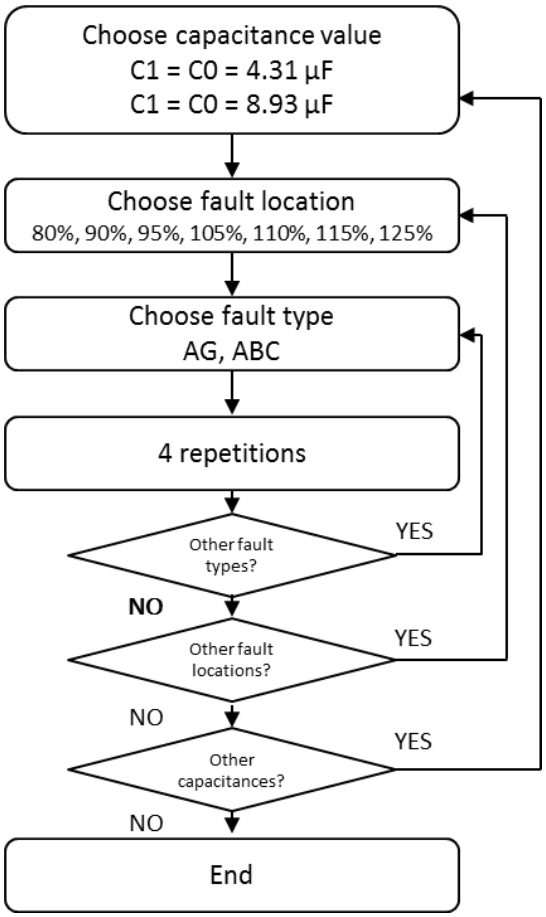

B.4 Frequency deviation